5-2013

Comparison of Tumor Shrinkage and Cumulative Dose Distribution for Lung Cancers

Yi Pei Chen

COMPARISON OF TUMOR SHRINKAGE AND CUMULATIVE DOSE DISTRIBUTION FOR LUNG CANCERS`

By

Yi Pei Chen, B.S.

APPROVED:

_____
Laurence Edward Court, PhD.
Supervisory Professor

_____
Lei Dong, Ph.D.

_____
Kenneth R. Hess, Ph.D.

_____
Xiaorong Ronald Zhu, Ph.D.

_____
Zhongxing Liao, M.D.

APPROVED:

_____
Dean, The University of Texas
Graduate School of Biomedical Science at Houston

COMPARISON OF TUMOR SHRINKAGE AND CUMULATIVE DOSE DISTRIBUTION FOR LUNG CANCERS

A

THESIS

Presented to the Faculty of

The University of Texas

Health Science Center at Houston

and

The University of Texas

M.D. Anderson Cancer Center

Graduate School of Biomedical Sciences

in Partial Fulfillment

of the Requirements

for the Degree of

MASTER OF SCIENCE

By

Yi Pei Chen, B.S.

Houston, TX

May, 2013

DEDICATION

To my husband, your love has carried me through every circumstance, and

my new-born son, your smile has changed my world.

ACKNOWLEDGEMENTS

I would like to thank my previous advisor, Dr. Lei Dong, for his guidance, advice and dedication to excellence. He is the one who inspired me and many others to get into this field. After Dr. Lei Dong's departure from M.D. Anderson, Dr. Laurence Court became my current advisor. I am truly grateful and fortunate that Dr. Court took me in as his student to finish this thesis. His mentoring skills and commitment to all of his students have encouraged me in general. I value his caring and dedication throughout the entire process. I would also like to thank the members of my committee: Dr. Kenneth Hess, Dr. Zhongxing Liao, and Dr. Ronald Zhu for their valuable suggestions and feedbacks that helped the project especially Dr. Hess who helped me to design my statistical analysis.

Special thanks must be given to computation scientist, Dr. Joy Zhang, for developing the tool to deform contours and dose for this project. I truly appreciate her assistance.

Finally, I would like to thank my group and friends for their supports especially to Adam Yock, Mitchell Carroll, Dr. Heeteak Chung, Joey Cheung, Luke Hunter, and Dr. Peter Park.

This research was supported financially by grant PO1CA021239 from the National Cancer Institute.

ABSTRACT

COMPARISON OF TUMOR SHRINKAGE AND CUMULATIVE DOSE DISTRIBUTION FOR LUNG CANCERS

Publication No._____

Yi Pei Chen, B.S.

Supervisory Professor: Laurence E. Court, Ph.D.

Background: The physical characteristic of protons is that they deliver most of their radiation dose to the target volume and deliver no dose to the normal tissue distal to the tumor. Previously, numerous studies have shown unique advantages of proton therapy over intensity-modulated radiation therapy (IMRT) in conforming dose to the tumor and sparing dose to the surrounding normal tissues and the critical structures in many clinical sites. However, proton therapy is known to be more sensitive to treatment uncertainties such as inter- and intra-fractional variations in patient anatomy. To date, no study has clearly demonstrated the effectiveness of proton therapy compared with the conventional IMRT under the consideration of both respiratory motion and tumor shrinkage in non-small cell lung cancer (NSCLC) patients.

Purpose: This thesis investigated two questions for establishing a clinically relevant comparison of the two different modalities (IMRT and proton therapy). The first question was whether or not there are any differences in tumor shrinkage between

patients randomized to IMRT versus passively scattered proton therapy (PSPT). Tumor shrinkage is considered a standard measure of radiation therapy response that has been widely used to gauge a short-term progression of radiation therapy. The second question was whether or not there are any differences between the planned dose and 5D dose under the influence of inter- and intra-fractional variations in the patient anatomy for both modalities.

Methods: A total of 45 patients (25 IMRT patients and 20 PSPT patients) were used to quantify the tumor shrinkage in terms of the change of the primary gross tumor volume (GTVp). All patients were randomized to receive either IMRT or PSPT for NSCLC. Treatment planning goals were identical for both groups. All patients received 5 to 8 weekly repeated 4-dimensional computed tomography (4DCT) scans during the course of radiation treatments. The original GTVp contours were propagated to T50 of weekly 4DCT images using deformable image registration and their absolute volumes were measured. Statistical analysis was performed to compare the distribution of tumor shrinkage between the two population groups. In order to investigate the difference between the planned dose and the 5D dose with consideration of both breathing motion and anatomical change, we re-calculated new dose distributions at every phase of the breathing cycle for all available weekly 4DCT data sets which resulted 50 to 80 individual dose calculations for each of the 7 patients presented in this thesis. The newly calculated dose distributions were then deformed and accumulated to T50 of the planning 4DCT for comparison with the planned dose distribution.

Results: At the end of the treatment, both IMRT and PSPT groups showed mean tumor volume reductions of 23.6% (19.2%) and 20.9% (17.0 %) respectively. Moreover, the mean difference in tumor shrinkage between two groups is 3% along with the corresponding 95% confidence interval, [-8%, 14%]. The rate of tumor shrinkage was highly correlated with the initial tumor volume size. For the planning dose and 5D dose comparison study, all 7 patients showed a mean difference of 1 % in terms of target coverage for both IMRT and PSPT treatment plans.

Conclusions: The results of the tumor shrinkage investigation showed no statistically significant difference in tumor shrinkage between the IMRT and PSPT patients, and the tumor shrinkage between the two modalities is similar based on the 95% confidence interval. From the pilot study of comparing the planned dose with the 5D dose, we found the difference to be only 1%. Overall impression of the two modalities in terms of treatment response as measured by the tumor shrinkage and 5D dose under the influence of anatomical change that were designed under the same protocol (i.e. randomized trial) showed similar result.

TABLE OF CONTENTS

LIST OF FIGURES

LIST OF TABLES

Chapter 1

Introduction

1.1 Background

Introduction to IMRT and Proton Therapy

One of the major goals in radiation therapy is the local control of tumor. It is a well-known fact that higher dose to the tumor will increase success of local control. However, delivering high dose to a tumor is restricted by the radiation tolerance of organs at risks (OAR) or normal tissue surrounding the tumor volume. The field of radiation oncology and, in particular, its method of delivering external beam radiation have changed rapidly including new technologies in linear accelerator and computerized treatment planning over the last two decades. After the first introduction of 3-dimentional imaging technology such as computed-tomography (CT) in the early 1980s, the development of virtual simulation using a computerized treatment planning system (TPS) quickly followed (Bucci, Bevan et al. 2005). With these advancements in hand, many hospitals adopted 3-dimensional conformal radiation therapy (3DCRT) technique in which the dose distribution from each radiation beam is shaped to fit the contour of a given target in beam's eye view based on a computerized patient image data set. By employing many such beams, 3DCRT was able to significantly reduce the amount of dose to the surrounding normal tissues, thereby allowing dose escalation to the tumor for a better therapeutic outcome. Now, 3DCRT is considered the conventional technique for hospitals in many developed countries. Despite the huge improvement of

going from what was essentially a 2D plan radiation therapy to 3DCRT, it was very difficult or impossible to spare critical structures that push into or partially surround a target (Galvin, Ezzell et al. 2004). In order to further escalate dose to the target, a more conformal dose distribution was necessary. The idea of modulating the intensity of the incoming radiation beam using moving leaves in a motorized fashion attached to a gantry was first conceived by Dr. Takahashi in early 1960s (Takahashi and Matsuda 1960). Thirty years later, researchers started developing multileaf collimators (MLC) to create multiple collimated fields for existing 3DCRT units. This process was then fully automated and integrated to the TPS to deliver conformal radiation efficiently. (Brahme 1988; Galvin, Smith et al. 1992; Brewster, Mohan et al. 1995).

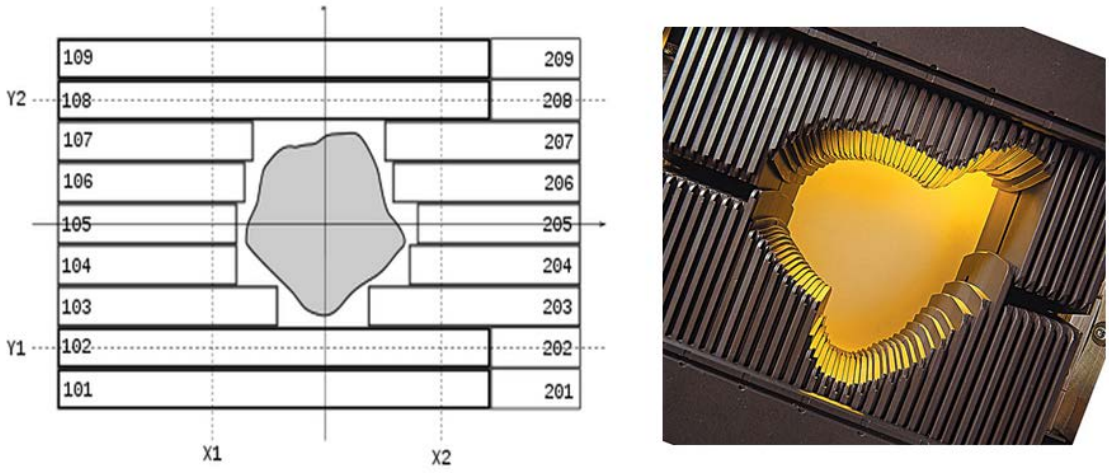

Figure 1.1 A schematic of MLC with its leaf position conforming to a target volume in beam's eye view (left) and an example of a working MLC that is attached to a IMRT unit by Varian SmartBeam^{TM} (right)

While the MLC technology was being developed, another important development known as inverse-planning was invented (Brahme 1988; Bortfeld, Burkelbach et al. 1990). The concept of inverse-planning is that a user indicates the desired goals of radiation therapy in terms of target coverage or dose constraint to nearby critical structures and computer tries to optimize the plan by determining the best treatment parameters. Traditionally, for 3DCRT, treatment plans have been designed using forward-planning. In forward- planning, the treatment planner must specify the number of fields, gantry angles, and collimator settings first, and then calculates the resultant dose distribution. With inverse-planning, it is possible to let a computer optimize any beam parameters of treatment planner's choice including the intensity of radiation beam that can be controlled with use of MLC. The integration of 3DCRT with MLC and inverse-planning became the basis of intensity modulated radiation therapy (IMRT). In a typical IMRT treatment planning, treatment planners can specify dosimetric goals with respect to the target and surrounding OARs. After preselecting basic plan parameters such as number of beams and gantry angles, an inverse-planning capable TPS will optimize the intensity of radiation beams and relative radiation beam weight to meet the planning objectives by manipulating collimator jaws and MLC leaf positions. The MLC leaves can move in and out of the open field in order to shape the dose profile and modulate transmission of the open beam, essentially allowing non-uniform beam intensities for each beam to be delivered (Webb *et al* 2003). Previously, many researchers and clinicians reported advantages of IMRT over 3DCRT both in treatment planning studies and clinical studies (Hall and Wuu 2003; Luxton, Hancock et al. 2004; Vlachaki, Teslow et al. 2005; Yom, Liao et al. 2007). The

advantages of IMRT over 3DCRT in terms of its ability to shape the dose to a target, spare dose to surrounding tissues, and specify dose objectives were so significant that it quickly became the state of art of external beam radiation therapy today.

In recent years, there has been increasing interests in treating cancer using high energy protons. The concept of treating cancer using high energy protons was first introduced by Wilson in 1946 (Wilson 1946 Wilson, RR. 1946. Radiological uses of fast protons. Radiology 47:487). The chief advantage of proton over photon is that it stops, giving the radiation beam a finite range in the patient body so that one can spare normal tissue distal to the tumor volume completely whereas for photon it is impossible to completely spare normal tissue directly along the direction of radiation beam. The depth dose curve of proton, which is often denoted as the Bragg curve, shows another important advantage of proton radiation compares to a typical depth dose curve obtained by photon radiation. When proton radiation interacts with a medium, it deposits relatively low dose at the entrance region but releases most of its energy at the end of its range before it falls to zero abruptly (see figure 1.2). However, a typical Bragg peak width is in the order of a few millimeters and it is not large enough to cover a typical tumor size. Therefore, many Bragg peaks are combined in order to generate a spread-out Bragg peak (SOBP). The width of an SOBP can be made to extend across any given target volume. However, in creating the SOBP, the low entrance dose given by the single Bragg peak must also be summed which increases entrance dose. Typically, this entrance dose is still on the order of 20% less than the dose given to the tumor volume for photon beam. Therefore, the advantage of proton over photon is still retained (See figure 1.2). However, due to the huge cost and size of facility required to

build a proton therapy center, the initial development of proton therapy was limited to high-energy physics facilities (Tobias, Lawrence et al. 1958). With the advancement of technology in accelerator physics, some vendors started to provide hospital based proton therapy facilities in the early 1990s (Slater, Miller et al. 1991). Since the beginning of 2000, the number of hospital based proton facilities increased dramatically and as of now there are 33 proton facilities in operation world-wide and 10 proton facilities in the United States. The number of hospital based proton facilities is expected to grow more in the next few years with many centers currently under construction or in the planning state. Even though, the theoretical advantage of proton therapy over the conventional external beam radiotherapy using photons was noted earlier. Since the birth of proton therapy in the early 1960's and its popularization into the early 2000, much technological advancements have occurred on the side of photon radiation therapy including IMRT that raises a question on whether or not proton therapy can demonstrate clinical advantage over IMRT.

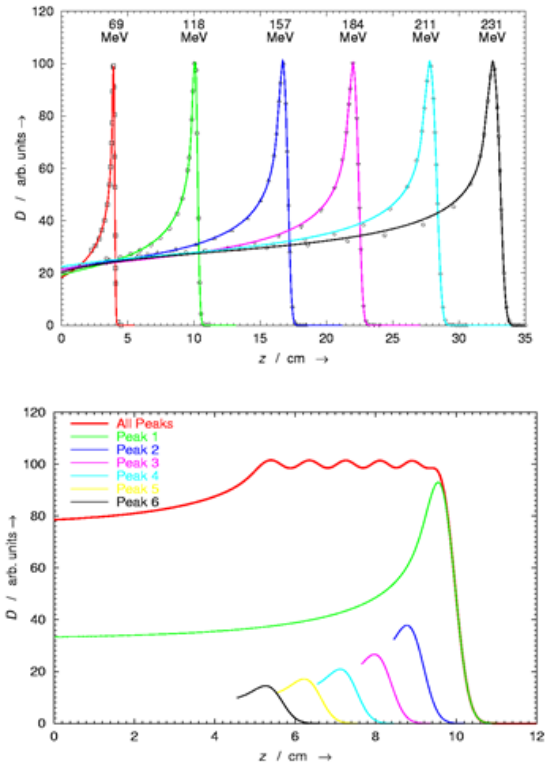

Figure 1.2 The Bragg peaks of different initial energy of protons (top) and an example of SOBP that is created by adding 6 different Bragg peaks of different energy and intensity. (Courtesy of Dr. Wayne D. Newhauser, Louisiana State University, USA)

Comparing IMRT vs. Proton Therapy

In recent years, the debate between IMRT vs. proton has been a hot topic in the radiation oncology community. As the number of proton therapy centers increases, there is a concern about whether or not the clinical advantage of proton therapy is well justified over the cost of building and maintaining proton centers (Brada, Pijls-Johannesma et al. 2007; Konski, Speier et al. 2007). Although the physical characteristic of proton's low entrance dose and no exit dose give clear theoretical advantages over IMRT, clinically feasible plans are not simple to be delivered. The actual clinical treatment plan is complicated with many parameters that can be vastly different between IMRT and proton plans. For example, a number of beam angles tend to be greater for IMRT which can potentially improve dose conformity in higher dose region. Also, treatment planning parameters (e.g. margins) can vary significantly between the two modalities that can potentially affect the final dose distribution. There have been many articles written in the past years comparing the dosimetric difference between IMRT and proton therapy in various treatment sites. A search of published manuscripts with both IMRT and proton as keywords on scopus.com resulted in a total number of 223 published scientific journals with increasing number of publications every year. Most of these publications are based purely on dosimetric studies that compared the dose distribution of IMRT and proton therapy plans but lack of clinical assessments such as patient follow-up morbidity, toxicity, or survival data. In 2007, Olsen *et al* conducted a comprehensive systematic literature review to survey the clinical effectiveness of proton therapy (Olsen, Bruland et al. 2007; Goitein and Cox

2008). In their study which looked at 54 different publications concluded that the evidence on clinical efficacy of proton therapy so far has relied on non-controlled studies that are poorly designed for the purpose of comparing IMRT and proton therapy.

1.2 NIH P01 Randomized Clinical Trial

Non-small cell lung cancer (NSCLC) is the leading cause of cancer deaths in the United States. (Chang, Zhang *et al*. 2006) Despite the recent advancement in cancer treatment, clinical outcome of NSCLC remains poor partly due to the difficulty in escalating dose to tumor in the presence of highly radiation sensitive critical structures such as lung, spinal cord, heart, and esophagus. With conventional radiotherapy, its 5 years survival rate is only 10-30% (Dosoretz, Katin et al. 1992). Although IMRT could deliver higher dose to the tumor, dose constraint to the surrounding healthy lung tissue has been the greatest barrier for further dose escalation. Recently, a few dosimetric studies demonstrated the advantage of proton therapy in lung cancer treatment over IMRT that can potentially allow further dose escalation to achieve better clinical outcome for lung cancer patient (Zhang, Li et al. 2009; Chang, Zhang et al. 2006). However, the lack of a proper randomized clinical trial to show the evidence of proton therapy's superiority over IMRT prompted many discussion in the radiation oncology community (Halperin 2000; Glasziou, Chalmers et al. 2007; Glimelius and Montelius 2007; Lodge, Pijls-Johannesma et al. 2007; Olsen, Bruland et al. 2007; Goitein and Cox 2008; Macbeth 2008). With recent developments and popularization of proton therapy in the United States, increasing interest to conduct a randomized trial prompted the

national institute of health (NIH) funded P01 randomized clinical trial of various tumor types and locations including NSCLC by the collaboration between Massachusetts General Hospital in Boston, Massachusetts and University of Texas M.D. Anderson Cancer Center in Houston, Texas. At the time of writing this thesis, this trial is still ongoing.

In this randomized clinical trial, patients are treated either with IMRT or passively scattered proton therapy (PSPT). This trial would not only answer whether or not PSPT is better than IMRT, but it would also help rectify the current challenges involved in lung cancer radiation therapy. As an example, in this thesis work, as one of many projects involved in the randomized clinical, will demonstrate a method of estimating delivered dose to a patient that takes into account of both breathing motion and anatomical change over the course of treatment for more accurate assessment of NSCLC therapy. All patient datasets (e.g. images, treatment plans, and etc.) related to this thesis work are sampled from the larger patient cohort of the randomized clinical trial. Only the patients with stage II-IIIB NSCLC who were enrolled for concurrent chemotherapy were eligible for this trial. Once the patient is enrolled, two radiation therapy plans were created, one for IMRT and one for PSPT, by following the identical planning goals and objectives (i.e. target coverage and dose constraint to critical structures). Only those patients with the plans that met the specific dose objectives for both IMRT and PSPT were allowed to enter the randomized trial. If either IMRT or PSPT plan did not meet the specified dose objectives, whichever plan that met the dose objectives was selected for treatment and the patient was removed from the trial. The process of creating a treatment plan is as follow: First, four-dimensional computed

tomography (4DCT) simulation is acquired for treatment planning purpose. The details of 4DCT simulation are discussed later in this chapter. Tumor motion is then evaluated using the 4DCT images at different breathing phases (Vedam *et al* 2002, Rietzel *et al* 2005). If the tumor motion is greater than 1cm, an active motion management technique such as voluntary breath-hold treatment is provided (Vedam, Keall et al. 2001; Ford, Mageras et al. 2002). However, in this study, those patients are excluded in order to minimize bias introduced by the motion management techniques. In order to assess anatomical change and its influence on dose distribution, each patient receives weekly 4DCTs throughout the course of treatment. For each weekly 4DCT, images are imported into the Pinnacle^3 treatment planning system (TPS) for contouring target and critical structures. For this study, every contour was delineated on the T50 phase of 4DCT because our analysis will be performed on this particular phase. T50 phase was chosen because the anatomy of patient is most stable during the end of exhale of breathing cycle ((Balter, Lam et al. 1998)). The target volumes are created by first delineating the gross tumor volume (GTV). The contour of GTV was expanded to form clinical target volume (CTV) to include surrounding microscopic diseases that are generally not visible on CT images. The contour of GTV on T50 phase is then deformed to other phases of breathing cycle to form the motion encompassing gross tumor volume called integrated-GTV (IGTV). The IGTV is further expanded to internal target volume (ITV) again to include microscopic disease and the ITV is then further expanded to planning target volume (PTV) isotropically using 5-7mm margins to compensate for possible setup error. For critical structures, brachial plexus, esophagus, liver, total lung, spinal cord and heart are contoured on the T50 phase image. Once

every contour is defined, treatment plans for both IMRT and PSPT are created based on the same predefined dosimetric objectives. The primary treatment planning goal is to deliver 74Gy to 95% of the planning target volume (PTV) while achieving various dose constraints to different critical structures as listed in table 1.1.

Table 1.1 Tolerance limits for critical structures

Critical Structures	**Dose Limits [Gy]**
PTV (Planning Target Volume)	> 99% volume receiving > 95% of 74Gy
Brachial plexus	Minimum dose to 2% highest dose volume < 60 Gy
Esophagus	1/3 volume < 65 Gy; 2/3 volume < 55 Gy
Liver	Mean dose to liver < 25 Gy; 1/3 liver < 35 Gy
Total Lung	Mean lung dose < 20 Gy; V20 < 37% of volume; Mean lung dose < 22Gy and V20 up to 40% are acceptable as minor deviations
Spinal Cord	Maximum dose to 2% highest dose volume < 50 Gy
Heart	1/3 volume < 60 Gy; 2/3 volume < 45 Gy; Mean heart dose < 30 Gy

For IMRT plan, 5 to 7 beam angles are typically used to cover the target area with prescribed dose while only 2 to 4 beam angles are used for PSPT plan. Once beam angles are chosen, the dose distributions for each plan are calculated and target coverage as well as tolerance limits to all critical structures are checked. A patient is randomized between IMRT and PSPT only if both IMRT and PSPT treatment plans meet these criteria. Otherwise, the patient is removed from the randomized trial and whichever plan provided better target coverage and normal tissue sparing is selected for treatment. The overall flow chart of NIH P01 randomized clinical trial is shown in figure 1.3 with details explained in the following sections.

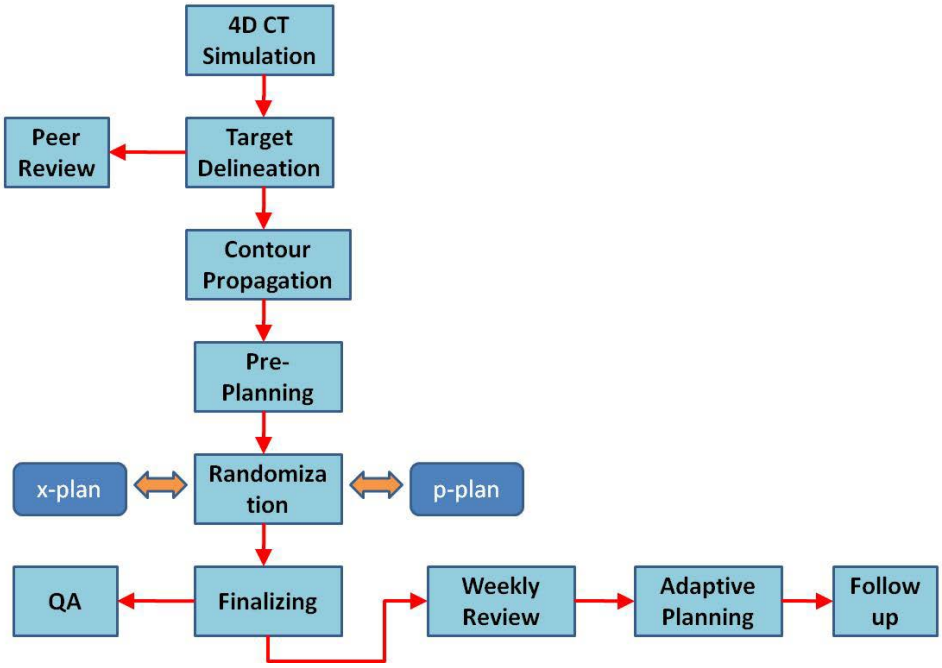

Figure 1.3 Overall flow chart for treatment planning process: Each patient is given a 4DCT simulation that is used to create both IMRT (x-plan) and PSPT plans (p-plan). Then, the patient is randomized between IMRT and PSPT only if both plans meet the given criteria. After randomization, the patient receives weekly 4DCT for treatment review to see if adaptive planning is necessary. (Courtesy of Dr. Lei Dong, M.D. Anderson Cancer Center, Houston, TX)

Four-dimensional Computed Tomography (4DCT)

In radiation therapy of thoracic site such as NSCLC cases, breathing motion introduces multiple problems such as image artifacts, inaccurate assessment of tumor position and its motion extent, and dose calculation (Keall, Mageras et al. 2006). In order to resolve the problems, 4DCT was developed to capture CT images of breathing motion at specified intervals which allowed accurate target delineation, motion assessment, and motion mitigating techniques such as breath-hold and gating treatment (Keall, Mageras et al. 2006). In order to collect and sort the CT images at a certain interval, each CT images must be time-stamped while patient's breathing cycle is tracked and recorded. The time stamping of CT images is done by the CT scanner machine during its data acquisition. The patient's breathing cycle can be tracked and recorded by using either internal or external markers. Most commonly used external markers are abdominal displacement or the flux of inhaled and exhaled volume of air respectively. The abdominal displacement can be tracked and recorded through infrared reflective plastic box placed on the patient's anterior abdominal surface and the flux of inhaled and exhaled volume of air can be traced using a spirometer. Internal marker can be patient anatomy itself which can be traced through real-time imaging such as ultrasound or fluoroscopy or it could be surgically implanted internal fiducial markers (Keall, Mageras et al. 2006). At M.D. Anderson Cancer Center, the acquisition of 4DCT follows a previous method reported by Pan *et al.* closely (Pan, Lee et al. 2004). In their method, CT images of patient are continuously acquired over a period greater than the normal breathing cycle (i.e. 15 images per any given table position for 3 to 4

seconds) using cine-mode that is available on multi-slice Discovery GE CT scanner (General Electric Medical Systems, Waukesha, Wisconsin) while recording external respiratory signal given by the Real-Time Position Management (RPM) respiratory gating system (Varian Medical Systems, Palo Alto, CA). Once both images and external motion signal are acquired, the sorting of images at different axial location according to their common breathing cycle time be binned together. The full cycle of breathing motion from RPM signal is divided into 10 bins that are equally spaced in time. Then, 3DCT images set corresponding to a single phase is derived by collecting images that have closest time-stamped to the selected phase at every table position. This process can be repeated for other phases to generate ten 3DCT image sets that represent different phase of breathing cycle. A simplified illustration of phase binning process is depicted in figure 1.4 (Pan, Lee et al. 2004).

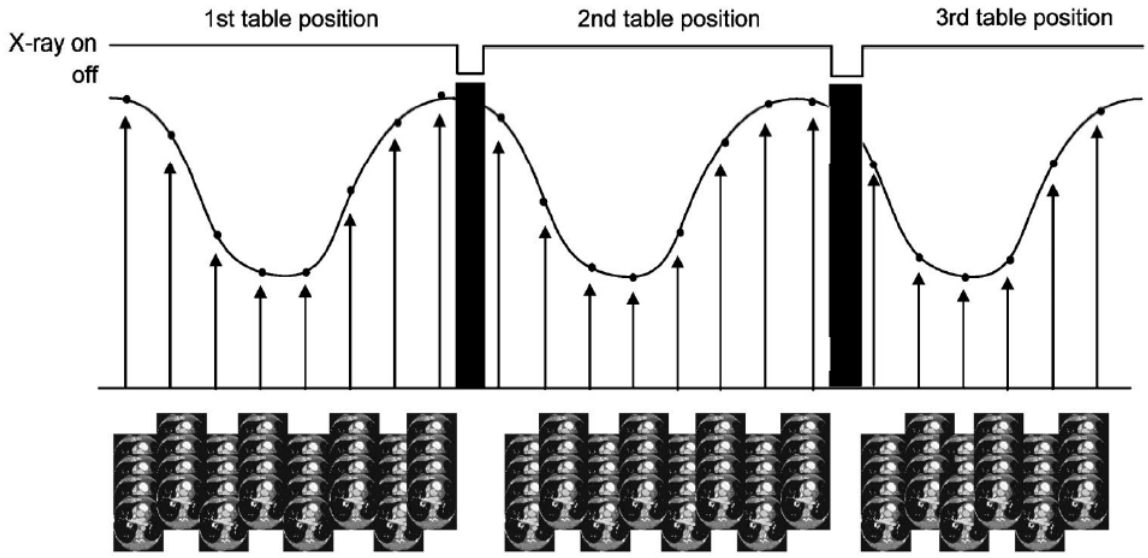

Figure 1.4 An illustration of scanning and image reconstruction of phase binned 4DCT: The sinusoidal wave represents breathing cycle (i.e. external signal from RPM). The dots on the wave represent individual phases. [Permission to publish this figure was obtained from Tinsu Pan, Ting-Yim Lee, Eike Rietzel, and George T. Y. Chen, Medical Physics, 2004, 31: 333-340]

During our 4DCT simulations, patients are immobilized with a T-bar handgrip, wing boards, and vacuum immobilization devices (Medical Solutions, Kalona, Indiana) in order to minimize inconsistency in patient setup. Each scan will be acquired using 50 cm field-of-view (FOV) with 2.5mm slice spacing. After the 4DCT simulation, extent of tumor motion can be measured (i.e. centroid motion of tumor mass) and based on the contours of GTV at individual phases, motion encompassing target volume (i.e. IGTV and ITV) can be defined. For patients exhibiting motion greater than 1cm, motion mitigating technique can be recommended based on assessment of 4DCT. Furthermore, in order to compensate for the breathing motion during dose calculation step, an averaged CT image set is derived by summing images of each phases of 4DCT. Because the averaged CT partially contains geometrical information of every phase, dose calculation based on this blurred image of patient anatomy can help mitigate dosimetric error caused by breathing motion (Admiraal, Schuring et al. 2008).

Deformable Image Registration for contour propagation

The purpose of specific aim I is to track tumor shrinkage throughout the treatment course using weekly 4DCT. Manual contouring is not feasible by the physicians in terms of labor cost and efficiency. Moreover, each patient receives 5 – 8 weekly 4DCT data sets, so it is a time-consuming process to delineate contours on every single week. Therefore, we are going to use a technique named deformable image registration that can automate this process efficiently. Deformable image registration is a technique of registering two images through spatial mapping of

corresponding locations using computer algorithm (Cachier and Pennec 2000). It allows two objects to be different in terms of size, orientation, and shape be deformed with respect to each other in two different images. The application of deformable image registration to radiation oncology has been extended to but not limited to auto segmentation of patient anatomy, contour propagation, and dose accumulation (Brock, McShan et al. 2003; Liang and Yan 2003). In this thesis work, we use deformable image registration to propagate contours to different sets of images. For example, contours at any given phase of 4DCT will be propagated to different phases of 4DCT. Also, the contours drawn on the simulation 4DCT will be propagated to the weekly 4DCTs. All of deformable image registration algorithms establish deformation vector field that contains displacement vector of corresponding points in 3D space. Figure 1.5 illustrates the concept of deformable image registration.

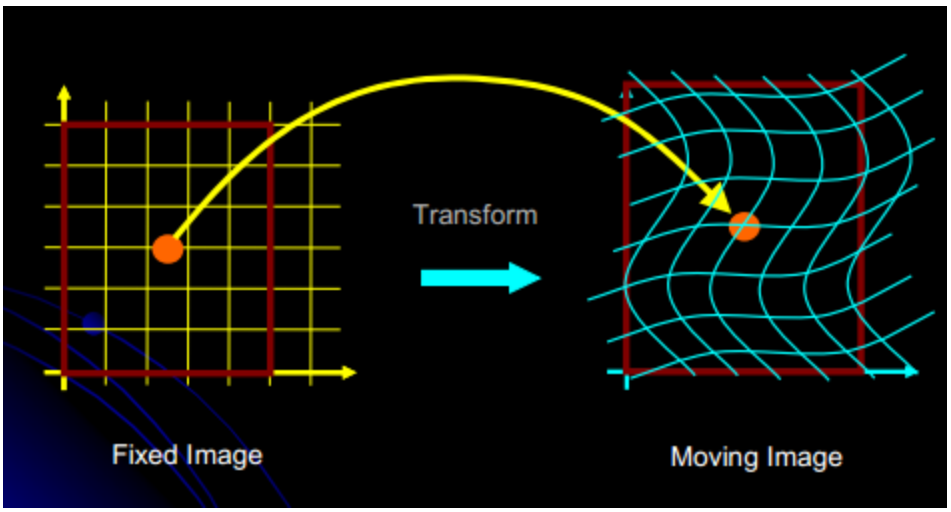

Figure 1.5 Illustration of deformable image registration between two images: Two points (orange dot) in different images are spatially correlated under the transformation that deforms fixed image to moving image under "assumed" action force. (Courtesy of Dr. Lei Dong, M.D. Anderson Cancer Center, Houston, TX)

In this thesis work, we employ an in-house developed deformable image registration software called CT-Assisted Targeting for Radiation Therapy (CAT) that uses 'demons' algorithm. In demons' algorithm, every pixel on the reference image is assumed to be under action force (i.e. local 'demon' is assumed to apply 'invisible' force) that moves pixel to the location given by the moving image (i.e. target image). The computer software seeks to solve this demon's force at every pixel by employing optical flow formula as follow:

---

where is the gradient of static image and is the internal force originating from the static image. The term is the differential force of the interaction between the static and moving images where m and s are the CT numbers (Thirion 1998; Wang, Dong et al. 2005) .The detail of how above optical flow solution is actually solved in computer is beyond the scope of a master's thesis but can be found in Wang's paper (Wang, Dong et al. 2005). Demons algorithm is based on the assumption that the corresponding pair of points on different images share the same image intensity values (i.e. gray scale value on CT images) thus the accuracy of registration relies heavily on similarity of intensity histogram of the images (Wang, Dong et al. 2005). In this thesis, all of deformable image registrations are performed to register CT to CT images (i.e. same modality) of the identical patients (i.e. phase to phase or week to week registration) and therefore the image intensity histograms of both target and reference images are assumed to be well-matched. Moreover, before deformable (non-rigid) image registration is perform, rigid registration is performed first by align two images

into the same location using bony structures (Wang, Dong et al. 2005). The accurate validation of any deformable image registration is difficult because the ground truth in real clinical problem is difficult to establish. However, limited scope of validation study by using mathematical or physical phantoms, as well as human assessment can be performed to boost the confidence in the registration algorithm in clinical setting. Previously, Wang *et al.* showed the validation of the demons' algorithm as implemented in the CAT software by applying mathematical transformation to real patient images and also on the physically deformable phantom (Wang, Dong et al. 2005). The result of their study provided an estimate of 2 mm accuracy to our current deformable image registration software.

Deformable Image Registration for Dose Accumulation

As mentioned in the previous section, deformable image registration produces deformation vector field which contains spatial relationship between two corresponding points on different sets of images. Not only this information can be used to propagate contours but also it can be used to combine dose values given to any tissue element on different sets of CT images. Because dose distribution is calculated based on the input CT images, the dose distribution is necessarily associated only with the anatomy given by that CT image. Thus, when a new dose distribution is calculated on a different CT image set (i.e. different phase of 4DCT or weekly 4DCT), one cannot simply add the two dose distributions in space coordinate to obtain accumulated dose. Rather, spatial location of a tissue element must be followed from one CT images set to another CT

images using deformation vector fields to accumulate dose to that element (Brock, McShan et al. 2003). Notice that for this thesis, in order to compare the planned dose vs. delivered dose, we chose T50 of 4DCT simulation as our reference. Although we can choose any other phase as our reference phase, T50 is chosen since it already has contours on it and it is the most stable phase as mentioned before. The application of deformable image registration for dose accumulation has been used in adaptive radiotherapy (Schaly, Kempe et al. 2004). However, it should be noted that dose accumulation via deformable image registration is not well established in clinical setting due to the difficulty of interpretation of such result. Unlike contour propagation, dose accumulation is more complicated by the fact that the "deformed" dose distribution is much harder to visually assess its accuracy compare to the propagated contour because dose distribution does not necessarily needs to conform to well-defined, visually detectable boundary of anatomy or tissues (Bender, Hardcastle et al.) Currently, active research is underway to develop accurate method of accessing accumulated dose through deformable image registration. For example, recently published work by Yeo *et al* showed that the accuracy of dose accumulation can be measured using a full 3D physically deformable gel dosimeter phantom (Yeo, Taylor et al.). In their study, they were able to deliver dose to the radiosensitive gel phantom before and after physical deformation and compared the 'measured' dose distribution against 'calculated' accumulated dose distribution using many commercially available deformable image registration software. In their study, they showed the accuracy of accumulated dose calculated using 'demons' based deformable image registration to be up to 34% using 3% dose and 3mm distance gamma criterion: 34% of the phantom's

measure accumulated dose were agreement with calculated dose within 3mm and 3%. However, it should be noted that their study is limited to the use of homogenous gel phantom whereas real patient anatomy is more heterogeneous and therefore the deformation introduced to the gel phantom may not mimic the realistic deformation that can occur inside the patient including disappearing of tissues and organ swelling.

1.3 Statement of the Problem

The goal of this thesis work is to improve cancer treatment for patients undergoing NSCLC radiation therapy. We can achieve this goal by questioning our current techniques. The first question is whether or not the difference in the uncertainties associated with both modalities would cause a difference in tumor shrinkage. It is a well-known fact that there are numerous uncertainties associated with our inability to deliver the intended dose to a target (Paganetti et al. 2012). A few major contributors are setup uncertainty, internal motion, changes in patient anatomy, and inaccuracies in imaging and simulation data. Previously, researchers reported that some of these uncertainties can result in greater effects for protons than photons 2011(Engelsman, DeLaney et al. ; Unkelbach, Chan et al. 2007; Lomax 2008; Lomax 2008). In particular, range uncertainties in proton therapy, primarily due to the error in estimated stopping powers of patient anatomy and the uncertainty in estimated relative biological effectiveness (RBE), are unique to proton therapy (Moyers, Sardesai et al.2010 ; Yang, Zhu et al. ; Paganetti, Niemierko et al. 2002). This noted difference leads to the question of whether or not the intended prescription dose to the tumor is

being delivered for both modalities. If there is indeed a significant difference in delivered dose between the two modalities, then we might be able to see the difference in terms of tumor shrinkage. The second question is how much difference is there between the delivered dose and planned dose for both modalities and how changes in patient anatomy will affect the delivered dose distribution. Changes in anatomy can cause changes in the dose distribution, which can be more significant for proton therapy than IMRT (Zhang, Dong et al. 2007; Albertini, Bolsi et al. 2008; Hui, Zhang et al. 2008). However, there are subtle differences in the treatment planning process for both modalities, such as different margins and different techniques involved in accounting for the uncertainties, which is hard to judge the sensitivity without direct assessment of the delivered dose. For the purpose of this thesis, from now on, we will refer delivered dose as "5D" dose such that 5D dose is the cumulative dose distribution from all 10 phases and from all available weekly 4DCT data sets for one patient.

1.4 Hypothesis and Specific Aims

1.4.1 Hypotheses

Hypothesis 1: We hypothesized that there is a statistically significant difference in tumor shrinkage between lung cancer patients treated with IMRT and those treated with PSPT.

Hypothesis 2: We hypothesized that there is a statistically significant difference between planned and 5D dose in both IMRT and PSPT plans of the lung cancer patients.

1.4.2 Specific Aims

Specific Aim 1: To compare tumor shrinkage between Intensity Modulated Radiation Therapy (IMRT) and Passively Scattered Proton Therapy (PSPT) using weekly 4DCT and deformable image registration

Specific Aim 2: To establish a method of estimating the 5D dose of both IMRT and PSPT using weekly 4DCT and deformable image registration and to perform a pilot study of comparing planned dose to 5D dose for both modalities

Chapter 2

Comparison of Tumor Shrinkage in IMRT and PSPT of Lung Cancer

*Specific Aim I: To compare tumor shrinkage in Intensity Modulated Radiation Therapy (IMRT) and Passively Scattered Proton Therapy (PSPT) using weekly 4DCT and deformable image registration**

*****This study was presented at 2011 Joint AAPM/COMP meeting as a short oral presentation.

2.1 Introduction

Patients who receive radiation therapy show significant change in tumor shape and volume as the tumor responses to radiation or concurrent chemotherapy (Barker, Garden et al. 2004; Hansen, Bucci et al. 2006; O'Daniel, Garden et al. 2007). As an effort to correctly identify treatment response, a treatment response criterion called Response Evaluation Criteria in Solid Tumors (RECIST) was introduced by the European Organization for Research and Treatment of Cancer (EORTC) and National Cancer Institutes of the United States and Canada (Therasse *et al* 2000). According to RECIST, tumor shrinkage is considered a standard measure of therapy response. In RECIST, it is recommended that the size of lesions (i.e. sum of the longest diameter of all lesions) should be calculated and reported. Based on the evaluation of tumor size, it provides response criteria ranging from complete response (i.e. disappearance of all lesions), partial response (i.e. at least 30% decrease), stable disease (i.e. no significant

change), and progressive disease (i.e. at least 20% increase). With the innovation and improvement of computed tomography (CT), it is now a routine practice to use CT to measure tumor volume at the simulation and to track tumor shrinkage throughout the treatment course if repeated CT is available. Currently, there is a randomized clinical trial of intensity-modulated radiotherapy (IMRT) vs. passively scattered proton therapy (PSPT) for non-small cell lung cancer patients (NSCLC) at M.D. Anderson Cancer Center. The details of this randomized trial were discussed in chapter 1. Although the end goal of this randomized clinical trial is to cross-compare the clinical outcome in long term survival rate of the patients who were treated either with IMRT or PSPT, understanding the tumor shrinkage in both modalities can provide us with immediate assessment of therapy response.

In the design of this randomized clinical trial, it was assumed that the same prescription dose, 74 Gy, was delivered to the clinical target volume (CTV) of patients treated with IMRT and PSPT. However, there are uncertainties in the beam delivery process such that the CTV coverage shown in the nominal plan (i.e. plan at the time of simulation) may not be what was actually delivered. It has been argued before, that there are unique aspects of proton therapy which makes it more sensitive to the error caused by patient setup, internal motion, anatomical deformation, and range uncertainty (Lomax 2008; Lomax 2008). If our ability to deliver the prescribed dose to the CTV is worse in PSPT than IMRT, we would expect to see the difference in tumor shrinkage in patients treated with PSPT.

Another unique uncertainty in proton therapy is the relative biological effectiveness (RBE). Previously, researchers have found a wide range of RBE values

both in vivo and in vitro studies using protons (Gerweck and Kozin 1999; Paganetti, Niemierko et al. 2002). It is now believed that the true RBE value can vary for different linear energy transfer (LET), dose, and tissue type (Wilkens and Oelfke 2004; Chen and Ahmad 2012). However, the true RBE is difficult to determine in practice as it requires a map of LET which in turn requires a Monte-Carlo simulation that is difficult and time consuming for practical purpose (Wilkens and Oelfke 2004). Furthermore, even after the LET distribution is known, matching the correct RBE values that varies for different tissue types is still a challenge (Paganetti, Niemierko et al. 2002). For these reasons, most proton therapy centers including M. D. Anderson Cancer Center have adopted a constant RBE value of 1.1 for prescribing and reporting proton dose (Paganetti, Niemierko et al. 2002). If this assumption of the RBE value for PSPT is significantly off, then we would expect to see a difference in tumor shrinkage caused by the difference in the magnitude of tumor response when compare with IMRT patients.

In summary, the main goal of the specific aim 1 is to compare the tumor shrinkage in non-small cell lung cancer patients who underwent randomized clinical trial between two different treatment modalities (protons vs. photons). It gives a unique opportunity to assess tumor response to proton or photon therapy because patients are randomized to receive the same dose prescription.

2.2 Methods and Materials

2.2.1 Patient Selection

A total of 45 patients (25 IMRT and 20 PSPT patients) who had completed their treatment courses were included in our analysis. Patients with an initial tumor size less than 5 cc were excluded from this study due to limitation of in-house deformable image registration, CT-Assisted Targeting For Radiation Therapy - CAT$^{V3.0}$. Our power analysis revealed that in order to detect 10% difference in tumor shrinkage between the two modalities with desired power of 0.8 and under the assumption that the data is normally distributed with standard deviation of 10% would require 16 samples from each group. The patients included in this study were the subset of the patient population who were enrolled in the NIH P01 randomized clinical trial between IMRT and PSPT with concurrent chemotherapy. So far, this on-going clinical trial has accrued 150 locally advanced NSCLC patients (stage II-IIIb) who were randomized to receive either photon (IMRT) or proton (PSPT) therapy. The details of the randomized trial were discussed in chapter 1 and only a short description that is relevant to this chapter is given here. The protocol includes several dose levels (74Gy, 66Gy, and 60Gy) as shown in figure 2.1. The primary objective was to deliver 74 Gy to CTV but if the adequate target coverage levels are not met at the highest dose level (74 Gy), then the next lower dose level (66Gy or 60 Gy) is assigned. If both IMRT and PSPT plans meet the criteria for adequate target coverage level which is defined as the 95% of planning target volume (PTV) receiving 74 Gy to CTV and if the mean lung dose is less than 22Gy and V20 is less than 40%, then patients are randomly assigned to either IMRT or PSPT.

For our study, only patients who were randomized to the 74 Gy dose level (i.e. 2 Gy per fraction, a total of 37 fractions) were selected.

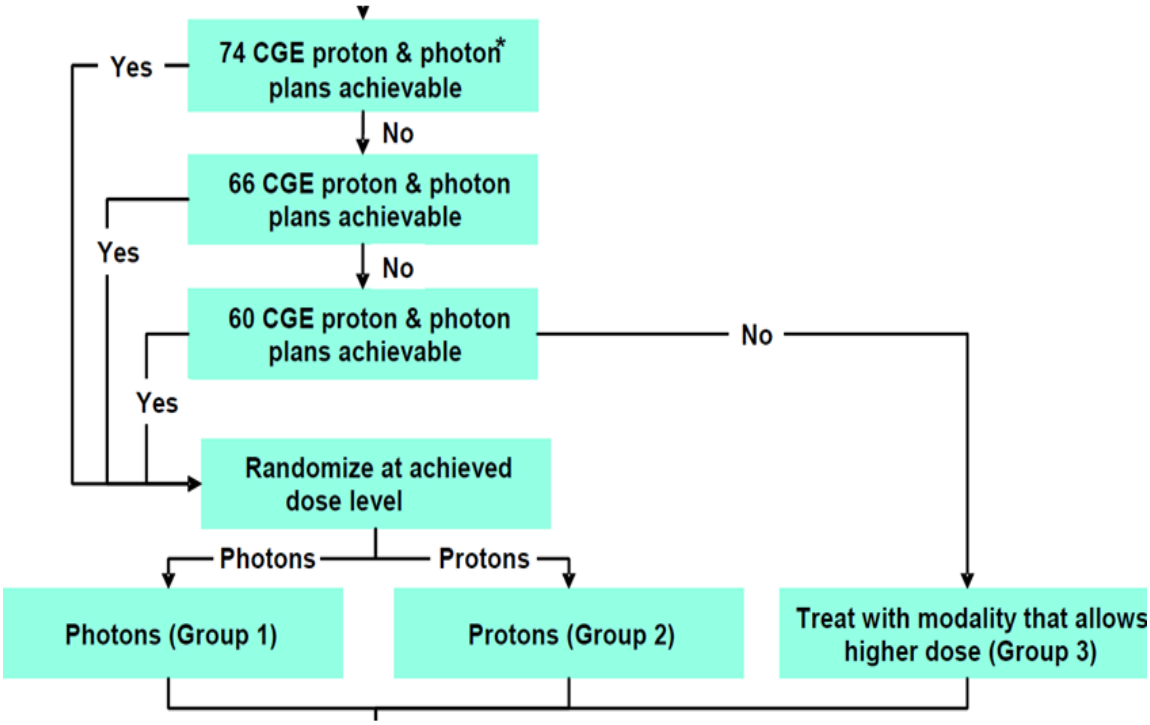

Figure 2.1 Three different dose levels for the lung protocol. At first, for all candidate patients, a treatment plan is designed with intention of delivering 74 Gy to CTV while meeting the dose objectives for other organs at risk for each IMRT and PSPT. If either plan can't achieve 74 Gy to CTV without compromising the dose objectives, the prescription is lower to 66 Gy. If the dose objectives are still not met, it is further lower to 60 Gy. Once the appropriate dose level for CTV is determined, patient is randomized between IMRT and PSPT. In this study, only the patients who received 74 Gy were analyzed to reduce variability in patient population.

2.2.2 Contouring and Deformable Image Registration

Weekly four-dimension computed tomography (4DCT) images were acquired for all patients in this protocol. In order to measure tumor shrinkage, we kept track of the volume of primary gross tumor volume (GTVp) using weekly 4DCT data sets throughout the treatment course. Previous study showed that GTV was the most reliable parameter to predict disease control probability (Strongin, Yovino et al.). Initially, the GTVp was contoured by the board certified physicians on the end-of-expiration phase (T50) of the planning 4DCT data sets. All manual contours were performed using a Pinnacle^3 treatment planning system (Phillips Medical Systems, Andover, MA). However, re-contouring the GTVp on every weekly 4DCT posed great demand from clinical staffs. Therefore, we used the deformable image registration to propagate the original GTVp drawn by the physicians on the newly acquired weekly 4DCT data sets. First, the original planning CT images and contours were exported from Pinnacle^3 treatment planning system and imported into CT-Assisted Targeting For Radiation Therapy (CAT$^{V3.0}$) which is an in-house developed deformable image registration based on demons algorithms. The utility of this deformable image registration software were validated elsewhere (Wang, Dong et al. 2005) and the details of the deformable image registration were discussed in chapter 1. Then, the original GTVp from T50 of 4DCT simulation was deformed to T50 of all available weekly 4DCT data sets. The changes in volumes were measured and recorded for all weeks. Figure 2.2 shows the interface of CAT$^{V3.0.}$ software and the "Daily" windows show the newly acquired CT image set (i.e. T50 of weekly 4DCT) and the "Ref" window shows the original CT image set (i.e.

T50 of simulation 4DCT). The red box region is first defined in order to preselect area which deformable image registration should occur and the deformation vector fields are computed. Once the deformable image registration is completed, the newly generated contours were visually inspected to make sure there are no obvious discrepancies (e.g. contours were in the wrong region of interest or discontinuity in contours). Notice that I have generated every new contour myself. Finally, we compared the individual tumor shrinkage, group average tumor shrinkage, tumor volume at the end of treatment, week by week tumor shrinkage, and rate of volume change.

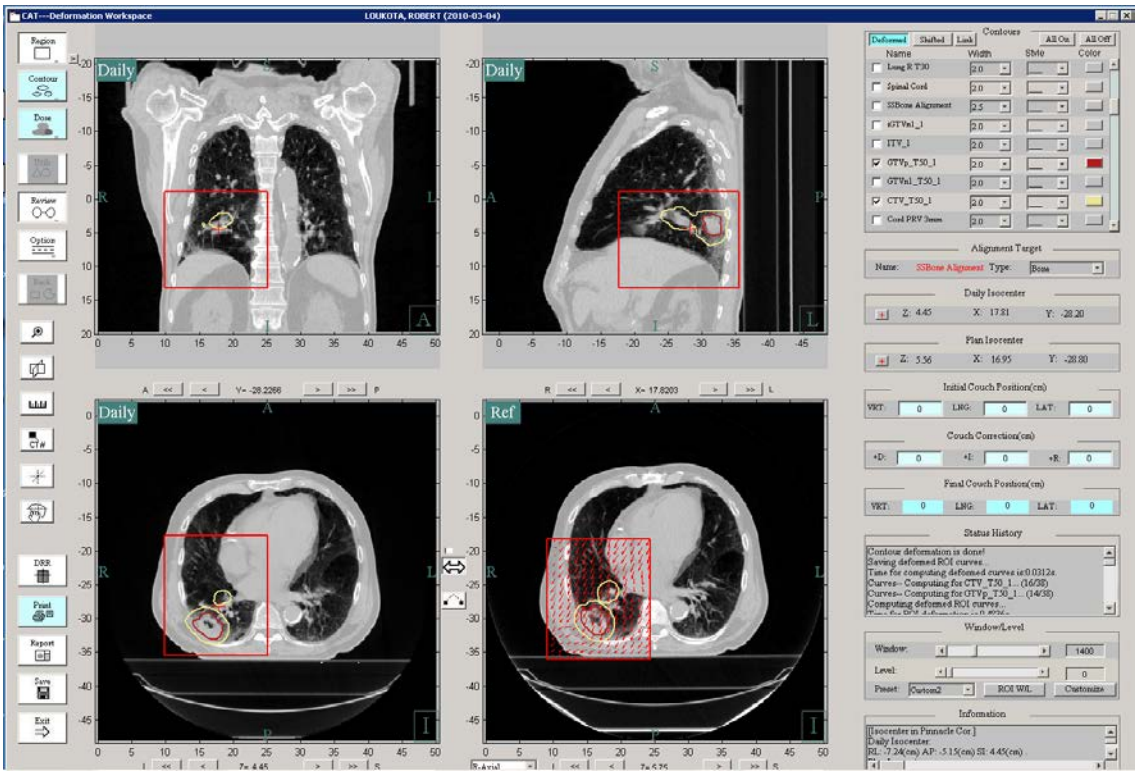

Figure 2.2 The graphical user interface of the CAT. In this user-friendly environment where both "Daily" and "Reference" images are cross compared. The red box region represents the pre-selected area where deformable image registration occurs. The newly deformed GTVp contours (bottom left) were visually assessed for its overall integrity by comparing it to the original contour (bottom right).

2.3 Results

Individual Tumor Shrinkage

The individual tumor shrinkage curves for all patients from each group are shown in figure 2.3. Each deformed volume was normalized to its initial volume measured at the first week CT data set. It should be noted that that the "Days after start of treatment (i.e. day 0)" to the time of weekly 4DCT scan date varies slightly among the patients; not all patients received weekly 4DCT scan on the same day of the week. The comprehensive data that includes the volume change of GTVp for all patients of all weeks are shown in table 2.1 and 2.2 . Out of 25 IMRT patients, 3 patients showed no sign of tumor shrinkage (i.e. greater or equal GTVp volume at the end of treatment course). For PSPT patients, 1 out of 20 patients showed no sign of tumor shrinkage.

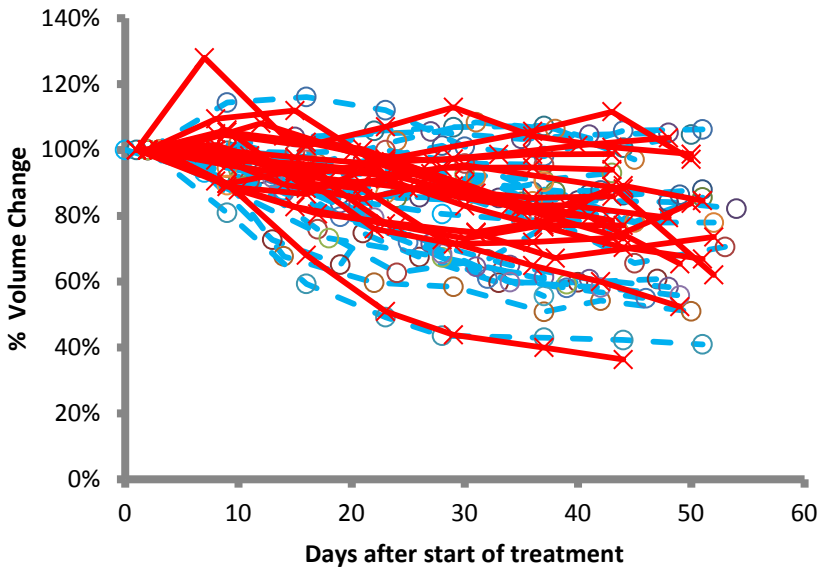

Figure 2.3 The GTVp volume change over elapsed treatment day for both IMRT (red) and PSPT (blue) patients

Table 2.1 The absolute and relative volumes of deformed GTVp of each week for IMRT patients. The weekly GTVp volumes were normalized to the GTVp volume at week 1.

	Week 1		Week 2		Week 3		Week 4		Week 5		Week 6		Week 7		Week 8	
Patient No.	[cc]	[%]	[cc]	[%]	[cc]	[%]	[cc]	[%]	[cc]	[%]	[cc]	[%]	[cc]	[%]	[cc]	[%]
1	14	100	14	100	13	93	13	93	12	87	12	86	12	88		
2	298	100	217	73	194	65	223	75	201	67	178	60	178	60	181	61
3	9	100	8	91	8	91	7	85	7	85	8	87	7	78	7	86
4	106	100	99	93	92	86	91	86	91	85	90	85	89	84	87	82
5	55	100	55	100	54	98	58	106	59	107	59	107	55	101	58	105
6	202	100	137	68	120	60	118	58	103	51	109	54	103	51		
7	10	100	9	93	10	97	10	101	9	87	9	88	9	86		
8	283	100	264	93	248	88	238	84	228	81	223	79	221	78		
9	18	100	18	104	19	106	18	103	18	105	18	105				
10	14	100	15	102	14	96	15	103	16	108	15	106	14	97		
11	40	100	46	114	47	116	45	112	41	101	40	98	43	106	43	106
12	30	100	27	91	23	76	19	63	20	67	24	78	20	66	21	71
13	53	100	50	94	50	93	50	94	49	93	48	91	50	93		

Table 2.1 Continued.

	Week 1		Week 2		Week 3		Week 4		Week 5		Week 6		Week 7		Week 8	
Patient No.	[cc]	[%]	[cc]	[%]	[cc]	[%]	[cc]	[%]	[cc]	[%]	[cc]	[%]	[cc]	[%]	[cc]	[%]
14	255	100	230	90	214	84	183	72	166	65	155	61	149	58		
15	520	100	421	81	309	59	256	49	227	44	224	43	220	42	213	41
16	54	100	51	95	48	89	47	87	49	92	45	84	42	78	42	78
17	197	100	183	93	157	80	142	72	120	61	115	58	108	55		
18	15	100	15	100	15	99	15	100	15	96	15	96				
19	146	100	107	73	98	67	86	59	94	65	95	65				
20	56	100	49	87	36	65	34	61	32	56						
21	64	100	57	89	36	56	30	47	32	49						
22	46	100	41	89	40	86	42	90	40	85	39	85				
23	32	100	31	97	30	94	26	80	25	77	24	76				
24	49	100	45	92	39	79	33	68	29	60	28	58	27	56		
25	63	100	64	101	58	91	58	92	59	93	57	90	55	87		

Table 2.2 The absolute and relative volume of deformed GTVp of each week for PSPT patients. The weekly GTVp volumes were normalized to the GTVp volume at week 1 because radiation treatment has started by then.

	Week 1		**Week 2**		**Week 3**		**Week 4**		**Week 5**		**Week 6**		**Week 7**		**Week 8**	
Patient No.	[cc]	[%]	[cc]	[%]	[cc]	[%]	[cc]	[%]	[cc]	[%]	[cc]	[%]	[cc]	[%]	[cc]	[%]
1	5	100	6	108	5	99	5	97	5	98	5	101	5	104		
2	13	100	13	99	12	90	11	85	12	89	11	83				
3	198	100	208	105	201	101	212	107	224	113	207	104	200	101	196	99
4	622	100	621	100	559	90	549	88	452	73	403	65	373	60	326	52
5	32	100	32	101	30	94	24	76	23	71	23	72	23	73	27	84
6	104	100	109	105	106	102	101	97	93	90	84	81	92	89	88	85
7	7	100	7	98	7	91	6	88	6	83	6	83	6	79		
8	150	100	136	91	124	83	115	77	113	75	119	79	134	89	93	62
9	582	100	564	97	559	96	545	94	511	88	498	85	500	86		
10	335	100	355	106	296	88	305	92	278	83	256	77	235	70	224	67
11	48	100	46	95	45	92	43	90	46	95	46	95	45	94		
12	184	100	179	98	176	96	179	97	181	99	181	99				

Table 2.2 Continued.

	Week 1		Week 2		Week 3		Week 4		Week 5		Week 6		Week 7		Week 8	
Patient No.	**[cc]**	**[%]**	**[cc]**	**[%]**	**[cc]**	**[%]**	**[cc]**	**[%]**	**[cc]**	**[%]**	**[cc]**	**[%]**	**[cc]**	**[%]**	**[cc]**	**[%]**
13	9	100	8	89	7	87	8	96	7	87	7	80	6	73		
14	41	100	40	99	38	94	37	92	39	95	36	88				
15	228	100	204	90	215	94	177	76	166	73	176	77	175	77		
16	64	100	70	109	72	112	62	96	68	106	72	112	62	97		
17	39	100	38	97	36	93	37	96	35	89	32	83	31	79		
18	152	100	195	128	158	104	152	100	141	93	124	81	121	80	99	65
19	149	100	131	88	120	81	111	75	100	67	110	74				
20	465	100	418	90	316	68	237	51	204	44	186	10	169	36		

Group Average Tumor Shrinkage

In order to minimize potential bias that can be introduced by daily time difference, we interpolated the weekly measured data given in table 2.1 and 2.2 to generate daily tumor shrinkage by using linear piece-wise interpolations between two consecutive weeks: in between two weekly measurements, we assigned daily progression of tumor volume change by fitting a line between the two end points (See Appendix A: Table A.1 and Table A.2). Figure 2.4 shows the mean change of GTVp for each group. The dashed lines representing the $\pm 1^{st}$ standard deviation of the average are also plotted to indicate the population variation.

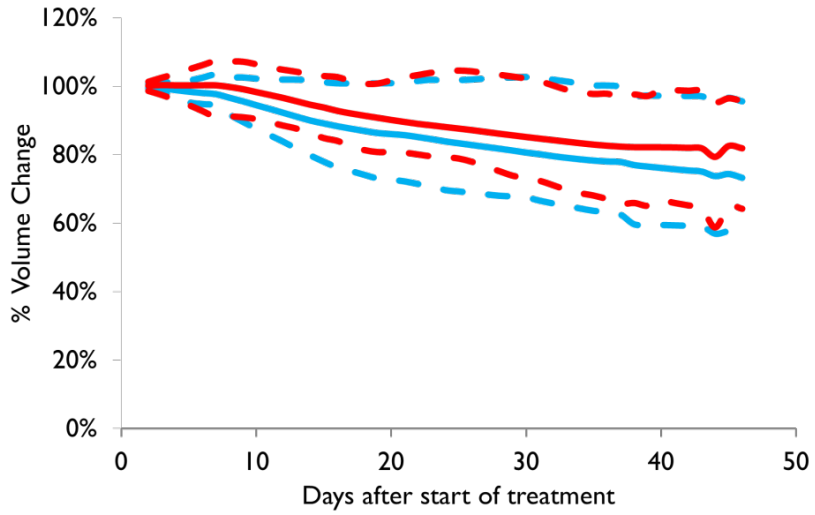

Figure 2.4 The population average of volume change of GTVp (solid line) and the standard deviation (dashed line) over elapsed treatment day for both IMRT (blue) and PSPT (red) patients is shown.

Comparison of Tumor Volume at the End of Treatment

Tumor volume at the end of treatment was used as the end point for this study to detect any clinical significant difference in tumor shrinkage between IMRT and PSPT. Table 2.3 shows the normalized GTVp volume and amount of shrinkage for all patients. Based on the tumor volume measured at the last 4DCT data sets, we found that on average, GTVp was reduced by 24% (19%) and 21% (17 %) for IMRT and PSPT respectively. The mean difference in tumor shrinkage between IMRT and PSPT was calculated to be 3% and its corresponding 95% confidence interval was calculated to be [-8%, 14%].

The distribution of the "end-of-study" tumor volume measurements are compared as box plots in figure 2.5. In order to determine if the observed difference in tumor shrinkage is statistically significant, we used the last recorded volume of GTVp for all patients from the two groups and performed the unpaired t-test with Welch's correction using the statistical package software R (GNU general public open source code). We found that there is no statistical difference in mean tumor shrinkage between the two arms (p-value $0.65 > 0.05$). In this study, our null hypothesis was that the mean tumor shrinkages between the two modalities are the same. According to this statistical test, based on our sampled means for two group (i.e. 24% and 21% for IMRT and PSPT respectively) and under the 95 % confidence interval, we cannot reject the null hypothesis, meaning that there is no evidence that the tumor shrinkage between the two groups is different.

Table 2.3 Tumor volumes measured at the last 4DCT for IMRT and PSPT patients

	IMRT patient No.	Normalized Volume*	Tumor Shrinkage	PSPT patient No.	Normalized Volume*	Tumor Shrinkage
	1	0.88	0.12	1	1.04	-0.04
	2	0.61	0.39	2	0.83	0.17
	3	0.86	0.14	3	0.99	0.01
	4	0.82	0.18	4	0.52	0.48
	5	1.05	-0.05	5	0.84	0.16
	6	0.51	0.49	6	0.85	0.15
	7	0.86	0.14	7	0.79	0.21
	8	0.78	0.22	8	0.62	0.38
	9	1.05	-0.05	9	0.86	0.14
	10	0.97	0.03	10	0.67	0.33
	11	1.06	-0.06	11	0.94	0.06
	12	0.71	0.29	12	0.99	0.01
	13	0.93	0.07	13	0.73	0.27
	14	0.58	0.42	14	0.88	0.12
	15	0.41	0.59	15	0.77	0.23
	16	0.78	0.22	16	0.97	0.03
	17	0.55	0.45	17	0.79	0.21
	18	0.96	0.04	18	0.65	0.35
	19	0.65	0.35	19	0.74	0.26
	20	0.56	0.44	20	0.36	0.64
	21	0.49	0.51			
	22	0.85	0.15			
	23	0.76	0.24			
	24	0.56	0.44			
	25	0.87	0.13			
mean			0.24			0.21
STD			0.19			0.17

*Normalized Volume = Volume divided by baseline volume

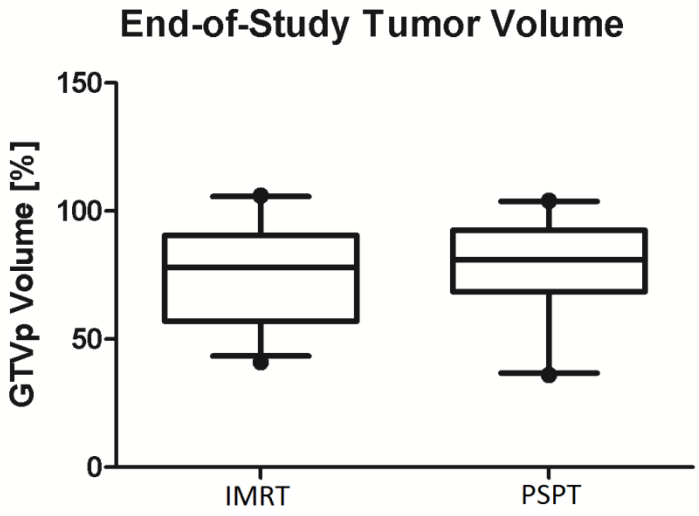

Figure 2.5 The boxplot comparison of tumor volume measured at the "end-of-study" between IMRT and PSPT. (The midline = mean, box = lower and upper quartile, and the outer lines = 10% and 90%)

Week by week Tumor shrinkage comparison between IMRT and PSPT

Since the last recording date of tumor volume was different for different patients, there may be a bias in comparing the "end-of-study" data points. We have performed the same statistical analysis based on the tumor shrinkage measured at the end of each week separately. The result of week by week tumor shrinkage comparison is summarized in table 2.4. Despite the fact that the mean tumor shrinkage of IMRT group was lower than PSPT group in all weekly comparisons, these differences were not statistically significant.

Table 2.4 Week by week Tumor shrinkage comparison between IMRT and PSPT

	Mean Difference (IMRT - PSPT)	**P-Value (Welch's t-test)**	**95% Confidence Intervals of the Mean Difference**
End of Week1	-2.5%	0.21	[-6.6%, 1.6%]
End of Week2	-4.2%	0.16	[-10.1%, 1.7%]
End of Week3	-3.6%	0.34	[-11.2%, 3.9%]
End of Week4	-3.9%	0.40	[-13.2%, 5.4%]
End of Week5	-4.0%	0.42	[-13.9%, 5.9%]
End of Week6	-5.9%	0.29	[-16.9%, 5.2%]
End of Week7	-1.9%	0.80	[-17.2%, 13.3%]

Rate of volume change for IMRT and PSPT patients

Another interesting factor of radiation therapy is the rate of volume change or how fast tumor responds to the radiation therapy. The rate of volume change was computed from the slope of observed data for each patient as shown in table 2.5 and 2.6 and negative values indicated tumors were getting smaller. Figure 2.6 shows the linear relationship between initial volume and the rate of volume change for both IMRT and PSPT patients. Red color represents IMRT patients and blue color represents PSPT patients. The slope is the same, 0.07, for both IMRT and PSPT patients.

Table 2.5 Rate of volume change for IMRT patients

Patient No.	Rate of volume change [cc/week]
1	-0.35
2	-12.89
3	-0.19
4	-2.20
5	0.44
6	-13.17
7	-0.21
8	-10.27
9	0.13
10	0.07
11	-0.31
12	-1.15
13	-0.53
14	-18.47
15	-40.94
16	-1.60
17	15.72
18	-0.15
19	-8.66
20	-6.36
21	-9.27
22	-1.31
23	-1.79
24	-3.81
25	-1.33

Table 2.6 Rate of volume change for PSPT patients

Patient No.	Rate of volume change [cc/week]
1	-0.006
2	-0.45
3	-0.35
4	-46.11
5	-1.22
6	-6.21
7	-0.26
8	-5.12
9	-15.28
10	-18.07
11	-0.30
12	-0.13
13	-0.30
14	-0.85
15	-9.37
16	-0.24
17	-1.34
18	-10.14
19	-8.51
20	-52.28

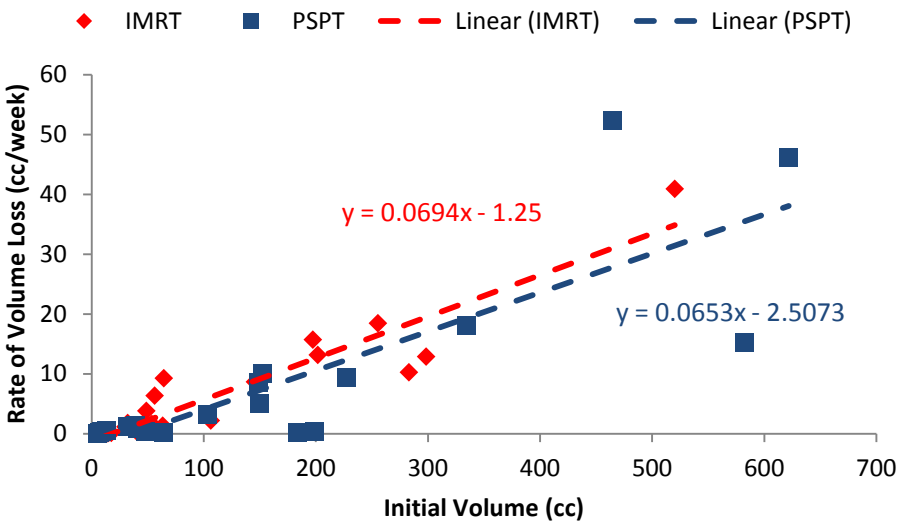

Figure 2.6 Linear regression fitted Lines for GTV of IMRT (red) and PSPT groups (blue).

2.4 Discussion

In this study, we analyzed gross tumor volume changes in patients who received IMRT and PSPT radiation therapy. The tumor volumes drawn by the physicians at the beginning of the radiation therapy were followed through using deformable image registration to propagate the original contour to the newly acquired weekly 4DCT images throughout the entire treatment course. Based on the mean difference in tumor shrinkage between IMRT and PSPT, 3%, along with the corresponding 95% confidence interval, [-8%, 14%], we can conclude that the tumor shrinkage is similar between two treatment modalities. Moreover, the result of this study showed that there is no statistically difference for both modalities indicating that the same prescription dose (74 Gy) is delivered to the target for both modalities regardless of associated uncertainties in beam delivery process. This could be an indication that our current treatment planning procedure for PSPT is at least as robust as the conventional IMRT. During our analysis of tumor shrinkage, it was noted that an important contributing factor in large tumor volume reduction was the initial volume of tumor as shown in figure 2.7. We found that the rate of volume change is highly correlated with the initial volumes as indicated by the Pearson correlation coefficient (Pearson correlation coefficient =0.94 and 0.86 for IMRT and PSPT respectively). It was observed that the larger the initial tumor volume, the faster the volume shrunk. The relationship between the rates of volume change vs. initial volume of tumor was the same for both IMRT and PSPT.

2.5 Conclusion

Majority of IMRT and PSPT patients showed tumor shrinkages as they responded to the radiation treatment. Despite the fundamental difference in photon and proton radiation therapy, we found no statistically significant difference in tumor shrinkage between lung cancer patients randomized to receive IMRT or PSPT to 74 Gy. The average tumor shrinkage for patients receiving IMRT and PSPT was similar.

Chapter 3

Comparison of Dose Distributions in IMRT and PSPT of Lung Cancer

Specific Aim II: To establish a method of estimating the 5D dose of both IMRT and PSPT plans using weekly 4DCT and deformable image registration and to perform a pilot study of comparing planned dose to 5D dose for both modalities

*This study was presented at 2012 AAPM Annual Meeting as a poster.

3.1 Introduction

Radiation therapy involves many steps such as treatment simulation, tumor delineation, treatment planning, patient setup, and finally, the delivery of the external radiation beam. Each of these steps comes with uncertainties that can influence the delivery of dose to a patient (Cho *et al.*, 2007; Lomax, 2008a, b; Zhu *et al.*, 2008; Zhang *et al.*, 2012; Yang *et al.*, 2012). Some of these uncertainties can be addressed during the treatment planning process and their impacts on the anticipated delivered dose can be assessed before the treatment begins. For example, in IMRT, patient set up error can be accounted by using a planning target volume (PTV) which is an expansion of clinical target volume (CTV) with margins corresponding to the expected errors. In another word, PTV includes areas larger than the disease sites that will be irradiated. In passively scattered proton therapy (PSPT), both patient set up and range uncertainty

have been accounted for during the treatment planning process by use of beam-specific hardware such as the lateral expansion of the aperture or block and smearing of the compensator (Moyers *et al.*, 2001; Engelsman and Kooy, 2005). In order to evaluate the potential dosimetric error to the target and organs at risk (OAR), the dose-volume parameters can be assessed. However, the uncertainties related to changing in patient anatomy are inherently difficult to account for and assess at the time of treatment planning process. For example, both inter-fractional and intra-fractional changes in patient anatomy during the course of treatment are extremely difficult to predict. During the course of radiation treatment, a patient can lose weight leading to unwanted effects on the delivered dose (Albertini *et al.*, 2008). Also, as a patient responds to radiation therapy, tumor shape and size, along with other parts of anatomy can change significantly and degrade the planned dose distribution in a patient (Wang *et al.*, 2011; Hui *et al.*, 2008). Furthermore, radiotherapy involving either thoracic or gastrointestinal sites, breathing motion of the patient is another factor contributing to the change in patient anatomy (Engelsman and Kooy, 2005; Kang *et al.*, 2007). In order to mitigate the change in patient anatomy, adaptive re-planning during radiation treatment is necessary (Schwarz, 2011; Zhang *et al.*, 2011; Schwartz, 2012). Previously, researchers have shown that the change in patient anatomy during the course of treatment can significantly degrade planned dose distribution in IMRT (Hurkmans *et al.*, 2012; Jensen *et al.*, 2012; Ahn *et al.*, 2011; Nishimura *et al.*, 2011). It can be argued that with the plans that offer more conformal dose distributions, it is more difficult to deliver the planned dose without adaptive re-planning because it is harder to contain the tumor volume within a smaller volume of irradiation. Proton therapy has

been shown to be more conformal than IMRT in certain clinical cases (Lee *et al.*, 2007; Chang *et al.*, 2006; Mohan *et al.*, 2010) which could pose a greater risk. Furthermore, in proton therapy, beam range is heavily dependent on the tissue density along its beam path which makes proton therapy especially error-prone when dealing with changes in patient anatomy (Engelsman and Kooy, 2004). The ability of proton therapy to deliver dose to a pre-determined depth in a patient and deliver no dose beyond the depth can actually cause the beam to either over-shoot or under-shoot depending on the change in tissue density (see Figure 3.1). Although IMRT plan can undergo a small perturbation in dose distribution as a result of change in anatomy, the magnitude of such change is significantly less than that can be caused in proton therapy.

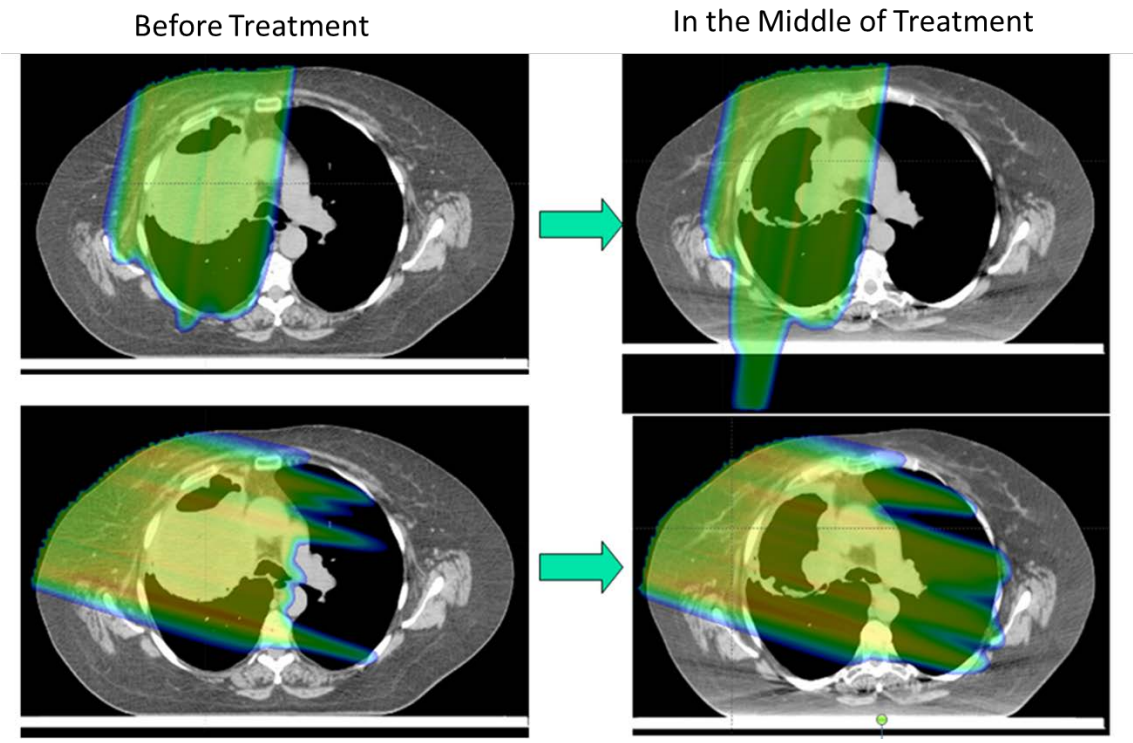

Figure 3. 1 Comparison of lung treatment plan and its dose distribution before treatment (left column) and in the middle of treatment (right column). The original tumor volume has shrunk significantly, and the protons penetrate further into the lower density lung volume. The deteriorated dose distribution overshoots further than original planned dose thereby increasing dose to both lung and heart tissue (courtesy of Lei Dong, M.D. Anderson Cancer Center, Houston, TX).

Figure 3.2 shows the perturbation of a dose distribution due to the breathing motion of a patient for both IMRT and proton therapy. Different isodose levels remain in the same position for IMRT but change significantly for proton therapy primarily due to the motion of liver (i.e. indicated with black arrow in the Figure 3.2). For example, 35 Gy isodose level (orange line) remains the same for IMRT but it moves 2 cm for proton therapy due to the motion of liver. Delivered dose distribution can be different from the planned dose distribution and the magnitude of such differences can be more significant for proton therapy than IMRT which challenges many previous studies compared the two modalities by only looking at the planned dose distribution and ignoring the effect on changing in patient anatomy (Lee *et al.*, 2007; Berman *et al.*, 2008; Mohan *et al.*, 2010; Krengli *et al.*, 2006; Yeung *et al.*, 2006; Ingram *et al.*, 2007). In Chapter 2, we investigated the difference in tumor shrinkage from patients who underwent a randomized clinical trial between IMRT and PSPT, and found no significant difference between the two modalities in terms of tumor shrinkage. Following the result of our previous study, in this chapter our primary goal is to assess delivered dose to tumor and other critical structures while accounting for both changing in patient anatomy throughout the entire treatment course and breathing motion. To date, no previous study has compared the delivered dose between IMRT and PSPT which takes into account both inter- and intra-fractional change in anatomy for non-small cell lung cancer patients. In multi-fractionated radiotherapy, the delivered dose to a patient can be closely approximated by accumulating dose to a patient. However, due to the change in patient anatomy, accumulating dose remains as a challenge. In this chapter we showed a method of explicitly accumulating dose to a patient over different

breathing cycles as well as different treatment days by using repeat four-dimensional CT (4DCT) and deformable image registration. Although, such accumulated dose is not the same as the true delivered dose, it closely resembles the true dose when compared to the planned dose. Since the accumulated dose in this work incorporates both breathing motion and anatomy change, we referred it as “5D” dose. Based on the 5D dose, we assessed the delivered dose to the planned dose for the patients who were treated either with IMRT or proton therapy according to the NIH P01 randomized clinical trial discussed in Chapter 1.

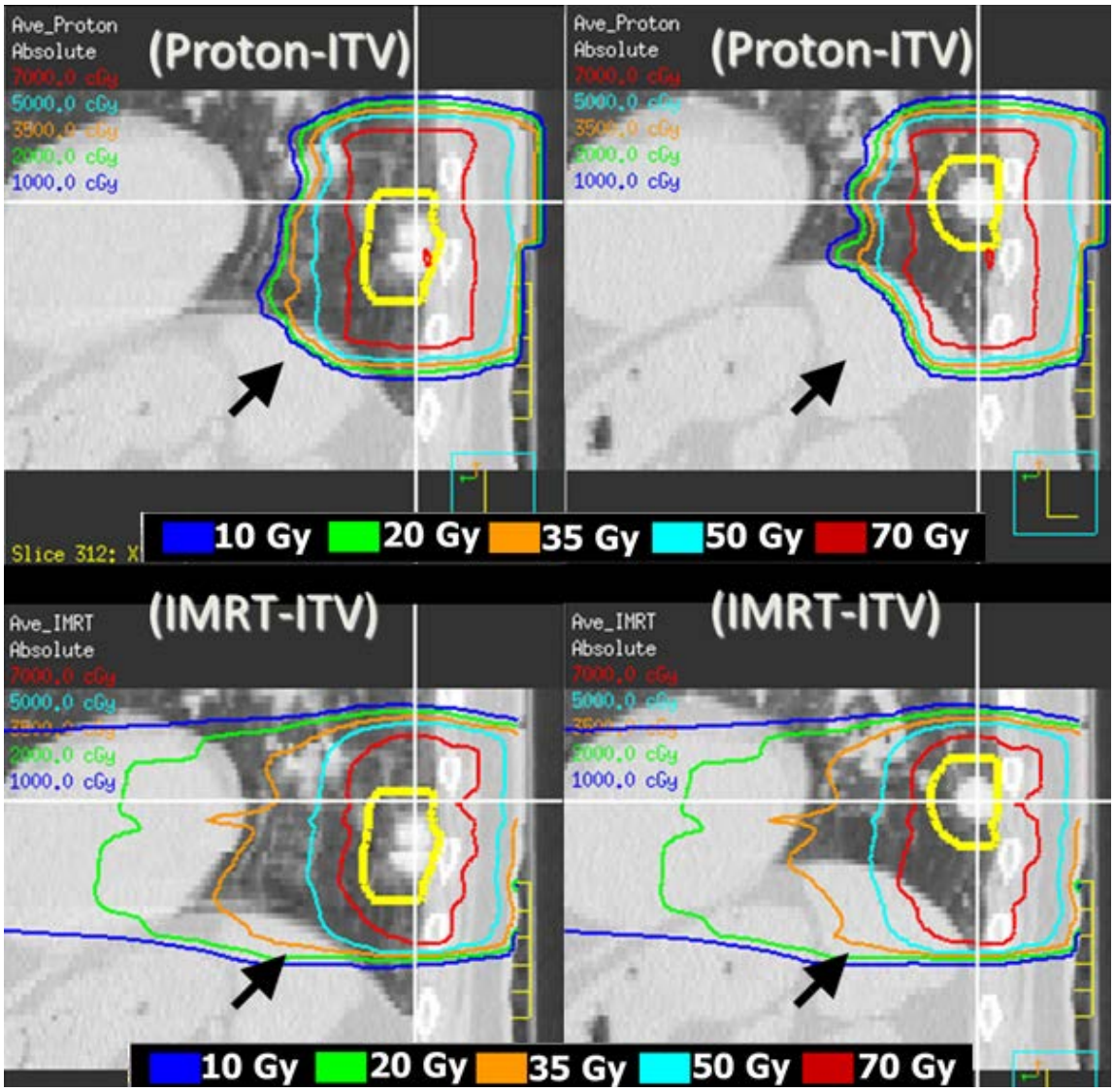

Figure 3.2 Comparison of dose distributions at inhale (right column) and exhale (left column) of breathing cycle for IMRT (bottom row) and proton therapy plan (top row). The arrow indicates region where a significant change in isodose level is shown for proton therapy and not for IMRT. (courtesy of Lei Dong, M.D. Anderson Cancer Center, Houston, TX).

3.2 Methods and Materials

An assessment of the 5D dose distribution to a lung cancer patient requires repeat 4DCT scans of the patient during the course of radiation therapy to track the breathing motion and change in patient anatomy. One 4DCT scan consists of 10 image data sets that are 3D images of one patient at different breathing cycle. The repeated 4DCT images sets can be aligned with respect to the specific respiratory phase of the planning CT images by deformable image registration. Deformable image registration is then used to accumulate dose distributions calculated from different CT images. The use of deformable image registration to establish voxel to voxel geo-spatial relationship between two different CT image sets for dose accumulation has been reported previously (Velec *et al.*, 2009; Lu *et al.*, 2006; Brock *et al.*, 2008; Janssens *et al.*, 2009). In this study, we used in-house developed deformable image registration software called CT-Assisted Targeting for Radiation Therapy - $CAT^{V3.0}$ that is based on the demon's algorithm (Wang *et al.*, 2005; Gao *et al.*, 2006; Wang *et al.*, 2006). A pilot study was designed to look at a group of 7 patients who represent the most typical patient population underwent the P01 randomized clinical trial for non-small cell lung cancer including two extreme cases. Patient number 2 has the largest tumor motion and patient number 7 has the largest initial tumor volume. Notice that these seven patients were chosen from specific aim I. Table 3.1 shows individual patient characteristics including age, sex, stage, histology, treatment modality, planning primary Gross Tumor Volume (GTVp), tumor motion, and tumor location. One tumor was located in the left upper lobe (LUL), two were in the right lower lobe (RLL), and four were in the right upper

lobe (RUL). The range of GTVp volume was between 13 – 622 cc. For each of these patients, physician approved IMRT plan and PSPT plans were designed using Pinnacle^3 (Philips Medical Systems, Andover, MA) and Eclipse^{TM} (Varian Medical System, Palo Alto, CA) respectively (see Figure B.1-B.14 from Appendix B). For each patient, both IMRT and PSPT plans were created to achieve dose objectives for different critical structures and approved for treatment. The plans were normalized to deliver 74Gy to 95% of the PTV with no hot spots greater than 110% of the prescription dose for more than 2cc volume. The detail description of the dose objectives used to create the treatment plans for both modalities was summarized in Table 1.1 of Chapter 1.

Table 3.1 Patient Characteristics used in this study

Patient #	**Sex**	**Age (y)**	**Stage**	**Histology**	**Treatment**	**Planning GTVp (T50) [cc]**	**Tumor Motion [mm]**	**Tumor Location**
1	M	68	IIIa	Squamous cell Carcinoma	PSPT	13	5.5	LUL
2	M	76	IIIa	Adenocarcinoma	PSPT	32	17	RLL
3	F	75	IIIb	Adenocarcinoma	IMRT	46	4.7	RUL
4	M	67	IIIa	Adenocarcinoma	IMRT	63	9	RLL
5*	M	63	III	Squamous cell Carcinoma	PSPT	149	3	RUL
6	F	74	IIIa	Carcinoma	IMRT	202	4	RUL
7¥	M	57	IIIb	Adenocarcinoma	PSPT	622	5.5	RUL

*Patient 5 had one adaptive replan.
¥Patient 7 had two adaptive replans.

Each of these patients received weekly 4DCT scans during their actual treatment course. These 4DCT data sets were backed up to our image archiving system and later imported into the Pinnacle and Eclipse treatment planning systems. Our 4DCT image sets consisted of 10 respiratory phases (T0 to T90). At all 10 phases, dose distributions were recalculated for all available weekly 4DCT data sets using Pinnacle and Eclipse treatment planning systems for IMRT and PSPT plans respectively. The number of weekly 4DCT sets received by patients ranged from 5 to 8 weekly 4DCT data sets for all patients. Therefore, for each patient, between 60 to 90 dose calculations were performed for both IMRT plans and PSPT plans including accumulating planned dose distribution. After the dose calculations were done, for each weekly 4DCT, the dose distributions calculated for the 10 different respiratory phases were deformed to the maximum exhale phase (T50) using the CAT software. The process of acquiring deformed vector fields that were later used to map dose started with rigid alignment of the two CT images sets based on the bony structures to establish a baseline prior to deformable image registration. Once the deformed vector fields were obtained, the newly calculated dose points associated with each of these voxels are mapped to the T50 phase of the same week except patient number 5 and 6 whose dose points are mapped directly to the T50 of planning 4DCT data sets. In order to inspect the result of deformable image registration, at least one contour which is typically a gross tumor volume (GTV) was visually assessed for any irregularities in contours and in deformed vector fields before and after the deformable image registration. These deformed doses from individual phases were summed with equal weight to represent the breathing time-resolved, 4D dose of the patient for that particular week represented on the T50 phase.

Next, the 4D doses calculated on all weekly 4DCT image sets were deformed to the T50 phase of the planning 4DCT image set. Again, these deformed doses were summed with equal weight. In this way, the 5D dose that are accumulated over all breathing phases and all weekly 4DCT image sets were represented as the single dose distribution overlaid on the top of the T50 phases of the planning CT for direct comparison with the planned dose distribution. Figure 3.3 illustrates the process of accumulating dose in this study. The 5D dose, which is a close approximation of the delivered dose, was compared to the planned dose using dose-volume histograms (DVHs). The planning parameters such as target coverage and dose limits to critical structures were compared to check if any significant deviation occurred.

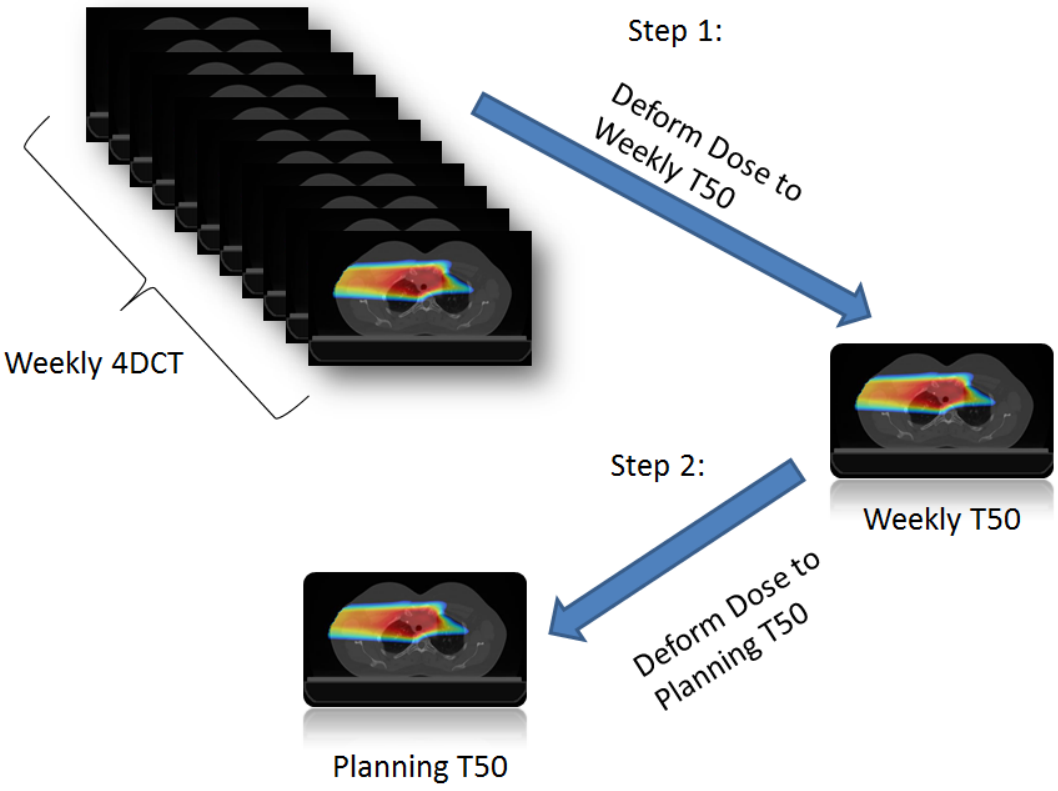

Figure 3.3 Process of dose accumulation. First, to obtain accumulated dose over the breathing cycle, dose calculations were performed on all 10 phases of weekly 4DCT scans. These dose distributions were mapped onto the T50 phases of CT images set. The cumulated dose at T50 of weekly 4DCT was deformed again to the T50 of planning 4DCT image set. This process was repeated for all available weekly 4DCT image sets.

3.3 Results

The differences between the 5D dose and the planned dose in terms of the dose coverage to target volume and dose objectives of the critical structures were compared for both IMRT and PSPT plans. Between 60 to 100 individual dose calculations were performed for each patient. Then, the accumulated dose distributions to T50 phase of the planning CT image were compared with the planned dose distribution calculated on the T50 phase of the planning CT image. For every patient, 5D dose distribution was visually inspected against the planned dose distribution for any unusual deviation introduced by human error while importing or exporting the data. The original planned dose distributions are shown in Appendix B for both IMRT and PSPT plans in 3 different views (axial, sagittal, and coronal) followed by the dose-volume histogram (DVH) comparisons between 5D dose and planned dose for target volume and critical structures for all patients. Below sections show results for target volume and critical structures in details.

CTV

Initial target coverage under the planned dose distribution was similar between IMRT and PSPT plans for all our patients, with less than 1% average difference of CTV V74Gy criteria indicating that our plans for both arms were designed according to our target coverage criteria. When comparing the CTV V74Gy of the planned dose distribution with the 5D dose distribution, we found that the original CTV V74Gy coverage was maintained in 5 out 7 patients for IMRT plans, and 6 out of 7 patients for PSPT plans. Patient No. 2 and 7 showed -2% and -7% decreases in CTV V74Gy in IMRT plan, respectively. But for PSPT plans, only the patient No. 7 showed -9% decreases (See figure 3.4).

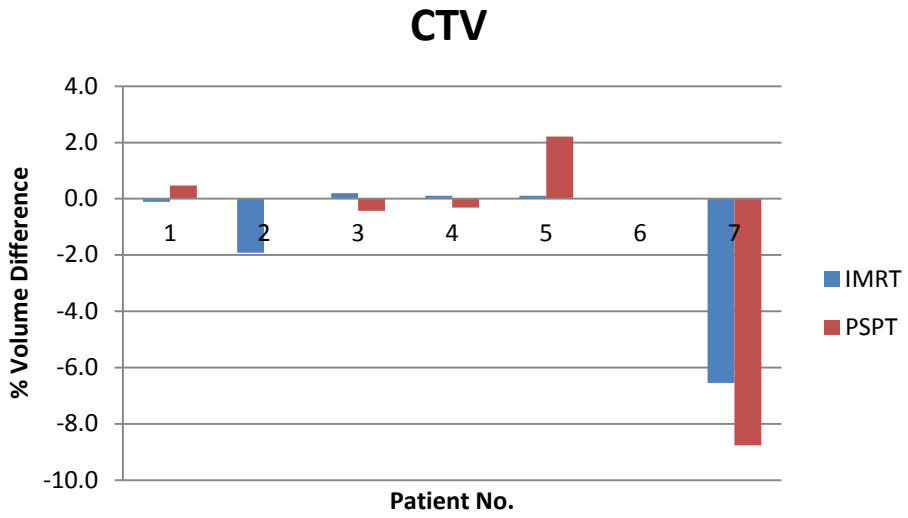

Figure 3.4 The difference of CTV receiving 74Gy between 5D and planned dose distributions for all patients for both IMRT (blue or left column) and PSPT (red or right column) plans.

Lung

For all dose objectives related to the total lung, (i.e. V5, V10, V20, Mean Lung Dose or MLD), we observed that the 5D doses were slightly larger than or equal to the planned doses for IMRT plans. Similarly, for PSPT plans the 5D doses were larger for most of the patients except for patient No. 7 who showed 47cGy reduction in MLD. Figure 3.5 shows the results related to the total lung dose objectives. The largest increase was observed for V5 and was 5% for IMRT plans, and 6% for PSPT plans.

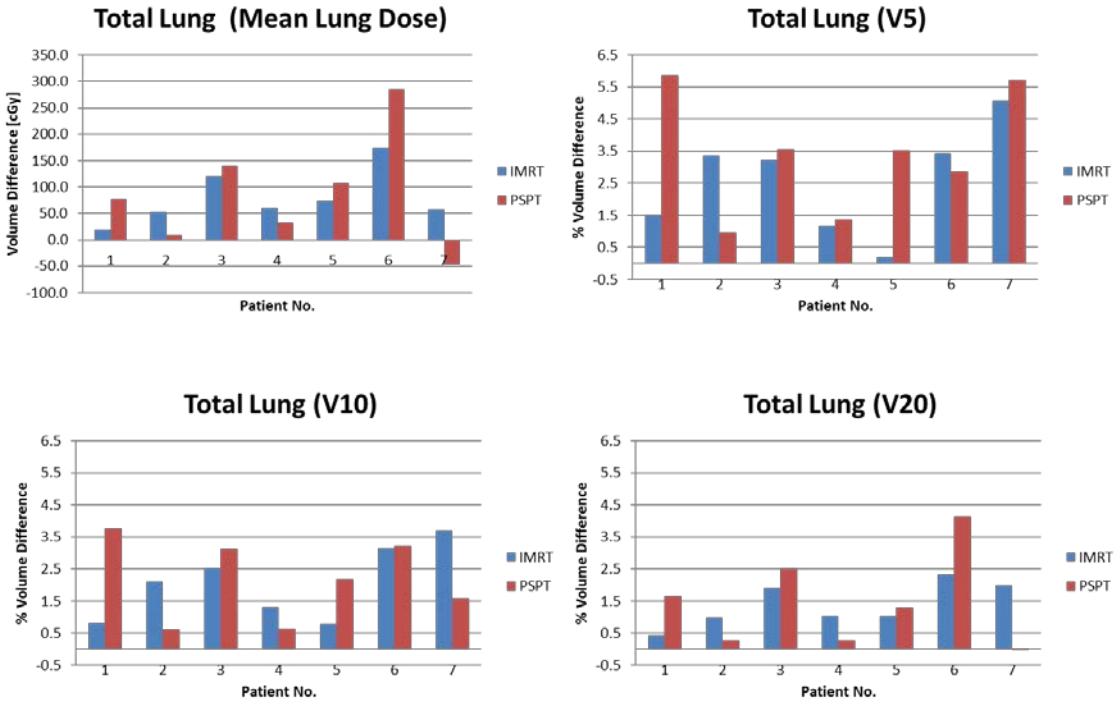

Figure 3.5 The difference of total lung receiving mean lung dose, 5Gy, 10Gy, and 20Gy between 5D and planned dose distributions for all patients for both IMRT (blue or left column) and PSPT (red or right column) plans.

Esophagus

For the esophagus V55 objective, 1 out of 7 patients showed greater than 3% increases for the IMRT plan, while for the PSPT plan, 1 out of 7 patients showed greater than 3% increases and patient NO. 1 showed a -1% decrease (see figure 3.6).

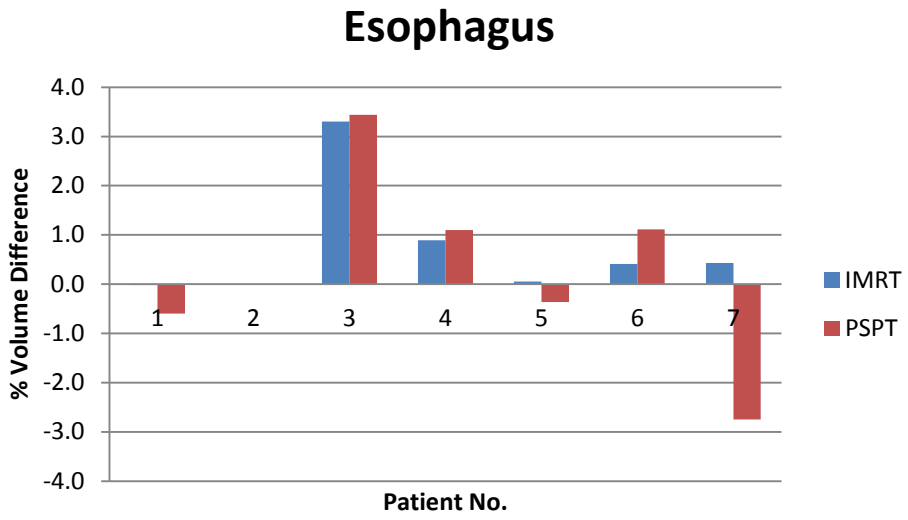

Figure 3.6 The difference of esophagus receiving 55Gy between 5D and planned dose distributions for all patients for both IMRT (blue or left column) and PSPT (red or right column) plans.

Heart

For the heart V45 dose objective, only a slight difference between the planned and 5D doses were observed for all patients (within 1% difference) except patient No. 7, who showed up to a 3% and 4% difference for IMRT and PSPT plans, respectively. Similarly, for the mean heart dose, except for patient No. 7, all differences were less than 200cGy (see figure 3.7).

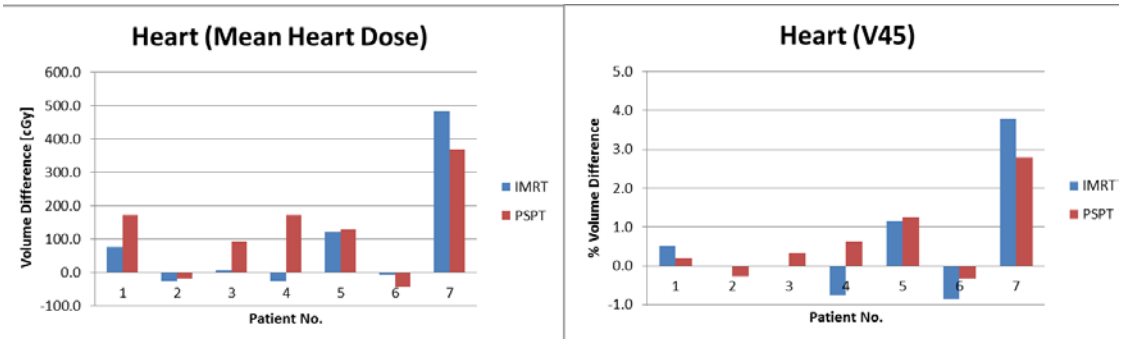

Figure 3.7 The difference of heart receiving mean heart dose and 40Gy between 5D and planned dose distributions for all patients for both IMRT (blue or left column) and PSPT (red or right column) plans.

Spinal Cord

For the maximum spinal cord dose objective, only one out of 7 patients indicated that the 5D dose was less than the planned dose for the IMRT plan, while 4 out of 7 patients indicated that the 5D dose was less than the planned dose for the PSPT plan. However, in all cases, the increased maximum cord dose calculated under the 5D dose distributions were still below our 50Gy criteria (see figure 3.8).

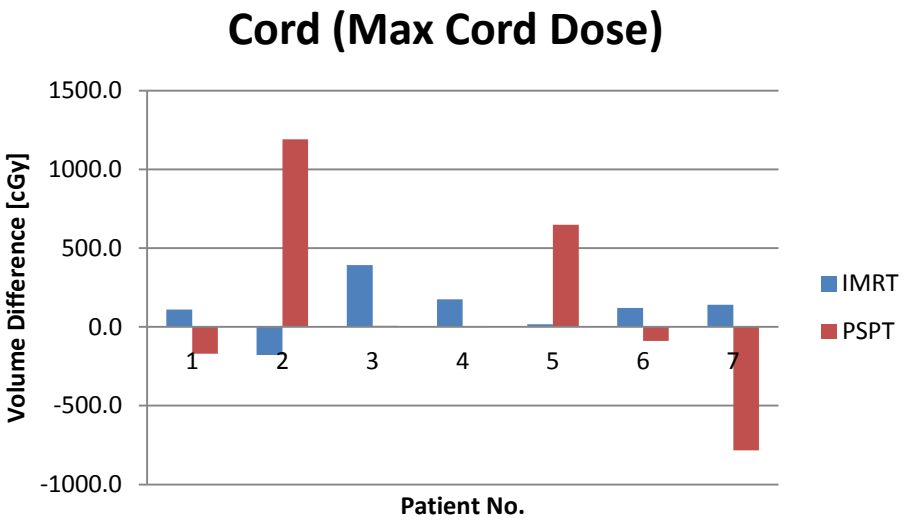

Figure 3.8 The difference of max dose of spinal cord for all patients for both IMRT (blue or left column) and PSPT (red or right column) plans.

3.4 Discussion

In this study, we established a method of estimating the 5D dose of both IMRT and PSPT plans using weekly 4DCT data sets and deformable image registration. The 5D dose closely approximates delivered dose by accumulating dose distributions calculated at every respiratory phase of weekly 4DCT data sets to account for both patient breathing motion and the change in anatomy during the course of treatment. For all 7 patients considered in this study, the 5D dose was very close to the planned dose except with patient No. 7. The average difference in CTV 74Gy coverage between 5D and planned dose was -1.7% and -1.3% for IMRT and PSPT respectively. For the patient No. 7, the difference in CTV 74GY coverage was -7 % and -9 % for IMRT and PSPT respectively. It is interesting to note that the patient No. 7 had the largest GTV volume at the time of treatment simulation (622 cc) and lost 52% of its initial volume over the course treatment. The greater difference in CTV coverage for this patient could be attributed to the huge reduction of GTV volume during the course of treatment that freed up more lung volume thereby changing tissue density along the beam path. During the time of simulation, significant portion of GTV volume and surrounding area were considered to be soft tissue. However, during the course of treatment, density surrounding the tumor becomes lower than the soft tissue as tumor shrinks thereby degrading the planned dose distribution.

Noticed that in this study, we did not separate patient groups by the modalities used for actual treatment because we were interested to find out, for a selected patient, if both IMRT and PSPT plans were given, how the 5D dose as calculated by utilizing weekly 4DCT compared to the planned dose. It should be noted that the weekly 4DCT

is taken during a course of treatment that was randomized to either IMRT or proton therapy. Therefore, there might be a bias introduced in our hypothetical treatment study: using the weekly 4DCT associated with one particular modality to study both arms. But from the result of Chapter 2 (Specific Aim I), we showed that there is no significant difference in terms of tumor shrinkage between IMRT and proton therapy patients. Therefore, we can assume that the tumor shrinkage is the same between the two treatment arms for specific aim II. The 5D dose is only an approximation to the true delivered dose because we ignore the other types of errors such as patient setup error and range error into our calculation. However, in general, these errors are considered during the treatment planning process in terms of target margin (i.e. for IMRT plan) or by shaping beam-specific hardware such as aperture and compensator (i.e. for PSPT plan) and therefore do not significantly degrade the target coverage or plan quality when compared to the error caused by anatomical deformation. However, due to the difficulty in predicting anatomical deformation, both breathing motion and anatomy change are not usually accounted for during treatment planning process. Moreover, there is no conventional method of estimating dosimetric errors due to anatomy change in advance. Although breathing motion is partially accounted for during treatment planning process by incorporating internal target volume (ITV), patient breathing pattern can change during the course of treatment.

This pilot study was intended to estimate the difference between 5D dose and planned dose of both IMRT and PSPT plans but the result of all our 7 patients only showed a mean difference of 1% (shown in Table 3.2). Moreover, if we assumed patient No. 7 to be an outlier, then the mean difference between 5D dose and planned

dose of both IMRT and PSPT plans is even smaller as shown in Table 3.3. The mean difference has changed from 1.1 to 0.3 for IMRT and 1.0 to -0.3 for PSPT if we exclude patient No. 7. Based on the narrow range of 95% confidence level shown below for both IMRT and PSPT, we can conclude that the difference between 5D dose and planned dose of both IMRT and PSPT are consistently small. Similarly, for the critical structures, the difference between the 5D dose and planned dose were in the clinically acceptable range for all patients including patient No. 7. Such small difference between the 5D dose and planned dose observed in our study indicates that the anticipated concerns of dosimetric errors caused by anatomical change during the course of treatment might have been over estimated especially for those patients with small initial tumor volume. The reason for such small difference in terms of CTV coverage can be attributed to the generous treatment margins during the treatment planning process. Although, the treatment margins are not directly design to account for the anatomical change, in our analysis, they are proven to be effective against the change in anatomy as well. However, when it comes to estimate the true 5D dose, we should include patient setup errors along with the anatomical deformation that could potentially cause the dosimetric difference than what was observed in this study. The scope of this study was limited that it did not incorporate setup errors associated with proton beam range for PSPT plans. A more comprehensive method of computing the 5D dose under the influence of both setup and range error is warranted for the future study.

Table 3.2 Mean, SD, and CI for both IMRT and PSPT CTV V74 for all 7 patients

Patient No.	IMRT CTV V74			PSPT CTV V74		
	Planned	5D	Planned-5D	Planned	5D	Planned-5D
1	100	100	0	99	99	0
2	100	98	2	100	100	0
3	98	98	0	97	97	0
4	100	100	0	98	98	0
5	100	100	0	97	99	-2
6	98	98	0	100	100	0
7	99	93	6	98	89	9
Mean			1.1			1.0
STD			2.3			3.6
95%CI			[-0.95,3.2]			[-2.3,4.3]

Table 3.3 Mean, SD, and CI for both IMRT and PSPT CTV V74 for all 6 patients

Patient No.	IMRT CTV V74			PSPT CTV V74		
	Planned	5D	Planned-5D	Planned	5D	Planned-5D
1	100	100	0	99	99	0
2	100	98	2	100	100	0
3	98	98	0	97	97	0
4	100	100	0	98	98	0
5	100	100	0	97	99	-2
6	98	98	0	100	100	0
Mean			0.3			-0.3
STD			0.8			0.8
95%CI			[-0.5,1.2]			[-1.2,0.5]

3.5 Conclusion

In this study, we established the method of estimating the 5D dose of both IMRT and PSPT plans using weekly 4DCT data sets and deformable image registration. In addition, we compared this 5D dose to the original planned dose to assess the effect of both breathing motion and the change in patient anatomy over the course of treatment on the final dose distribution the patient receives. Furthermore, by applying the same technique to both the IMRT and the PSPT therapy plan of an individual patient, we compared the sensitivity of the 5D dose distribution to the planned dose between both IMRT and PSPT therapy. All of the patients studied in this chapter showed that the 5D dose distribution closely follows the planned dose distribution within the limits of initial dose objectives. That is, some changes in the 5D dose distributions that were observed were still within the limits of our plan criteria. With limited patient numbers studied so far, we could not reach a definite conclusion in terms of whether or not PSPT plan is more sensitive to the anatomical change.

Chapter 4

Conclusions

4.1 Conclusions of Hypothesis 1

Hypothesis 1: We hypothesized that there is a statistically significant difference in tumor shrinkage between lung cancer patients treated with IMRT and those treated with PSPT.

The motivation of our *Hypothesis 1* derives from the speculation that proton therapy is inherent more sensitive to anatomical change due to the finite range of proton beam that is highly dependent on tissue density. In chapter 2, we investigated the tumor shrinkage of 25 Intensity Modulated Radiation Therapy (IMRT) and 20 Passively Scattered Proton Therapy (PSPT) patients who were randomly assigned to receive either IMRT or PSPT for locally advanced non-small cell lung carcinoma. In both groups, 24% (19%) and 21% (17 %) of initial primary Gross Tumor Volume (GTVp) were reduced for IMRT and PSPT respectively. The 95% confidence interval for the mean difference in tumor shrinkage between the two arms was [-8%, 14%]. According to our statistical test (i.e. Welch's non-paired t-test) with the null hypothesis that the mean tumor shrinkages for both modalities are the same, we obtained p-value = 0.65. This result suggests that we cannot reject the null hypothesis. Therefore, we

concluded that there is no statistical difference in mean tumor shrinkage between IMRT and PSPT patients. The clinical interpretation of this result can be that the overall therapy responses in terms of tumor shrinkage between the two modalities were similar and this is a positive result since our clinically intended goal was to deliver same prescription dose to both groups of patients. Although it is true that the proton beam is more sensitive to the tissue density change caused by the anatomical variation from breathing motion and tumor shrinkage, the original plan design method (i.e. beam shaping strategy and treatment margin) is vastly different between the two modalities and some of the uncertainties that are more pronounced in proton beam is being taken into special account during design of proton radiation therapy planning.

4.2 Conclusions of Hypothesis 2

Hypothesis 2: We hypothesized that there is a statistically significant difference between planned and 5D dose in both IMRT and PSPT plans of the lung cancer patients.

The motivation of our *Hypothesis 2* was similar to that of *Hypothesis 1*. In chapter 3, we established a method of estimating the 5D dose of both IMRT and PSPT plans using weekly 4DCT and the in-house developed deformable image registration software, CAT. Moreover, we performed a pilot study of comparing planned dose to 5D dose for both modalities using 7 patients selected from the randomized clinical trial. Unlike our previous study in chapter two which separates the patients by the chosen treatment modality, this study assumed that each patient received both IMRT and PSPT treatments at the same time. This assumption is valid since the conclusion from chapter two has showed us that the tumor shrinkage between IMRT and PSPT patients is similar. In order to approximate the 5D dose to a patient, individual dose was re-calculated on all 10 phases of weekly 4DCT data sets separately and then deformed to the T50 (end of exhale) phase of the same week. Finally, dose distributions from each week were all deformed to the T50 phase of the planning 4DCT data sets for direct comparison with the planned accumulated dose. In this study, for all 7 patients, the mean difference between the 5D dose and planned dose of both IMRT and PSPT plans was only 1% for the target volume. Based on the 95% confidence interval, [-0.95%,

3.2%] and [-2.3%, 4.3%] for IMRT and PSPT respectively, we can conclude that the difference between 5D dose and planned dose of both IMRT and PSPT are consistently small. However, with small number of patient sample size, we could not reach a conclusion if PSPT plan is more sensitive to the anatomical change than IMRT plan.

APPENDIX A:

Table A.1 It represents individual patient versus elapsed treatment days for primary GTV of IMRT patients. Linear interpolation was applied between two consecutive 4DCT weeks in order to interpret the result between them.

Patient no./ Days	**1**	**2**	**3**	**4**	**5**	**6**	**7**	**8**	**9**	**10**	**11**	**12**	**13**	**14**	**15**	**16**	**17**	**18**	**19**	**20**	**21**	**22**	**23**	**24**	**25**
0								1.0																	
1					1.0			1.0																	
2	1.0				1.0			1.0			1.0		1.0		1.0	1.0		1.0	1.0						
3	1.0		1.0		1.0			1.0		1.0	1.0	1.0	1.0		1.0	1.0		1.0	1.0			1.0			
4	1.0		1.0		1.0			1.0		1.0	1.0	1.0	1.0		0.9	1.0	1.0	1.0	1.0			1.0			
5	1.0	1.0	1.0	1.0	1.0			1.0		1.0	1.1	1.0	1.0		0.9	1.0	1.0	1.0	0.9			1.0			
6	1.0	1.0	1.0	1.0	1.0		1.0	0.9	1.0	1.0	1.1	1.0	1.0	1.0	0.9	1.0	1.0	1.0	0.9			0.9	1.0		
7	1.0	0.9	0.9	1.0	1.0	1.0	1.0	0.9	1.0	1.0	1.1	1.0	1.0	1.0	0.9	1.0	1.0	1.0	0.9	1.0	1.0	0.9	1.0	1.0	
8	1.0	0.9	0.9	1.0	1.0	1.0	1.0	0.9	1.0	1.0	1.1	0.9	1.0	1.0	0.8	1.0	1.0	1.0	0.9	1.0	1.0	0.9	1.0	1.0	1.0
9	1.0	0.9	0.9	1.0	1.0	0.9	1.0	0.9	1.0	1.0	1.1	0.9	0.9	1.0	0.8	0.9	1.0	1.0	0.9	1.0	1.0	0.9	1.0	1.0	1.0
10	1.0	0.8	0.9	0.9	1.0	0.9	1.0	0.9	1.0	1.0	1.1	0.9	0.9	1.0	0.8	0.9	1.0	1.0	0.9	0.9	1.0	0.9	1.0	1.0	1.0
11	1.0	0.8	0.9	0.9	1.0	0.8	1.0	0.9	1.0	1.0	1.1	0.9	0.9	0.9	0.7	0.9	0.9	1.0	0.8	0.9	0.9	0.9	1.0	0.9	1.0
12	1.0	0.8	0.9	0.9	1.0	0.8	0.9	0.9	1.0	1.0	1.2	0.9	0.9	0.9	0.7	0.9	0.9	1.0	0.8	0.9	0.9	0.9	1.0	0.9	1.0
13	1.0	0.7	0.9	0.9	1.0	0.7	0.9	0.9	1.0	1.0	1.2	0.9	0.9	0.9	0.7	0.9	0.9	1.0	0.8	0.9	0.9	0.9	1.0	0.9	1.0
14	0.9	0.7	0.9	0.9	1.0	0.7	0.9	0.9	1.0	1.0	1.2	0.8	0.9	0.9	0.7	0.9	0.9	1.0	0.8	0.9	0.9	0.9	1.0	0.9	1.0
15	0.9	0.7	0.9	0.9	1.0	0.7	0.9	0.9	1.0	1.0	1.2	0.8	0.9	0.9	0.6	0.9	0.9	1.0	0.8	0.9	0.9	0.9	1.0	0.9	1.0
16	0.9	0.7	0.9	0.9	1.0	0.7	0.9	0.9	1.0	1.0	1.2	0.8	0.9	0.9	0.6	0.9	0.9	1.0	0.8	0.8	0.9	0.9	1.0	0.9	1.0
17	0.9	0.7	0.9	0.9	1.0	0.6	0.9	0.9	1.0	1.0	1.2	0.8	0.9	0.9	0.6	0.9	0.8	1.0	0.7	0.8	0.9	0.9	1.0	0.9	1.0

Table A.1 Continued.

Patient no./ Days	1	2	3	4	5	6	7	8	9	10	11	12	13	14	15	16	17	18	19	20	21	22	23	24	25
18	0.9	0.7	0.9	0.9	1.0	0.6	0.9	0.9	1.0	1.0	1.1	0.7	0.9	0.9	0.6	0.9	0.8	1.0	0.7	0.8	0.8	0.9	1.0	0.8	1.0
19	0.9	0.7	0.9	0.9	1.0	0.6	1.0	0.9	1.0	1.0	1.1	0.7	0.9	0.8	0.6	0.9	0.8	1.0	0.7	0.8	0.8	0.9	1.0	0.8	1.0
20	0.9	0.7	0.9	0.9	1.0	0.6	1.0	0.8	1.0	1.0	1.1	0.7	0.9	0.8	0.5	0.9	0.8	1.0	0.7	0.8	0.8	0.9	1.0	0.8	0.9
21	0.9	0.7	0.9	0.9	1.0	0.6	1.0	0.8	1.0	1.0	1.1	0.7	0.9	0.8	0.5	0.9	0.8	1.0	0.7	0.8	0.8	0.9	0.9	0.8	0.9
22	0.9	0.7	0.9	0.9	1.1	0.6	1.0	0.8	1.0	1.0	1.1	0.7	0.9	0.8	0.5	0.9	0.8	1.0	0.7	0.8	0.8	0.9	0.9	0.8	0.9
23	0.9	0.7	0.9	0.9	1.1	0.6	1.0	0.8	1.1	1.0	1.1	0.6	0.9	0.8	0.5	0.9	0.7	1.0	0.7	0.8	0.8	0.9	0.9	0.8	0.9
24	0.9	0.7	0.9	0.9	1.1	0.6	1.0	0.8	1.1	1.0	1.1	0.6	0.9	0.8	0.5	0.9	0.7	1.0	0.7	0.7	0.8	0.9	0.9	0.8	0.9
25	0.9	0.7	0.9	0.9	1.1	0.6	1.0	0.8	1.1	1.0	1.1	0.6	0.9	0.7	0.5	0.9	0.7	1.0	0.7	0.7	0.7	0.9	0.9	0.7	0.9
26	0.9	0.7	0.9	0.9	1.1	0.6	1.0	0.8	1.1	1.0	1.1	0.6	0.9	0.7	0.5	0.9	0.7	1.0	0.7	0.7	0.7	0.9	0.9	0.7	0.9
27	0.9	0.7	0.9	0.9	1.1	0.6	1.0	0.8	1.1	1.1	1.1	0.6	0.9	0.7	0.4	0.9	0.7	1.0	0.7	0.7	0.7	0.9	0.9	0.7	0.9
28	0.9	0.7	0.9	0.9	1.1	0.6	1.0	0.8	1.1	1.1	1.0	0.6	0.9	0.7	0.4	0.9	0.7	1.0	0.7	0.7	0.7	0.9	0.9	0.7	0.9
29	0.9	0.6	0.8	0.9	1.1	0.6	1.0	0.8	1.1	1.1	1.0	0.7	0.9	0.7	0.4	0.9	0.7	1.0	0.7	0.7	0.7	0.9	0.9	0.7	0.9
30	0.9	0.6	0.8	0.9	1.1	0.6	1.0	0.8	1.0	1.1	1.0	0.7	0.9	0.7	0.4	0.9	0.6	1.0	0.7	0.7	0.7	0.9	0.9	0.7	0.9
31	0.9	0.6	0.8	0.9	1.1	0.6	1.0	0.8	1.0	1.1	1.0	0.7	0.9	0.7	0.4	0.9	0.6	1.0	0.7	0.6	0.6	0.9	0.8	0.6	0.9
32	0.9	0.6	0.8	0.9	1.1	0.6	0.9	0.8	1.0	1.1	1.0	0.7	0.9	0.7	0.4	0.9	0.6	1.0	0.6	0.6	0.6	0.9	0.8	0.6	0.9
33	0.9	0.6	0.8	0.9	1.1	0.5	0.9	0.8	1.0	1.1	1.0	0.7	0.9	0.7	0.4	0.9	0.6	1.0	0.6	0.6	0.6	0.9	0.8	0.6	0.9
34	0.9	0.6	0.8	0.9	1.1	0.5	0.9	0.8	1.0	1.1	1.0	0.7	0.9	0.7	0.4	0.9	0.6	1.0	0.6	0.6	0.6	0.9	0.8	0.6	0.9
35	0.9	0.6	0.8	0.9	1.1	0.5	0.9	0.8	1.0	1.1	1.0	0.7	0.9	0.6	0.4	0.9	0.6	1.0	0.6	0.6	0.6	0.9	0.8	0.6	0.9
36	0.9	0.6	0.9	0.9	1.1	0.5	0.9	0.8	1.0	1.1	1.0	0.7	0.9	0.6	0.4	0.8	0.6	1.0	0.6	0.6	0.6	0.9	0.8	0.6	0.9
37	0.9	0.6	0.9	0.8	1.1	0.5	0.9	0.8	1.0	1.1	1.0	0.8	0.9	0.6	0.4	0.8	0.6	1.0	0.6	0.6	0.6	0.9	0.8	0.6	0.9
38	0.9	0.6	0.9	0.8	1.1	0.5	0.9	0.8	1.0	1.1	1.0	0.8	0.9	0.6	0.4	0.8	0.6		0.6	0.6	0.5	0.9	0.8	0.6	0.9
39	0.9	0.6	0.9	0.8	1.1	0.5	0.9	0.8	1.0	1.1	1.0	0.8	0.9	0.6	0.4	0.8	0.6		0.6	0.6	0.5	0.9	0.8	0.6	0.9
40	0.9	0.6	0.8	0.8	1.0	0.5	0.9	0.8	1.0	1.0	1.0	0.7	0.9	0.6	0.4	0.8	0.6		0.6	0.6	0.5	0.9	0.8	0.6	0.9

Table A.1 Continued.

Patient no./ Days	1	2	3	4	5	6	7	8	9	10	11	12	13	14	15	16	17	18	19	20	21	22	23	24	25
41	0.9	0.6	0.8	0.8	1.0	0.5	0.9	0.8	1.0	1.0	1.0	0.7	0.9	0.6	0.4	0.8	0.6		0.6	0.6	0.5	0.9	0.8	0.6	0.9
42	0.9	0.6	0.8	0.8	1.0	0.5	0.9	0.8	1.0	1.0	1.0	0.7	0.9	0.6	0.4	0.8	0.6		0.6	0.6	0.5	0.9	0.8	0.6	0.9
43	0.9	0.6	0.8	0.8	1.0	0.5	0.9	0.8	1.0	1.0	1.0	0.7	0.9	0.6	0.4	0.8	0.6		0.6	0.6	0.5	0.9	0.8	0.6	0.9

Table A.2 It represents individual patient versus elapsed treatment days for primary GTV of PSPT patients. Linear interpolation was applied between two consecutive treatments in order to interpret the result between them.

Patient no./ Days	1	2	3	4	5	6	7	8	9	10	11	12	13	14	15	16	17	18	19	20
0																				
1						1.0			1.0	1.0									1.0	
2		1.0		1.0	1.0	1.0	1.0		1.0	1.0	1.0	1.0			1.0	1.0	1.0		1.0	
3		1.0		1.0	1.0	1.0	1.0		1.0	1.0	1.0	1.0		1.0	1.0	1.0	1.0	1.0	1.0	1.0
4	1.0	1.0		1.0	1.0	1.0	1.0	1.0	1.0	1.0	1.0	1.0		1.0	1.0	1.0	1.0	1.0	1.0	1.0
5	1.0	1.0		1.0	1.0	1.0	1.0	1.0	0.9	1.0	1.0	1.0		1.0	1.0	1.0	1.0	1.0	1.0	1.0
6	1.0	1.0		1.0	1.0	1.0	1.0	1.0	0.9	1.0	1.0	1.0		0.9	1.0	0.9	1.0	1.0	1.1	1.0
7	1.0	1.0	1.0	1.0	1.0	1.0	1.0	0.9	1.0	1.0	1.0		0.9	1.0	0.9	1.1	1.0	1.3	0.9	0.9
8	1.0	1.0	1.0	1.0	1.0	1.0	1.0	0.9	1.0	1.1	1.0	1.0	0.9	1.0	0.9	1.1	1.0	1.2	0.9	0.9
9	1.1	1.0	1.0	1.0	1.0	1.1	1.0	0.9	1.0	1.1	1.0	1.0	0.9	1.0	0.9	1.1	1.0	1.2	0.9	0.9
10	1.1	1.0	1.0	1.0	1.0	1.1	1.0	0.9	1.0	1.0	0.9	1.0	0.9	1.0	0.9	1.1	1.0	1.2	0.9	0.9
11	1.1	0.9	1.0	1.0	1.0	1.0	1.0	0.9	1.0	1.0	0.9	1.0	0.9	1.0	0.9	1.1	1.0	1.1	0.9	0.8
12	1.1	0.9	1.0	1.0	1.0	1.0	1.0	0.9	1.0	1.0	0.9	1.0	0.9	1.0	0.9	1.1	1.0	1.1	0.9	0.8
13	1.1	0.9	1.0	0.9	1.0	1.0	1.0	0.8	1.0	1.0	0.9	1.0	0.9	1.0	0.9	1.1	1.0	1.1	0.8	0.8
14	1.1	0.9	1.0	0.9	0.9	1.0	1.0	0.8	1.0	0.9	0.9	1.0	0.9	1.0	0.9	1.1	0.9	1.0	0.8	0.7
15	1.0	0.9	1.0	0.9	0.9	1.0	0.9	0.8	1.0	0.9	0.9	1.0	0.9	1.0	0.9	1.1	0.9	1.0	0.8	0.7
16	1.0	0.9	1.0	0.9	0.9	1.0	0.9	0.8	1.0	0.9	0.9	1.0	0.9	0.9	0.9	1.1	0.9	1.0	0.8	0.7
17	1.0	0.9	1.0	0.9	0.9	1.0	0.9	0.8	1.0	0.9	0.9	1.0	0.9	0.9	0.9	1.1	0.9	1.0	0.8	0.7

Table A.2 Continued.

Patient no./ Days	1	2	3	4	5	6	7	8	9	10	11	12	13	14	15	16	17	18	19	20
18	1.0	0.9	1.0	0.9	0.9	1.0	0.9	0.8	0.9	0.9	0.9	1.0	0.9	0.9	0.9	1.1	0.9	1.0	0.8	0.6
19	1.0	0.9	1.0	0.9	0.8	1.0	0.9	0.8	0.9	0.9	0.9	1.0	0.9	0.9	0.9	1.0	0.9	1.0	0.8	0.6
20	1.0	0.9	1.0	0.9	0.8	1.0	0.9	0.8	0.9	0.9	0.9	1.0	0.9	0.9	0.8	1.0	0.9	1.0	0.8	0.6
21	1.0	0.9	1.1	0.9	0.8	1.0	0.9	0.8	0.9	0.9	0.9	1.0	0.9	0.9	0.8	1.0	1.0	1.0	0.8	0.6
22	1.0	0.9	1.1	0.9	0.8	1.0	0.9	0.8	0.9	0.9	0.9	1.0	1.0	0.9	0.8	1.0	1.0	1.0	0.8	0.5
23	1.0	0.9	1.1	0.8	0.8	1.0	0.9	0.8	0.9	0.9	0.9	1.0	1.0	0.9	0.8	1.0	1.0	1.0	0.8	0.5
24	1.0	0.9	1.1	0.8	0.7	1.0	0.9	0.8	0.9	0.9	0.9	1.0	1.0	0.9	0.8	1.0	0.9	1.0	0.8	0.5
25	1.0	0.9	1.1	0.8	0.7	1.0	0.9	0.8	0.9	0.9	0.9	1.0	0.9	0.9	0.8	1.0	0.9	1.0	0.8	0.5
26	1.0	0.9	1.1	0.8	0.7	0.9	0.9	0.8	0.9	0.9	0.9	1.0	0.9	0.9	0.8	1.0	0.9	0.9	0.8	0.5
27	1.0	0.9	1.1	0.7	0.7	0.9	0.9	0.8	0.9	0.9	0.9	1.0	0.9	0.9	0.8	1.0	0.9	0.9	0.8	0.5
28	1.0	0.9	1.1	0.7	0.7	0.9	0.9	0.8	0.9	0.9	0.9	1.0	0.9	0.9	0.7	1.0	0.9	0.9	0.8	0.5
29	1.0	0.9	1.1	0.7	0.7	0.9	0.9	0.8	0.9	0.8	0.9	1.0	0.9	0.9	0.7	1.0	0.9	0.9	0.8	0.4
30	1.0	0.9	1.1	0.7	0.7	0.9	0.9	0.8	0.9	0.8	0.9	1.0	0.9	1.0	0.7	1.0	0.9	0.9	0.8	0.4
31	1.0	0.9	1.1	0.7	0.7	0.9	0.8	0.8	0.9	0.8	0.9	1.0	0.9	0.9	0.7	1.0	0.9	0.9	0.7	0.4
32	1.0	0.8	1.1	0.7	0.7	0.9	0.8	0.8	0.9	0.8	0.9	1.0	0.9	0.9	0.7	1.0	0.9	0.9	0.7	0.4
33	1.0	0.8	1.1	0.7	0.7	0.9	0.8	0.8	0.9	0.8	0.9	1.0	0.8	0.9	0.7	1.0	0.9	0.8	0.7	0.4
34	1.0	0.8	1.1	0.7	0.7	0.8	0.8	0.8	0.9	0.8	0.9	1.0	0.8	0.9	0.8	1.0	0.8	0.8	0.7	0.4
35	1.0	0.8	1.1	0.7	0.7	0.8	0.8	0.8	0.9	0.8	0.9	1.0	0.8	0.9	0.8	1.0	0.8	0.8	0.7	0.4
36	1.0		1.0	0.6	0.7	0.8	0.8	0.8	0.9	0.8	0.9	1.0	0.8	0.9	0.8	1.1	0.8	0.8	0.7	0.4
37	1.0		1.0	0.6	0.7	0.8	0.8	0.8	0.9	0.8	0.9	1.0	0.8	0.9	0.8	1.1	0.8	0.8	0.7	0.4
38	1.0		1.0	0.6	0.7	0.8	0.8	0.8	0.9	0.8	0.9	1.0	0.8	0.9	0.8	1.1	0.8	0.8	0.7	0.4
40	1.0		1.0	0.6	0.7	0.8	0.8	0.8	0.9	0.7	0.9	1.0	0.8	0.9	0.8	1.1	0.8	0.8	0.7	0.4

Table A.2 Continued.

Patient no./ Days	1	2	3	4	5	6	7	8	9	10	11	12	13	14	15	16	17	18	19	20
41	1.0		1.0	0.6	0.7	0.9	0.8	0.8	0.9	0.7	0.9	1.0	0.8	0.9	0.8	1.1	0.8	0.8	0.7	0.4
42	1.0		1.0	0.6	0.7	0.9	0.8	0.9	0.9	0.7	0.9	1.0	0.8	0.9	0.8	1.1	0.8	0.8	0.7	0.4
43	1.0		1.0	0.6	0.7	0.9	0.8	0.9	0.9	0.7	0.9	1.0	0.7	0.9	0.8	1.1	0.8	0.8	0.7	0.4

APPENDIX B:

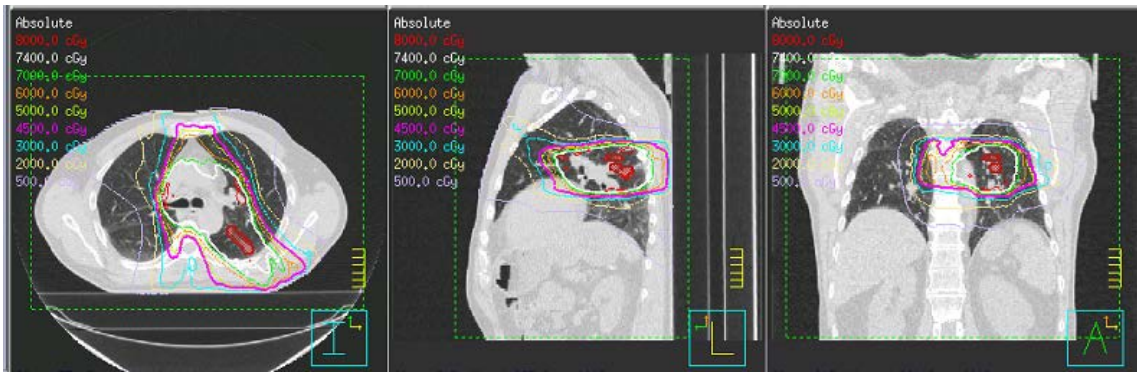

Figure B.1 Patient 1's clinical IMRT plan with GTVp in red and original isodose lines

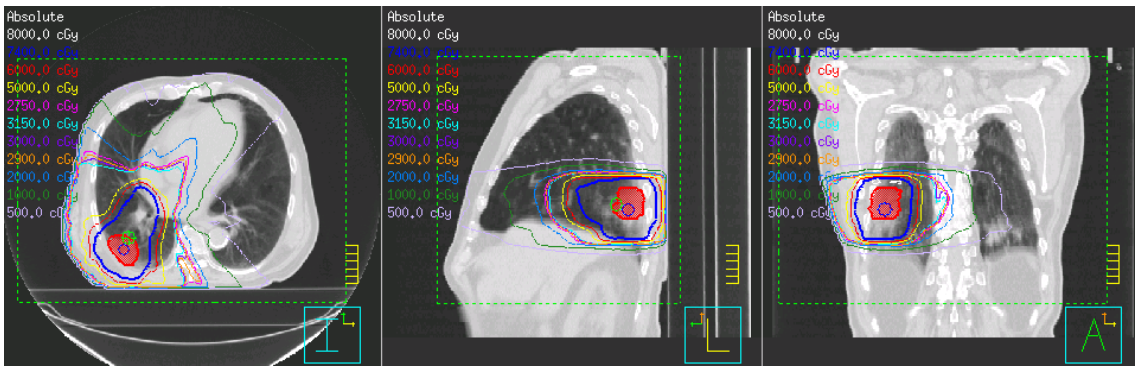

Figure B.2 Patient 2's clinical IMRT plan with GTVp in red and original isodose lines

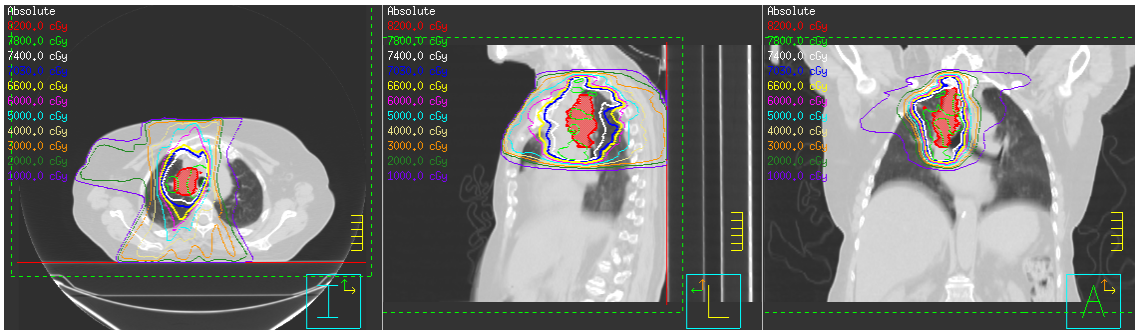

Figure B.3 Patient 1's clinical IMRT plan with GTVp in red and original isodose lines

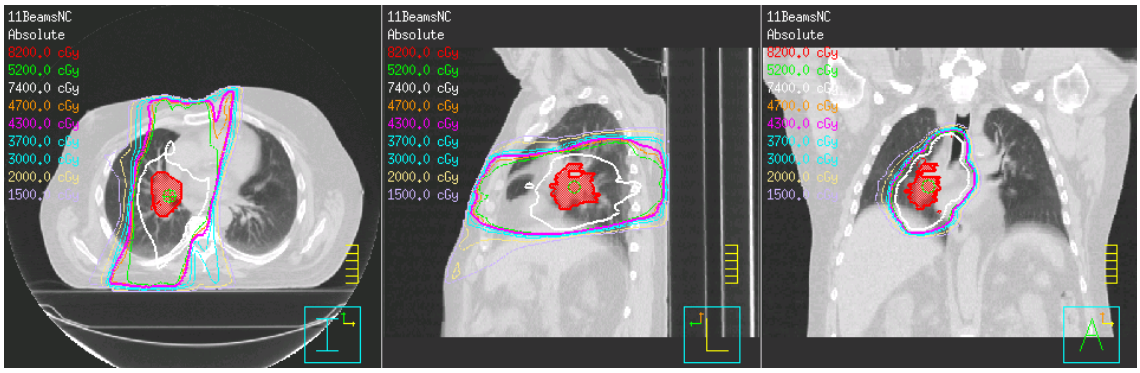

Figure B.4 Patient 4's clinical IMRT plan with GTVp in red and original isodose lines

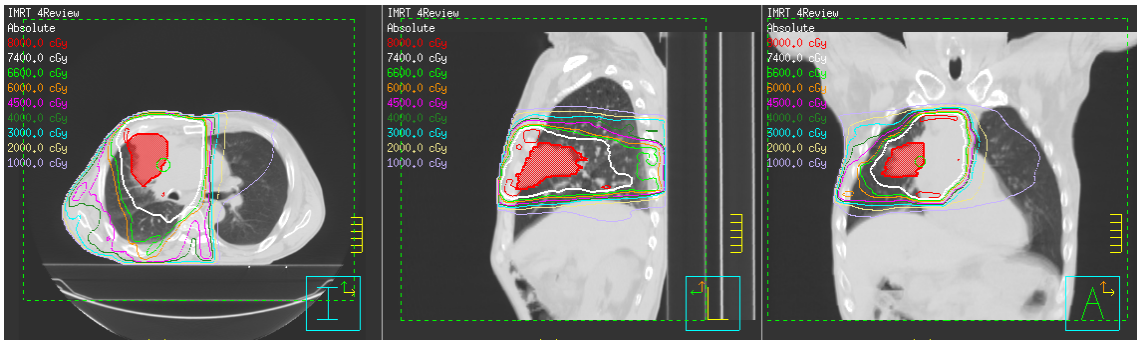

Figure B.5 Patient 5's clinical IMRT plan with GTVp in red and original isodose lines

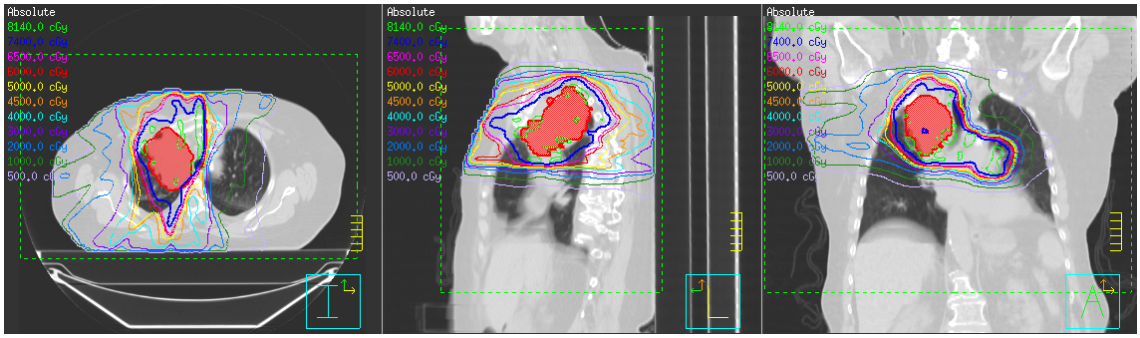

Figure B.6 Patient 6's clinical IMRT plan with GTVp in red and original isodose lines

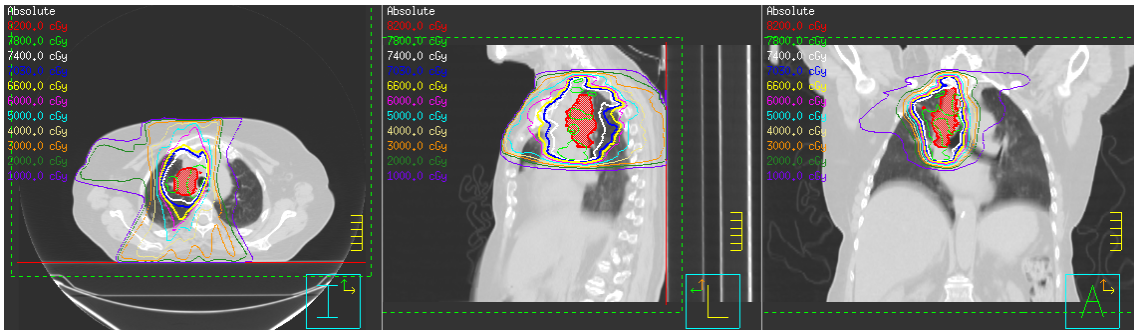

Figure B.7 Patient 7's clinical IMRT plan with GTVp in red and original isodose lines

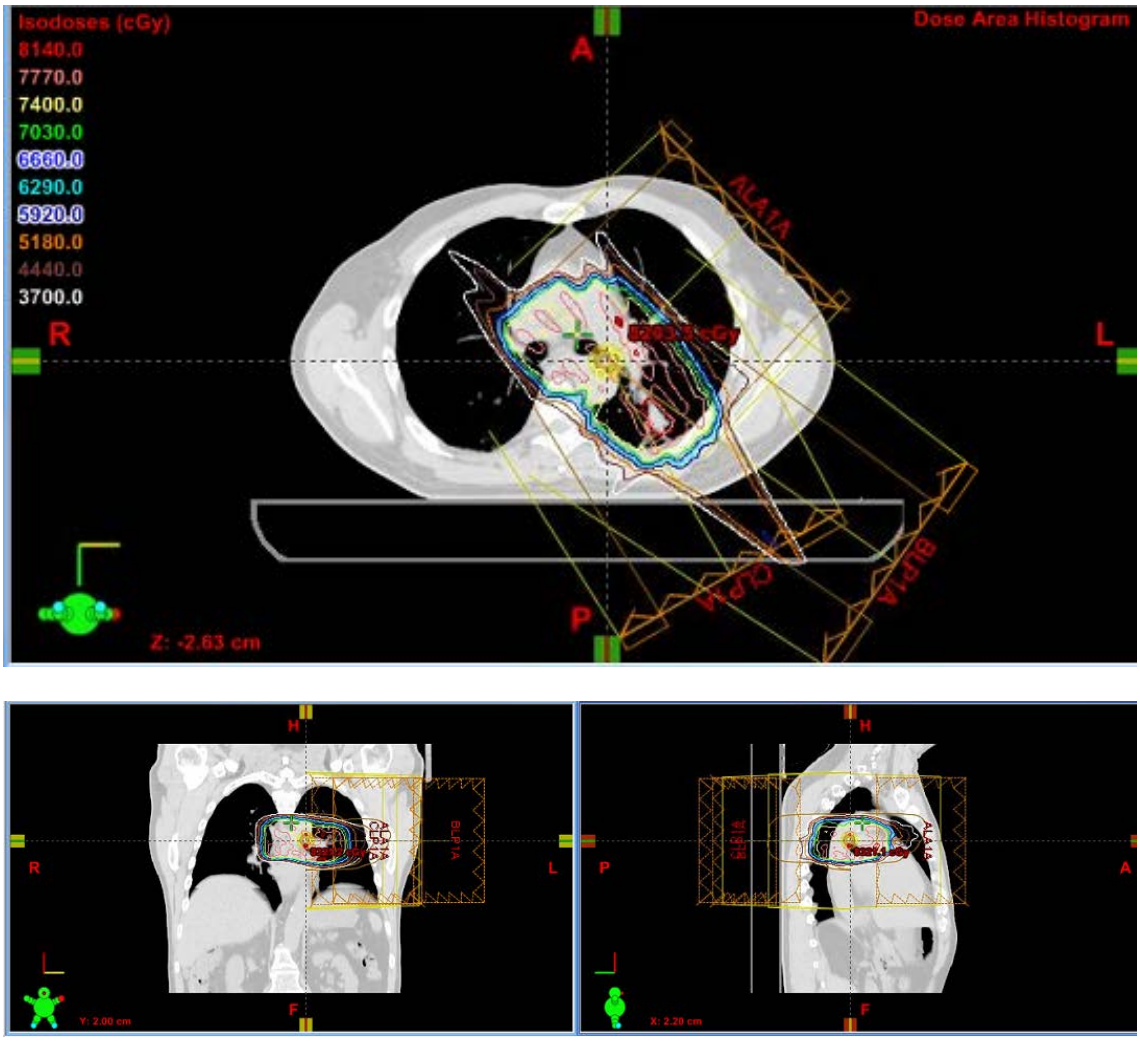

Figure B.8 Patient 1's clinical PSPT plan with GTVp in red and original isodose lines

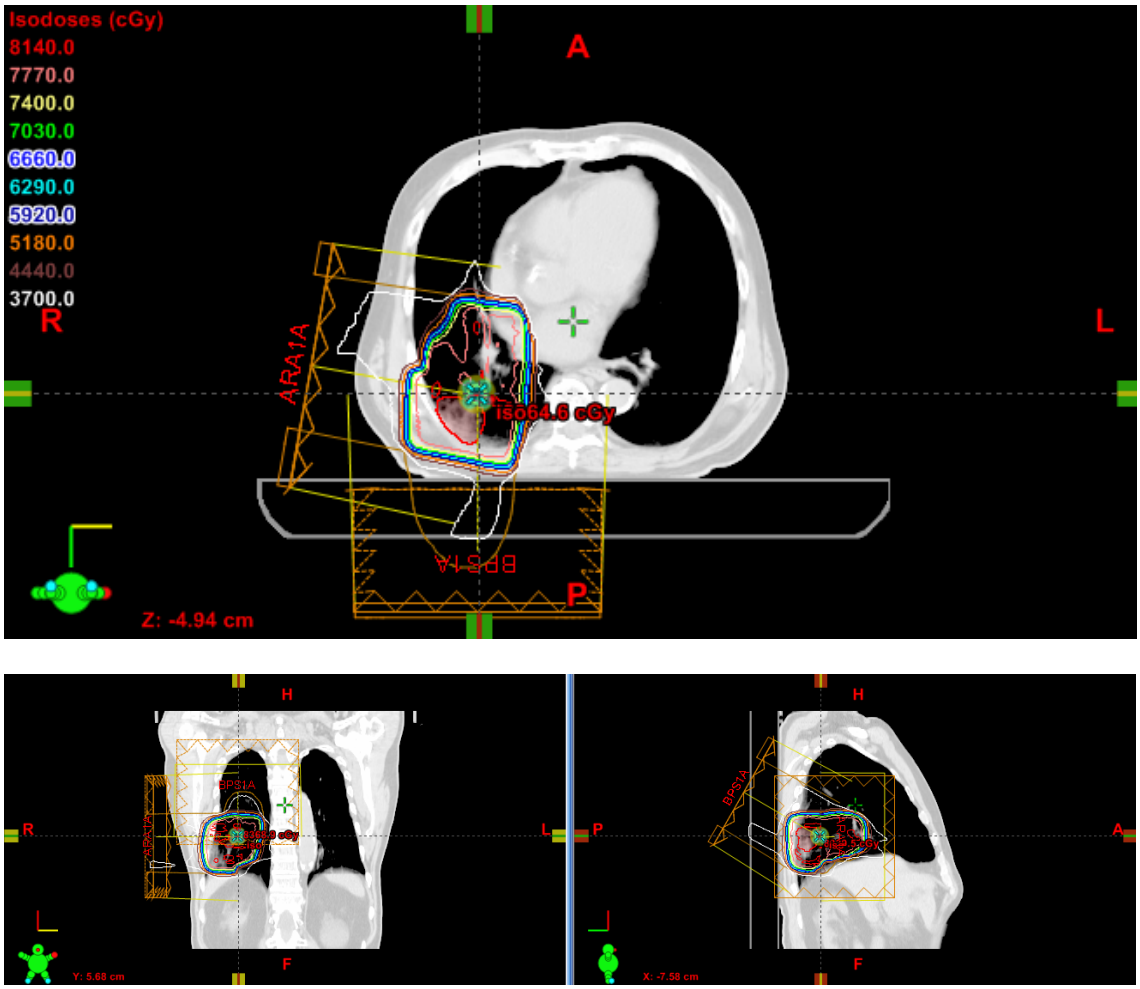

Figure B.9 Patient 2's clinical PSPT plan with GTVp in red and original isodose lines

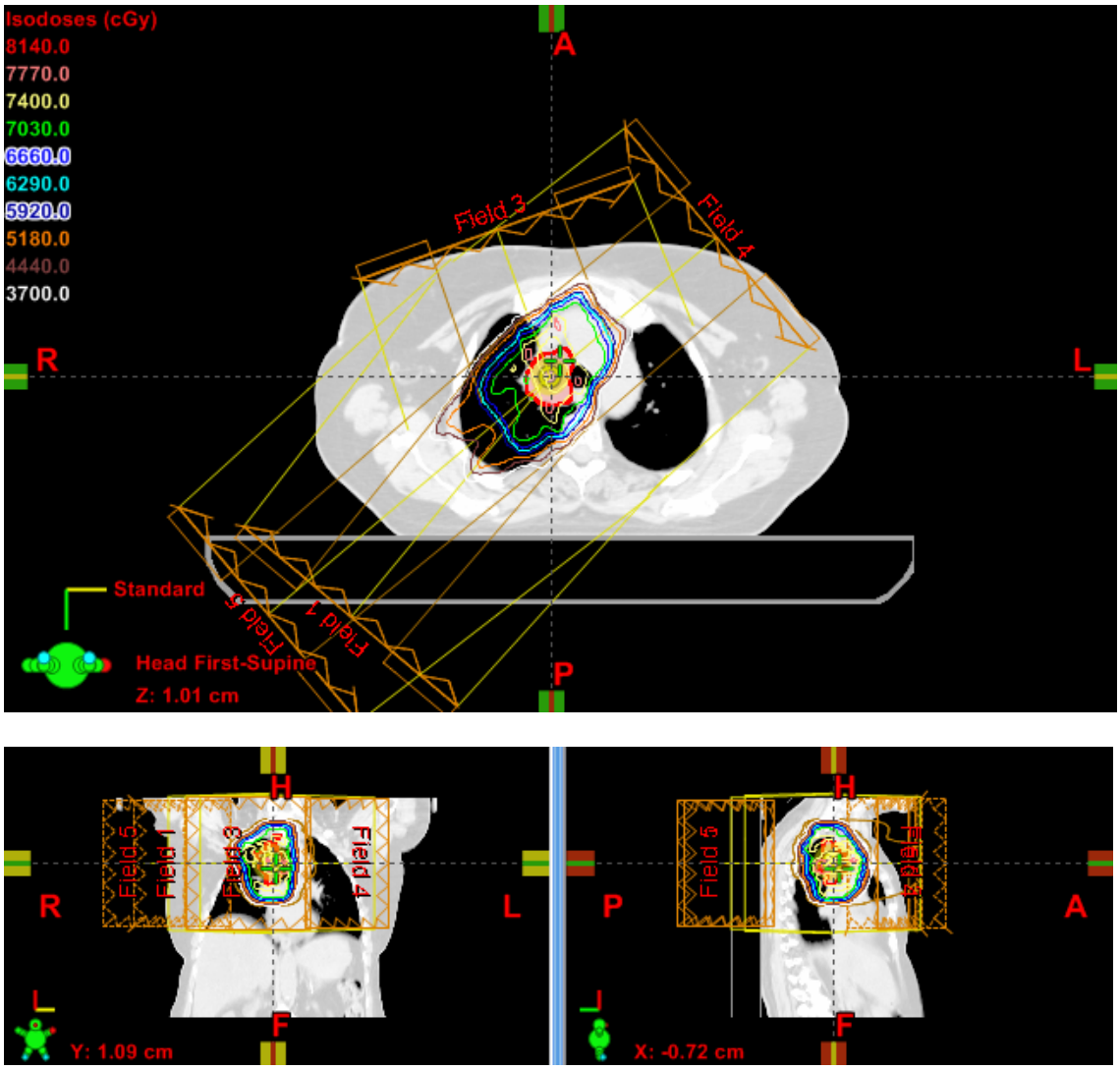

Figure B.10 Patient 3's clinical PSPT plan with GTVp in red and original isodose lines

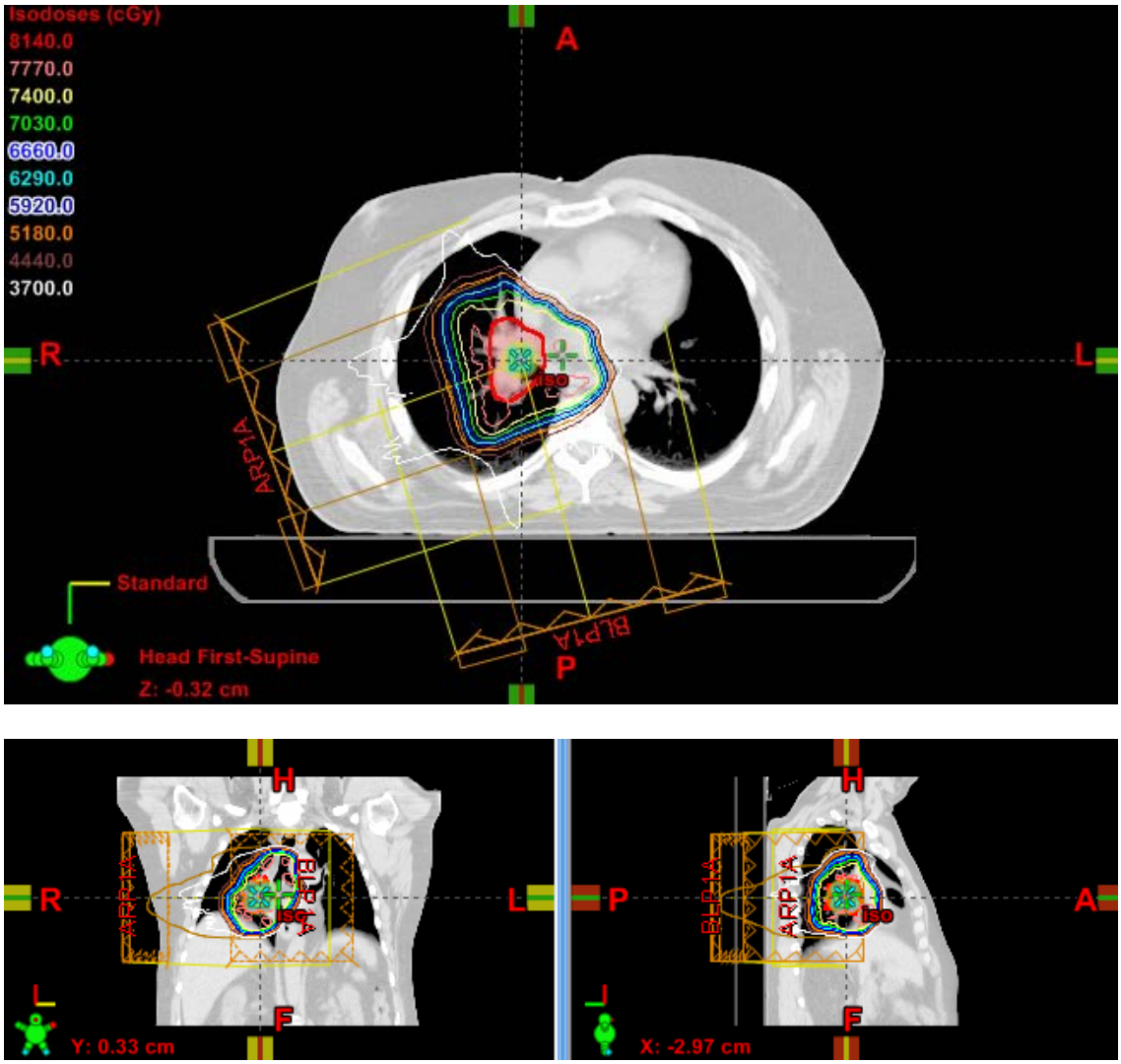

Figure B.11 Patient 4's clinical PSPT plan with GTVp in red and original isodose lines

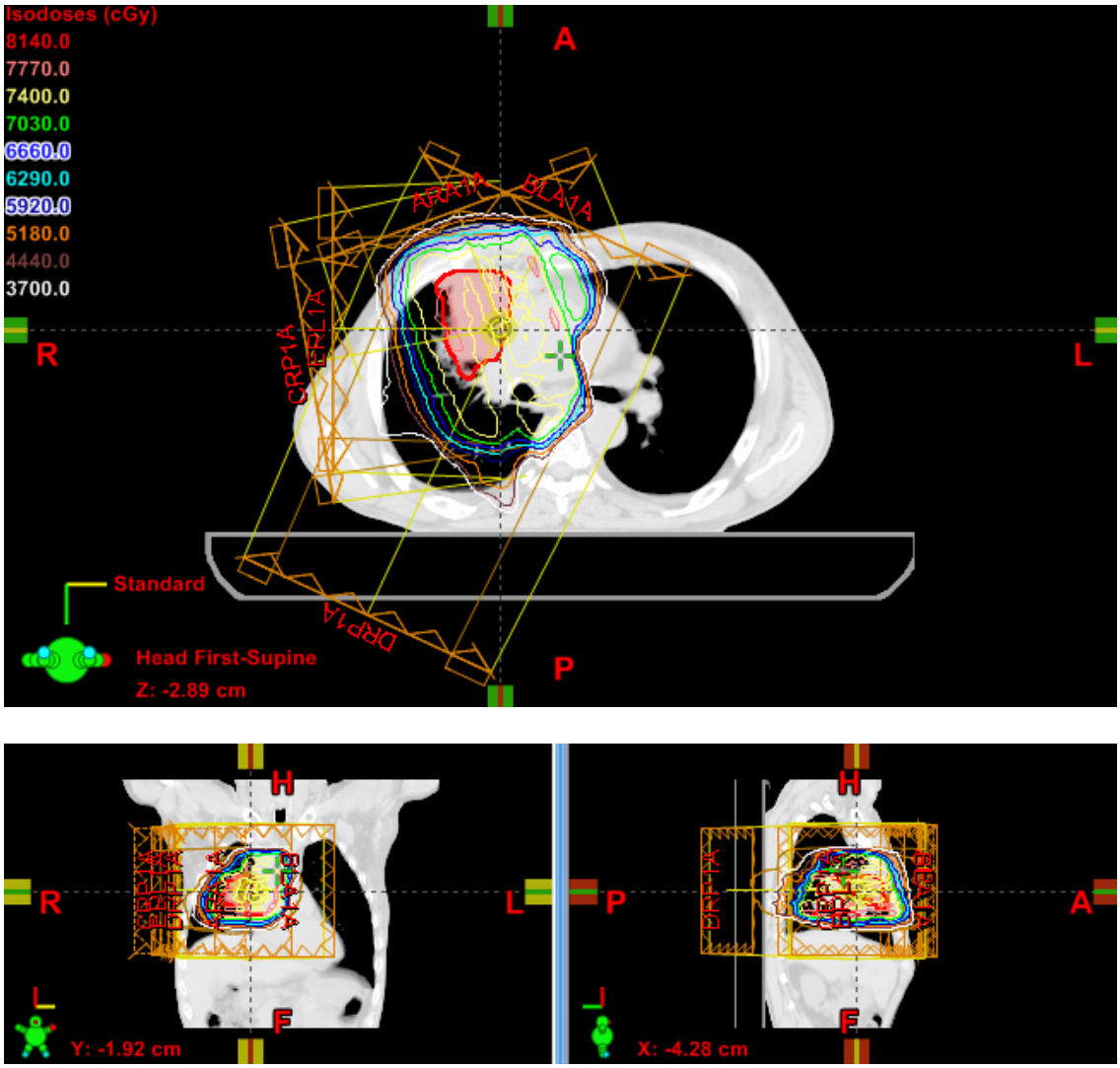

Figure B.12 Patient 5's clinical PSPT plan with GTVp in red and original isodose lines

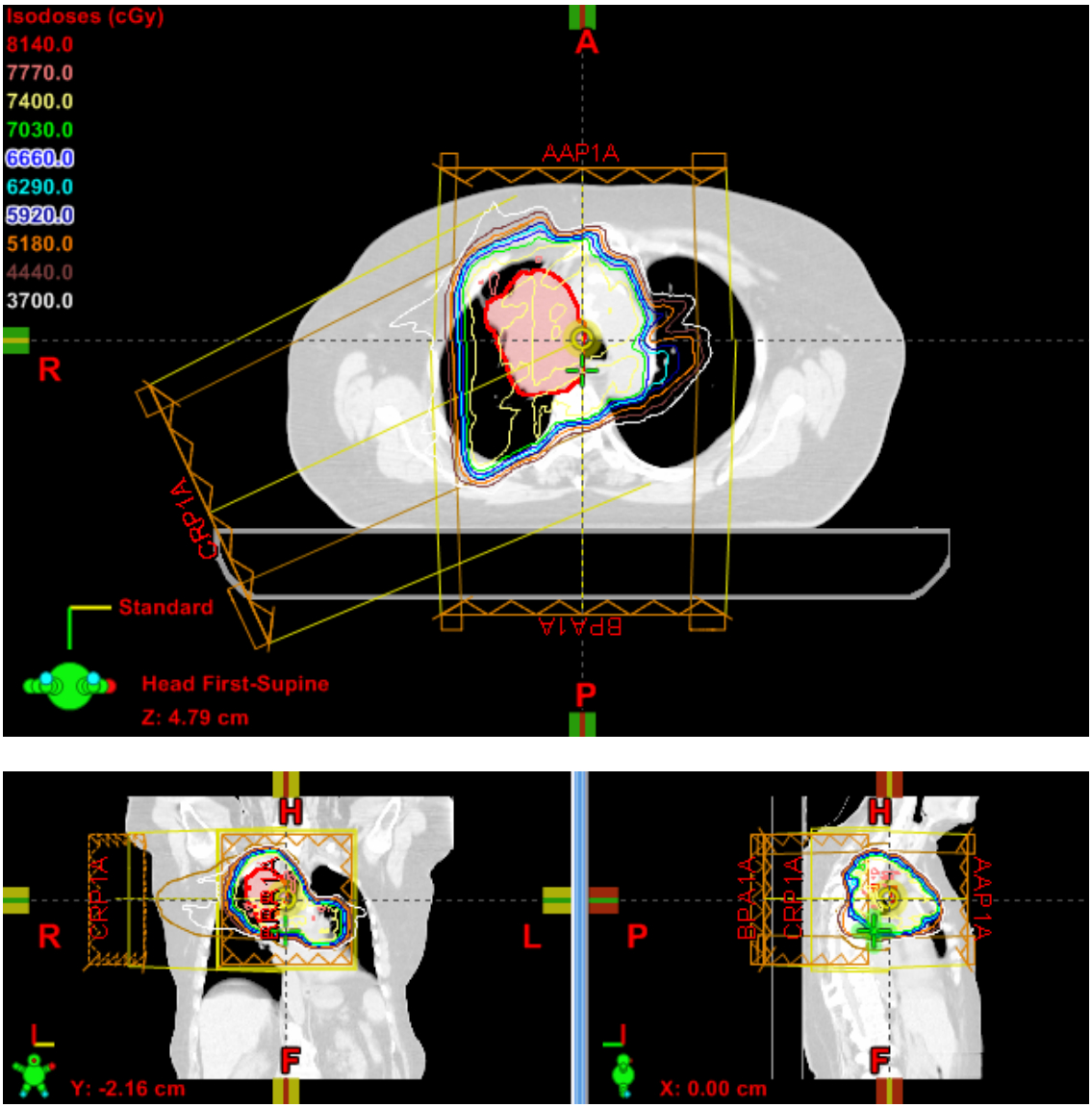

Figure B.13 Patient 6's clinical PSPT plan with GTVp in red and original isodose lines

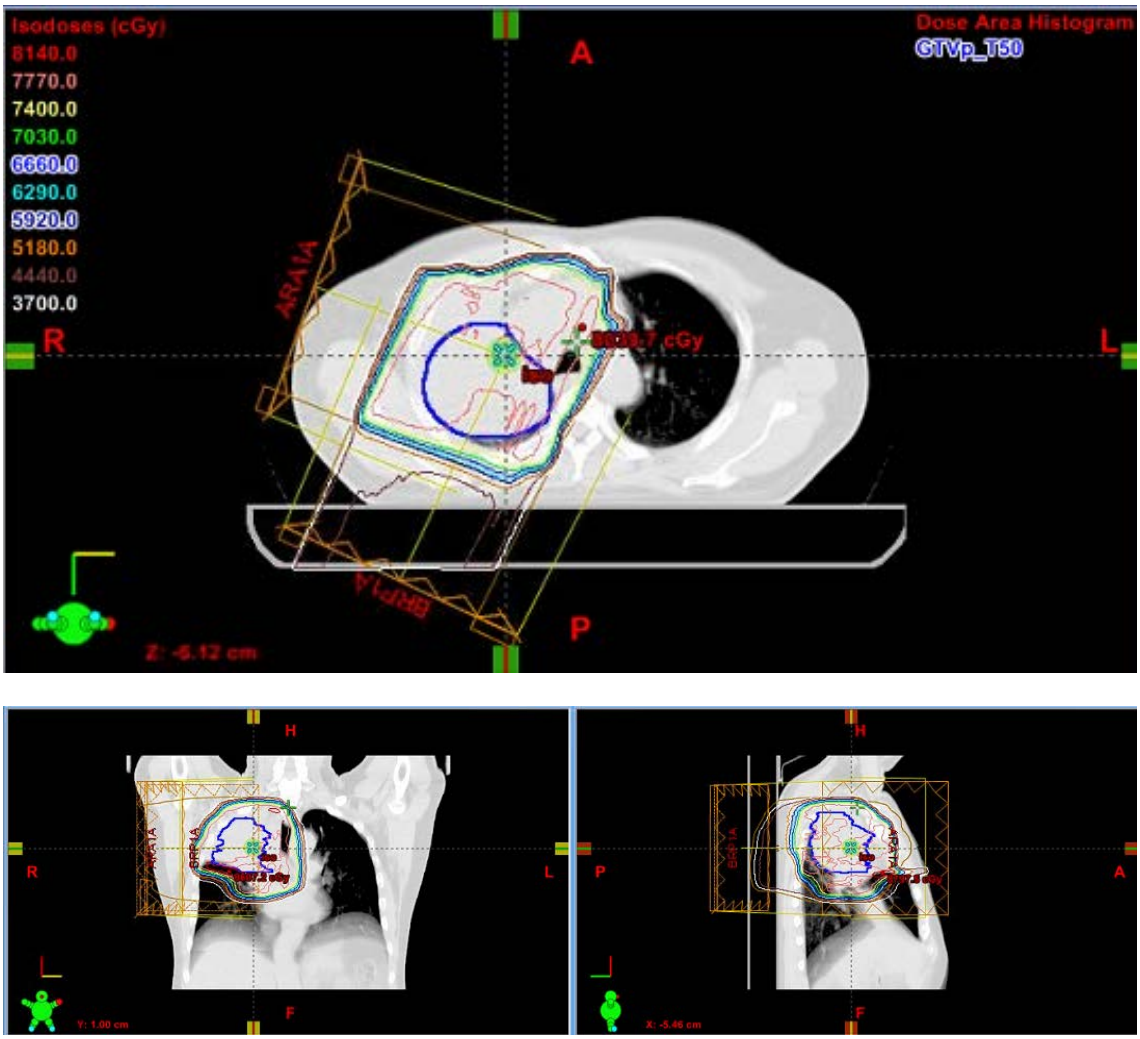

Figure B.14 Patient 7's clinical PSPT plan with GTVp in red and original isodose lines

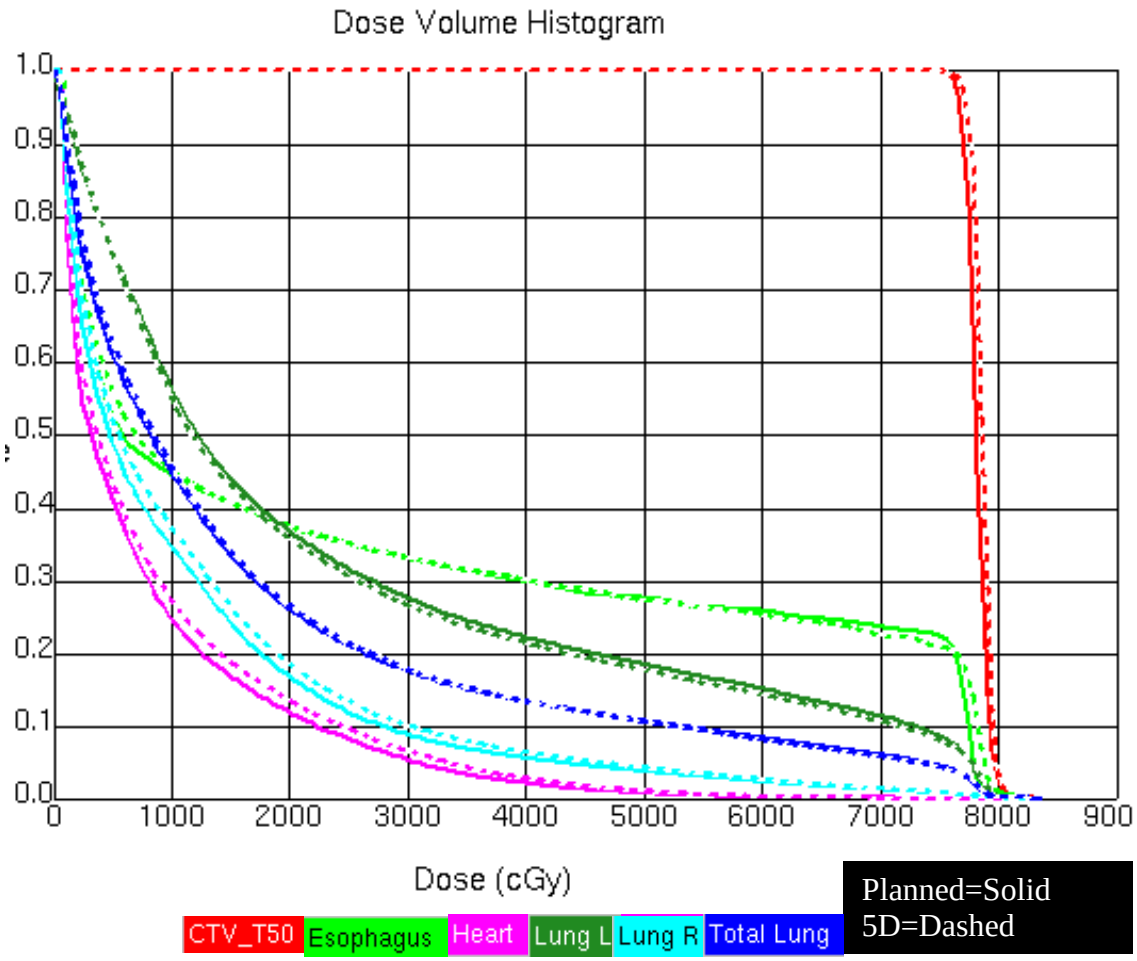

Figure B. 15 Patient 1 DVH for IMRT plan

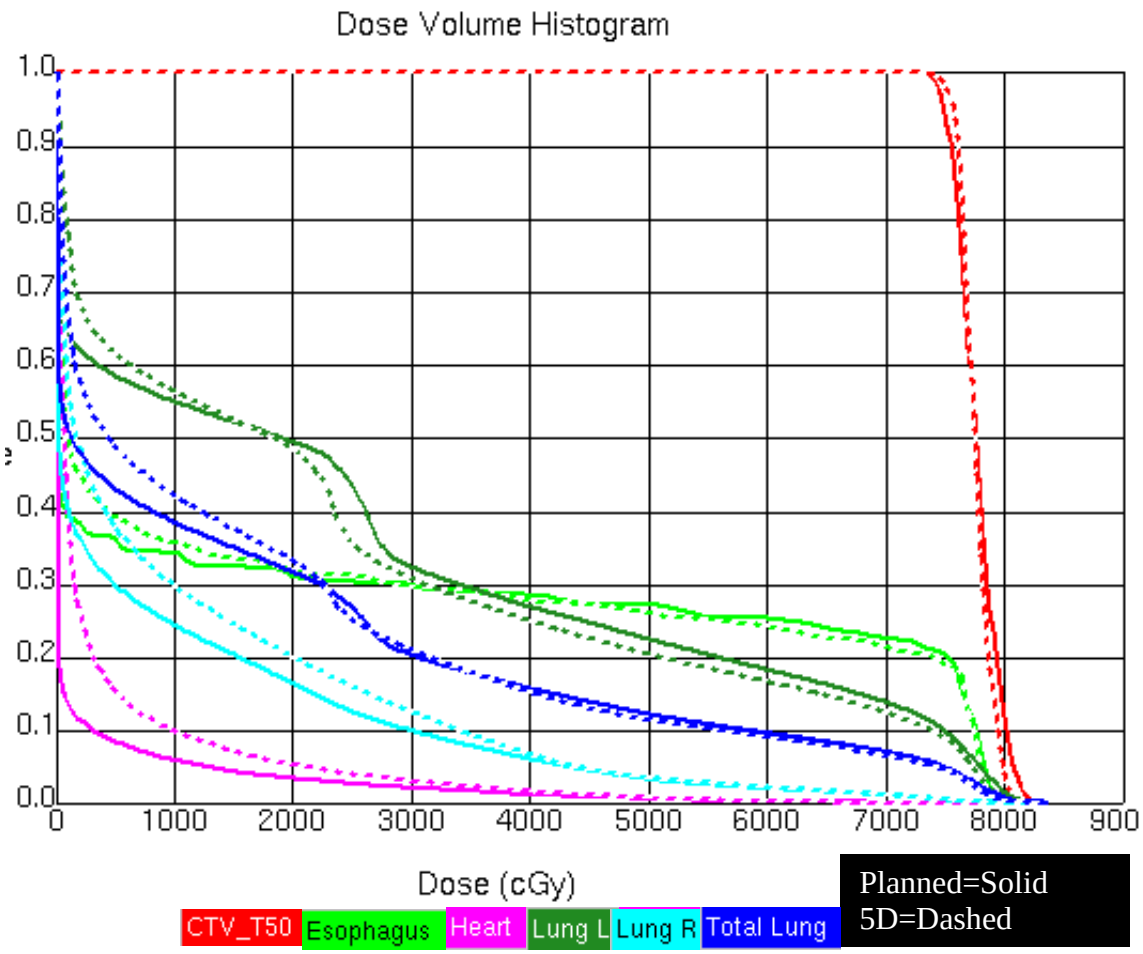

Figure B.16 Patient 1 DVH for PSPT plan

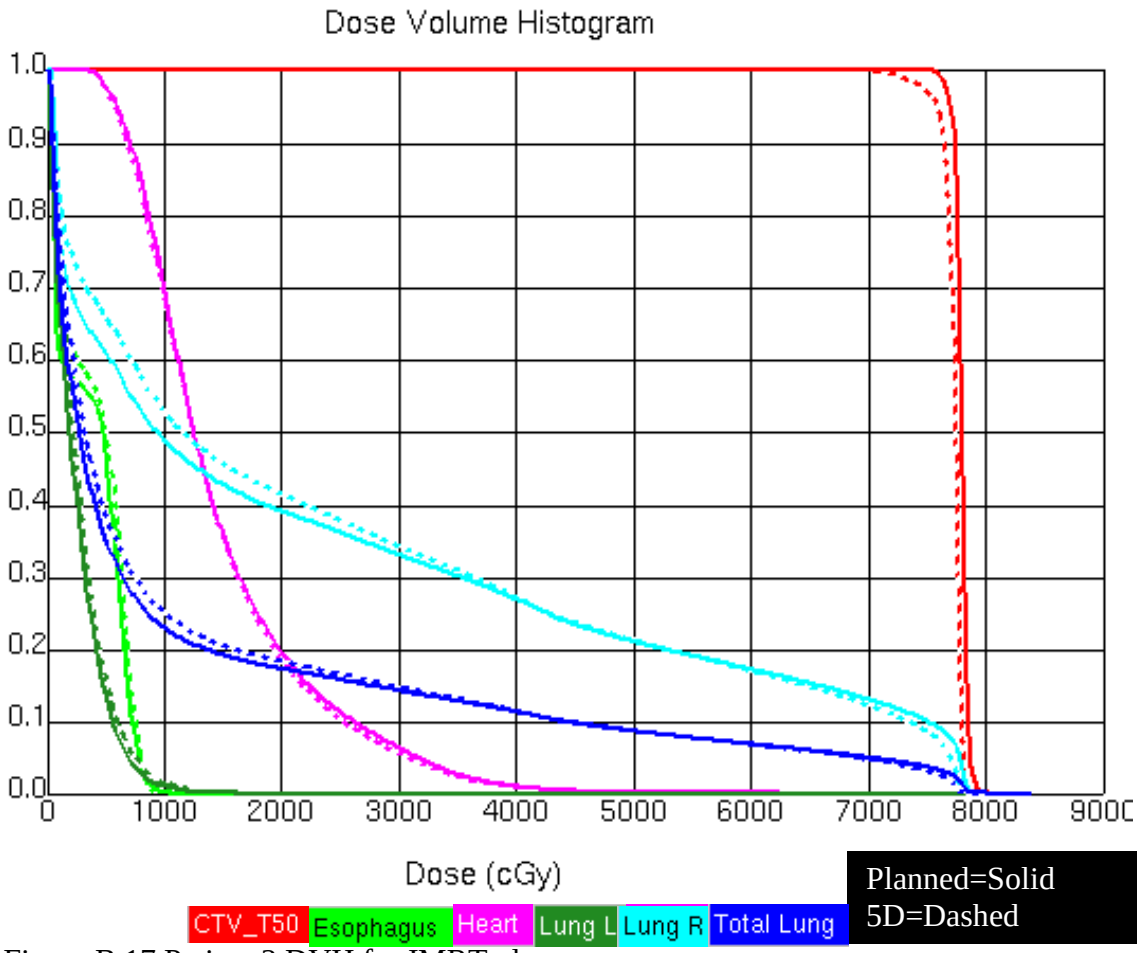

Figure B.17 Patient 2 DVH for IMRT plan

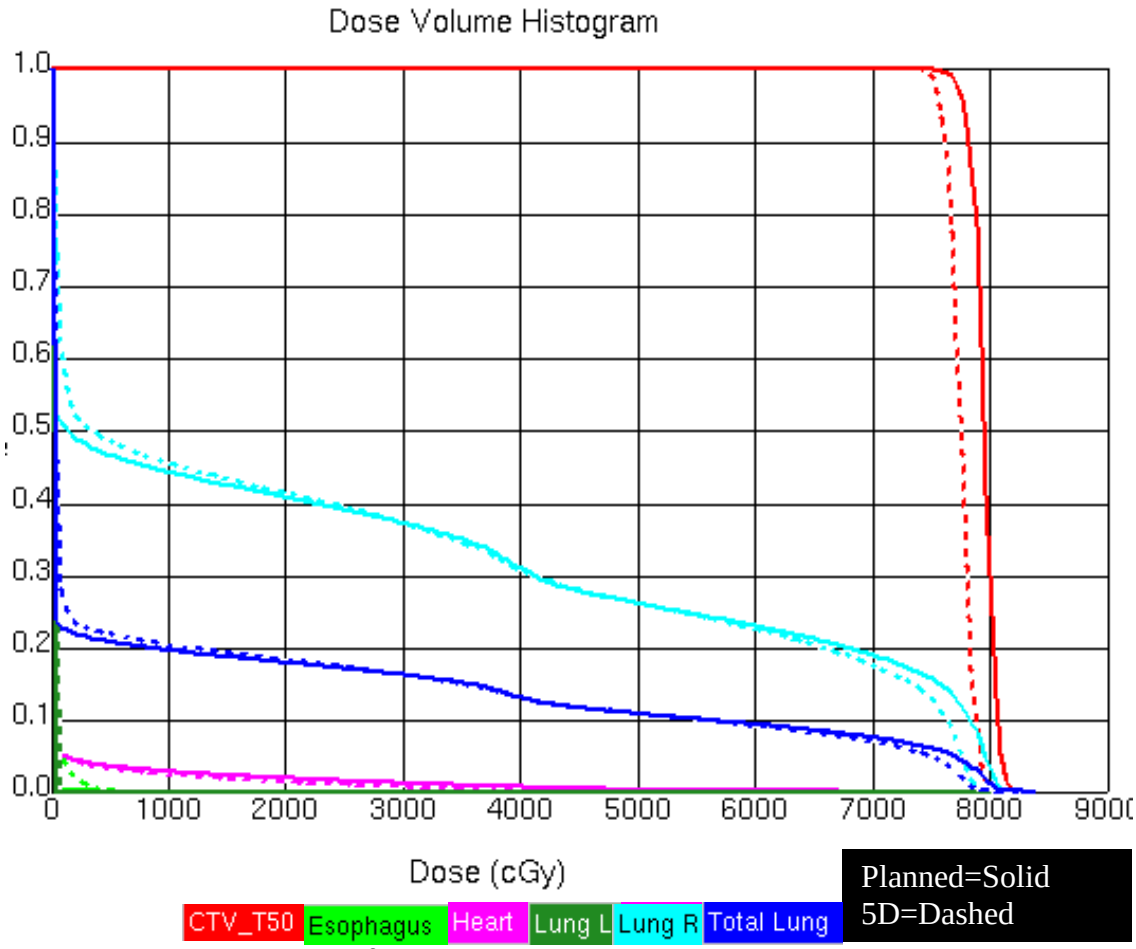

Figure B.18 Patient 2 DVH for PSPT plan

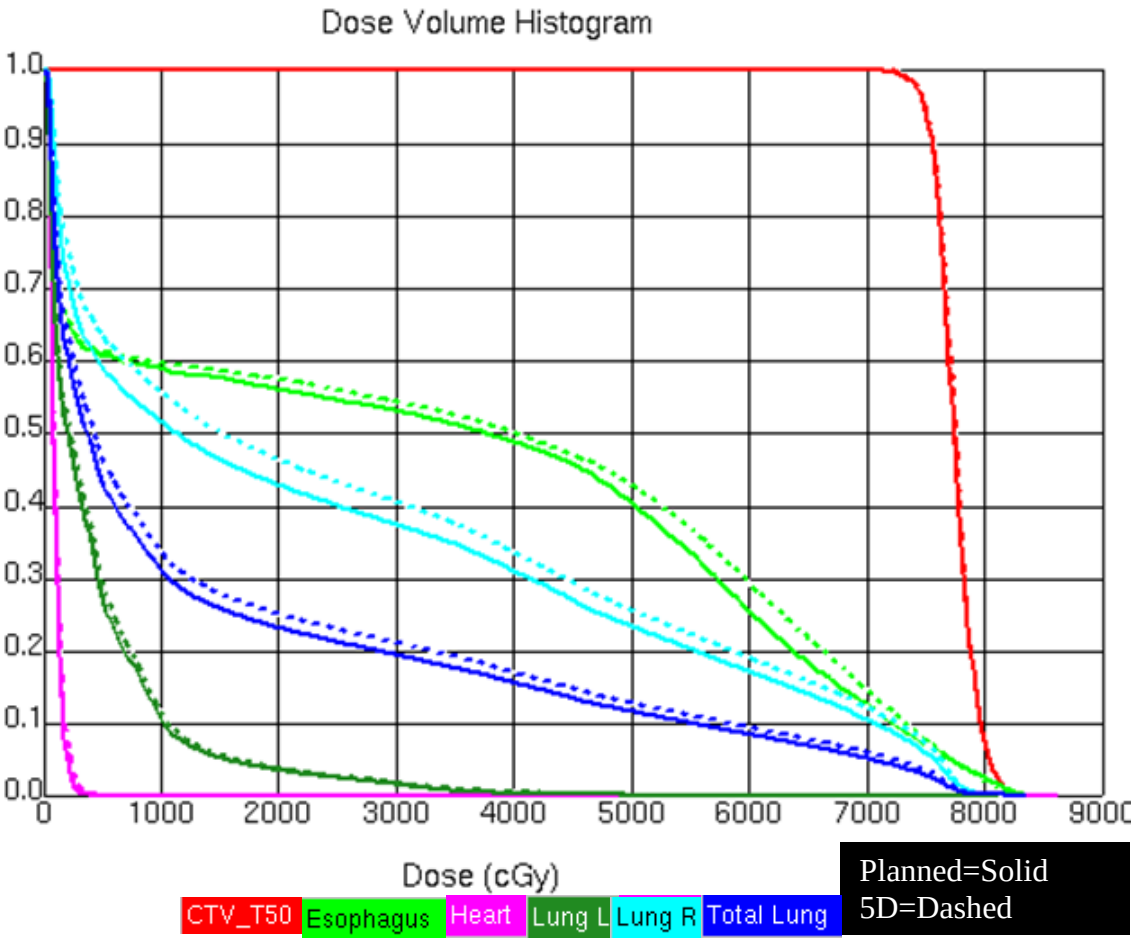

Figure B.19 Patient 3 DVH for IMRT plan

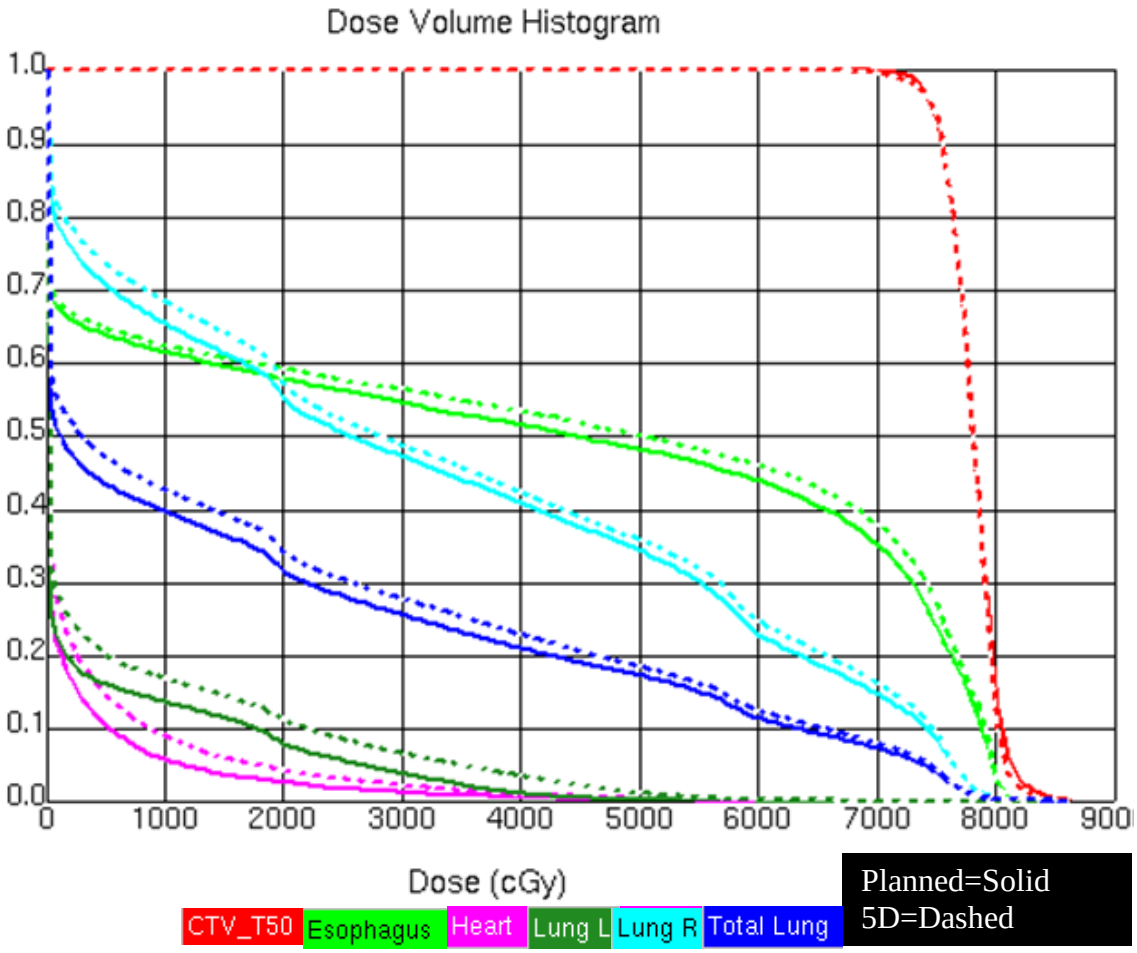

Figure B.20 Patient 3 DVH for PSPT plan

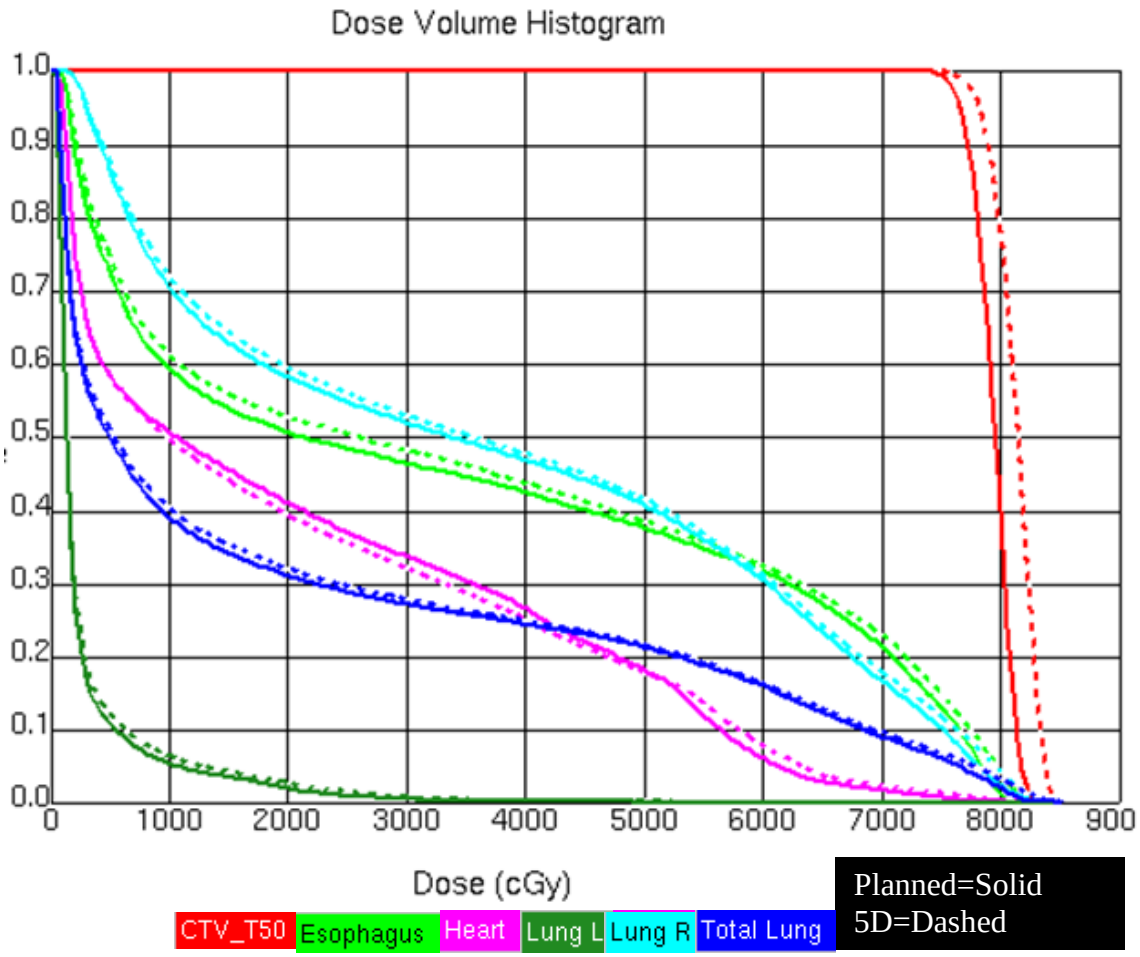

Figure B.21 Patient 4 DVH for IMRT plan

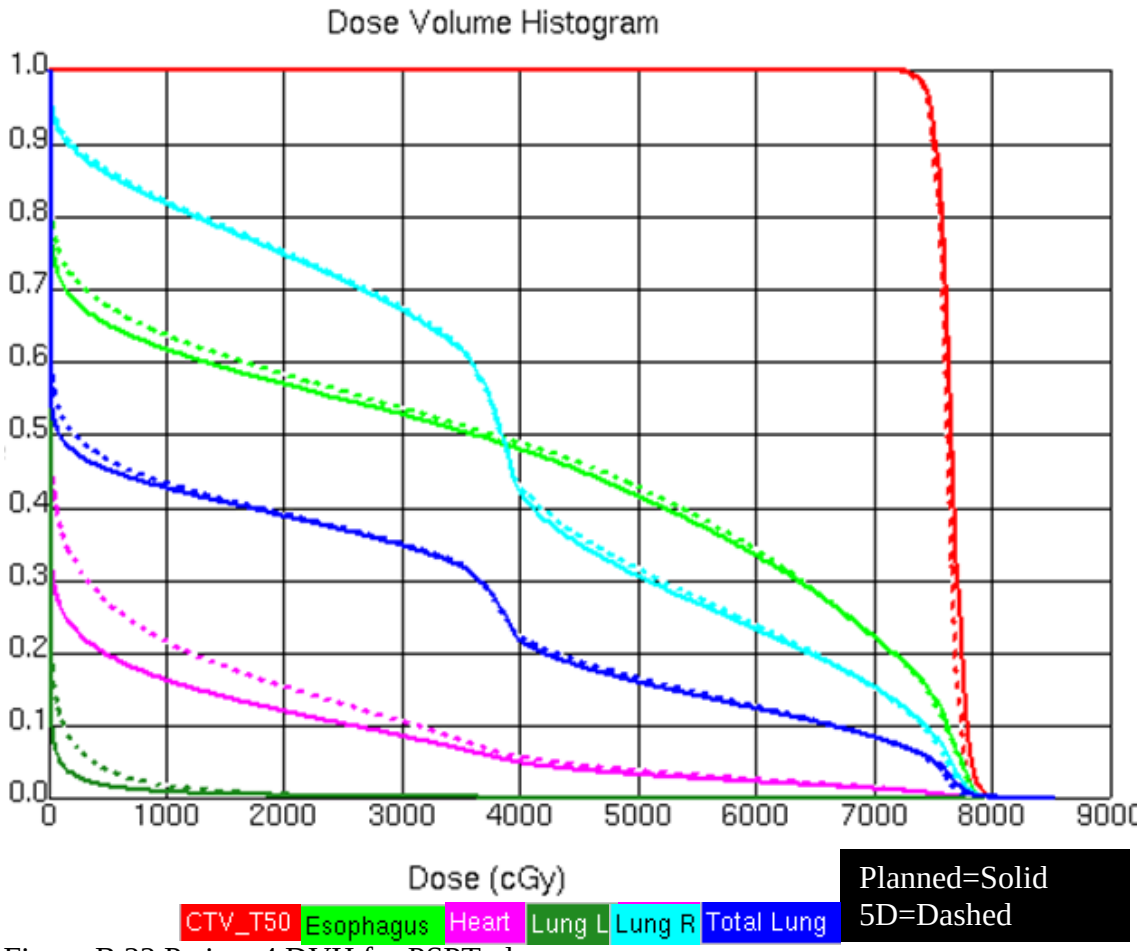

Figure B.22 Patient 4 DVH for PSPT plan

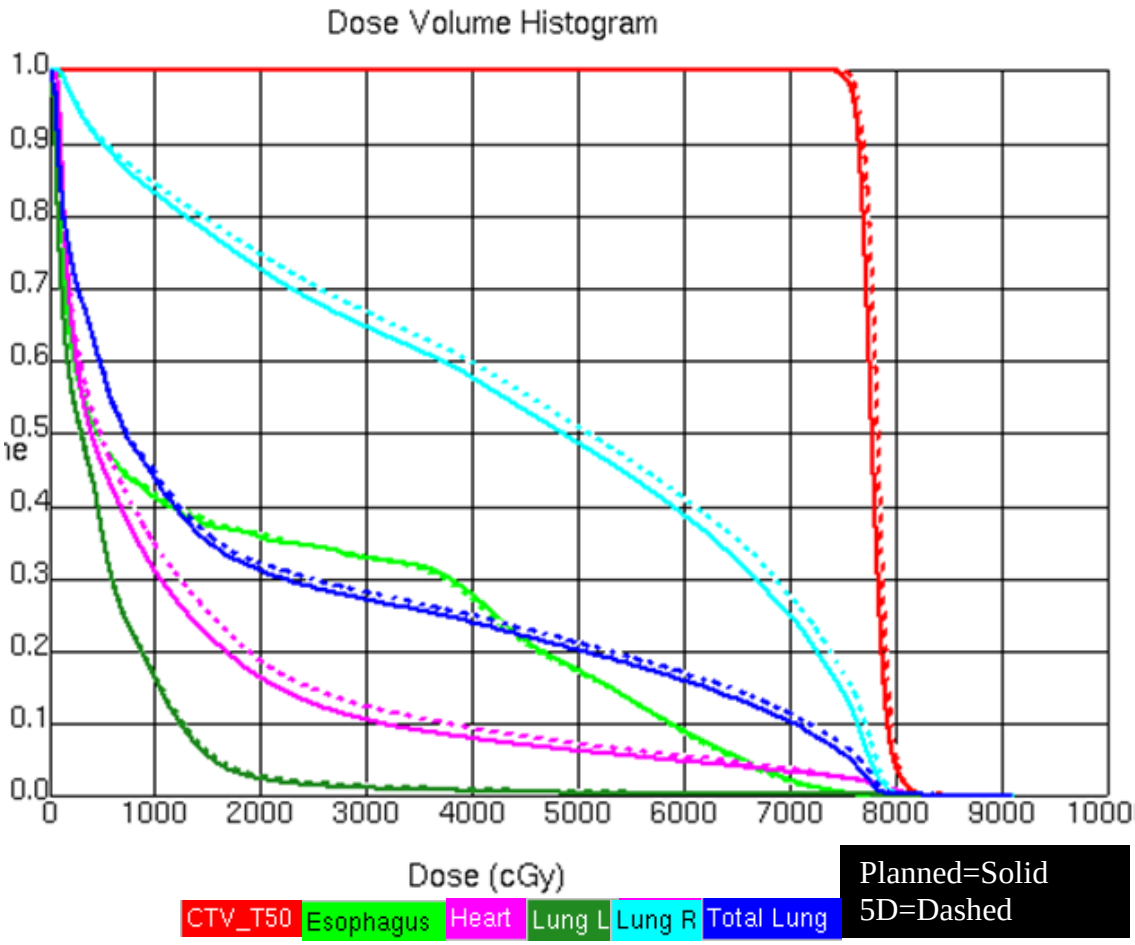

Figure B.23 Patient 5 DVH for IMRT plan

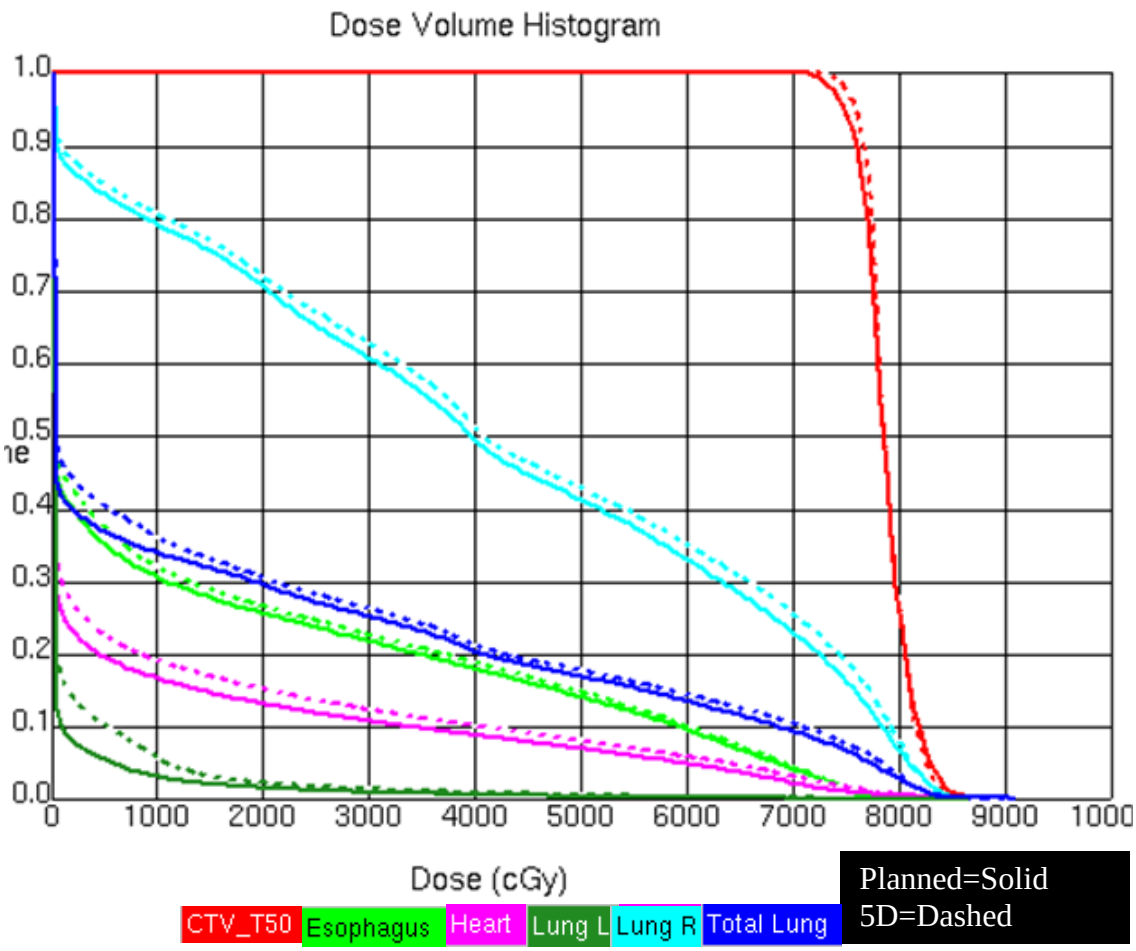

Figure B.24 Patient 5 DVH for PSPT plan

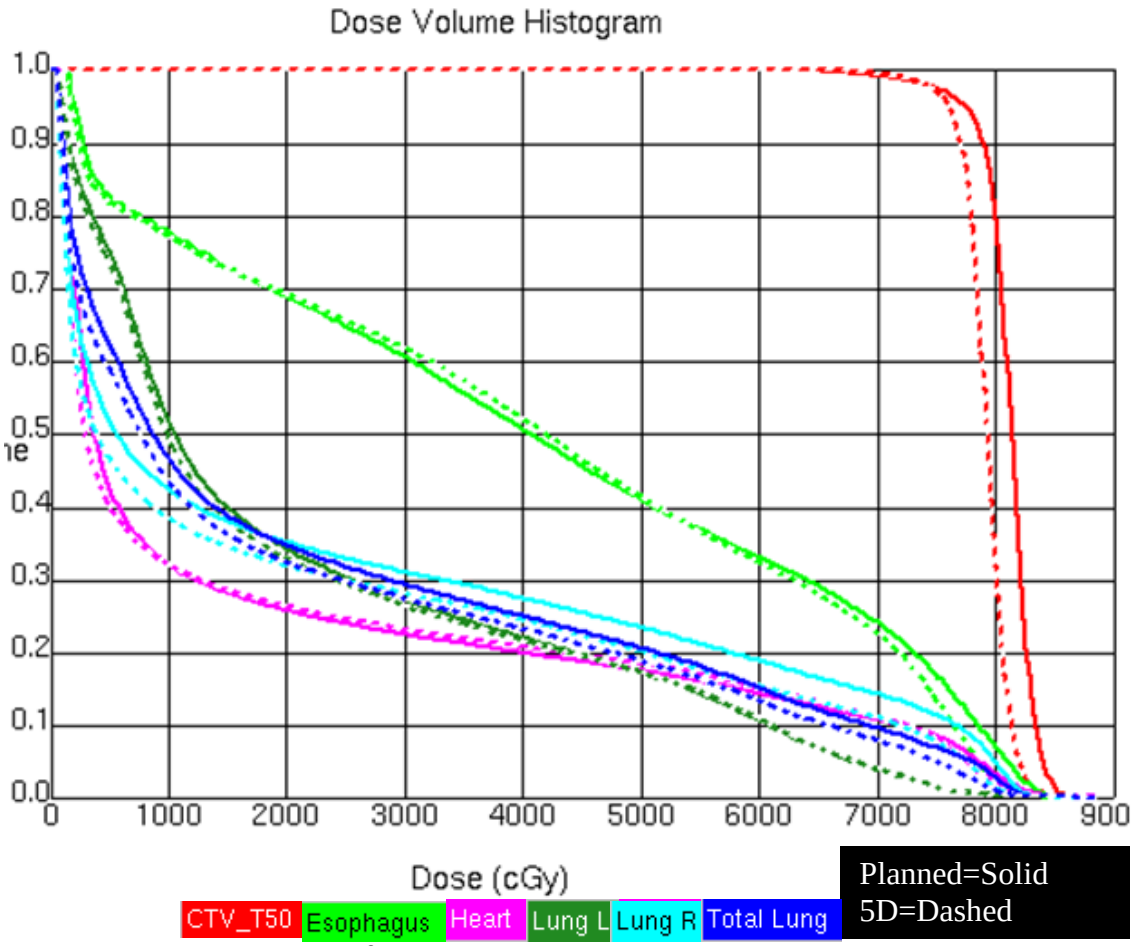

Figure B.25 Patient 6 DVH for IMRT plan

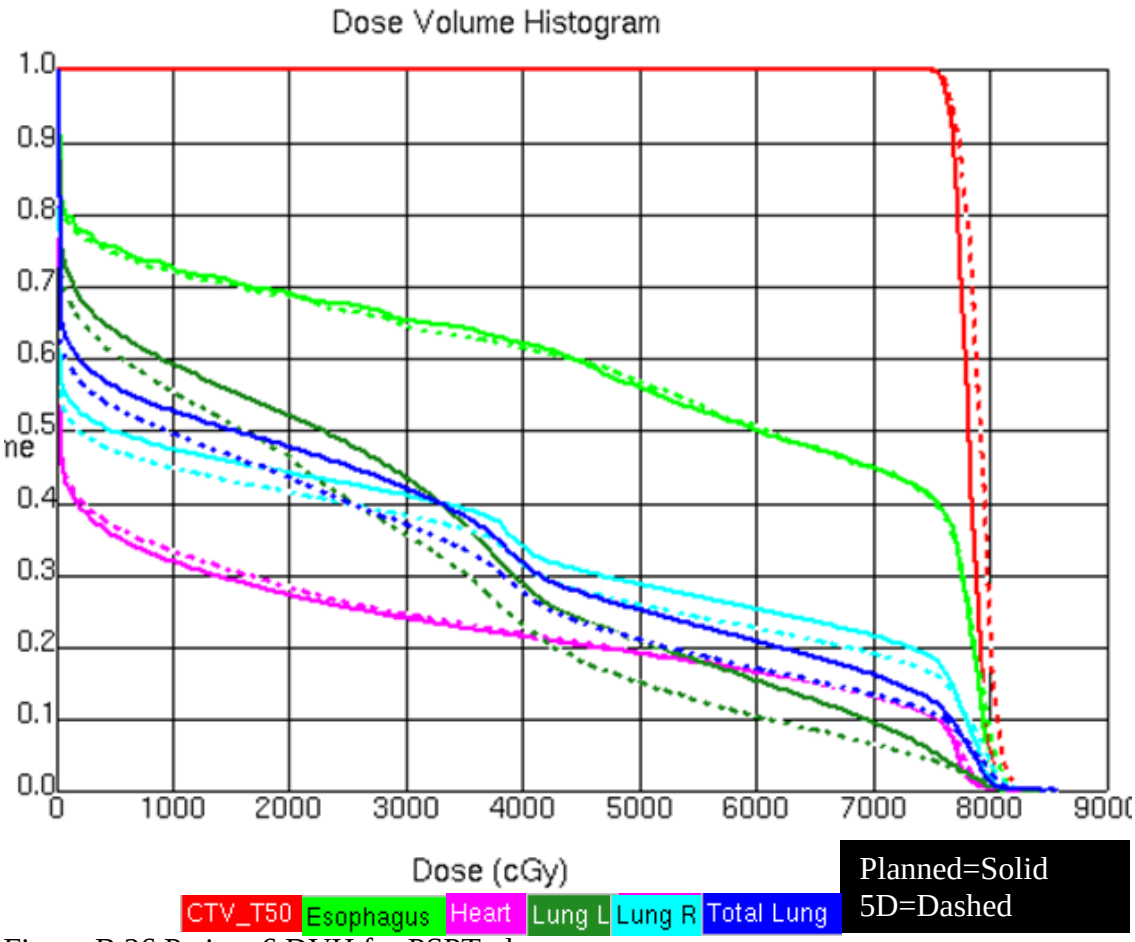

Figure B.26 Patient 6 DVH for PSPT plan

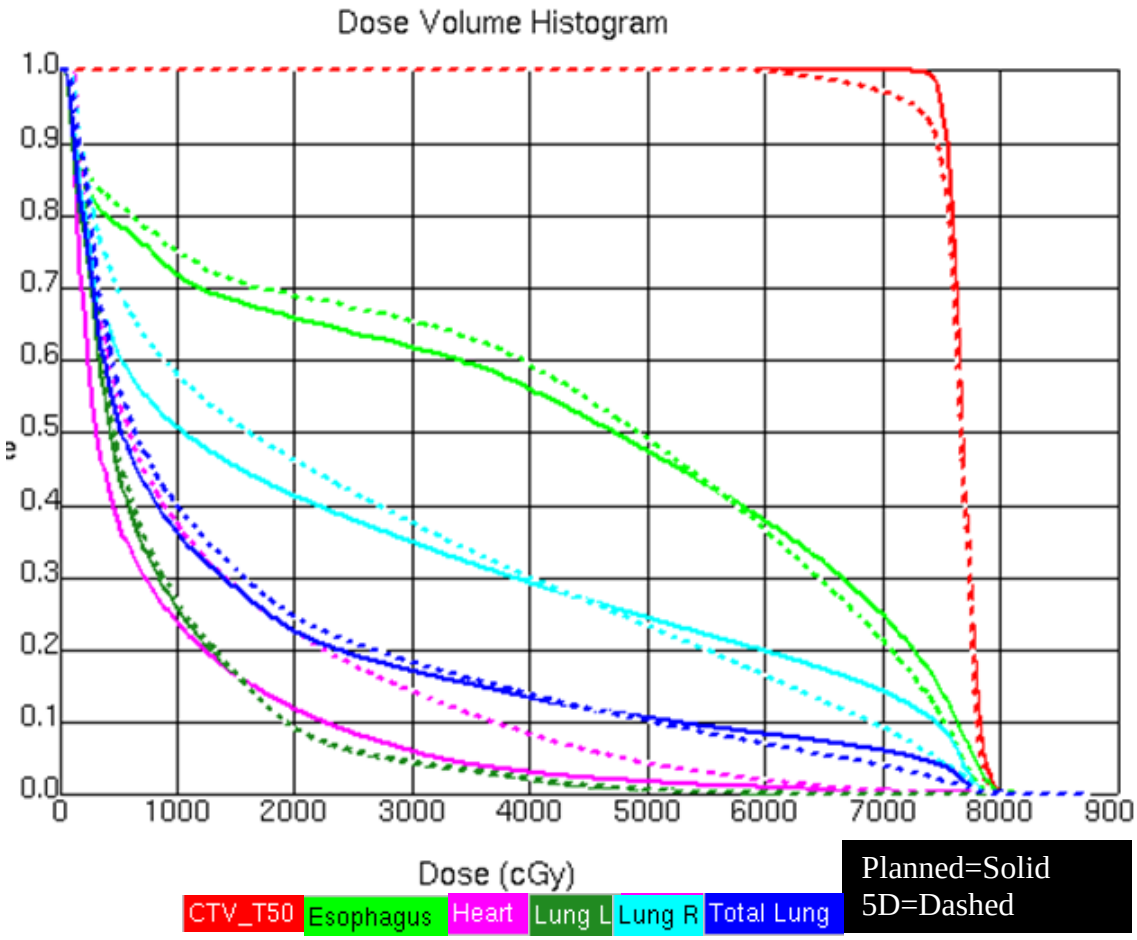

Figure B.27 Patient 7 DVH for IMRT plan

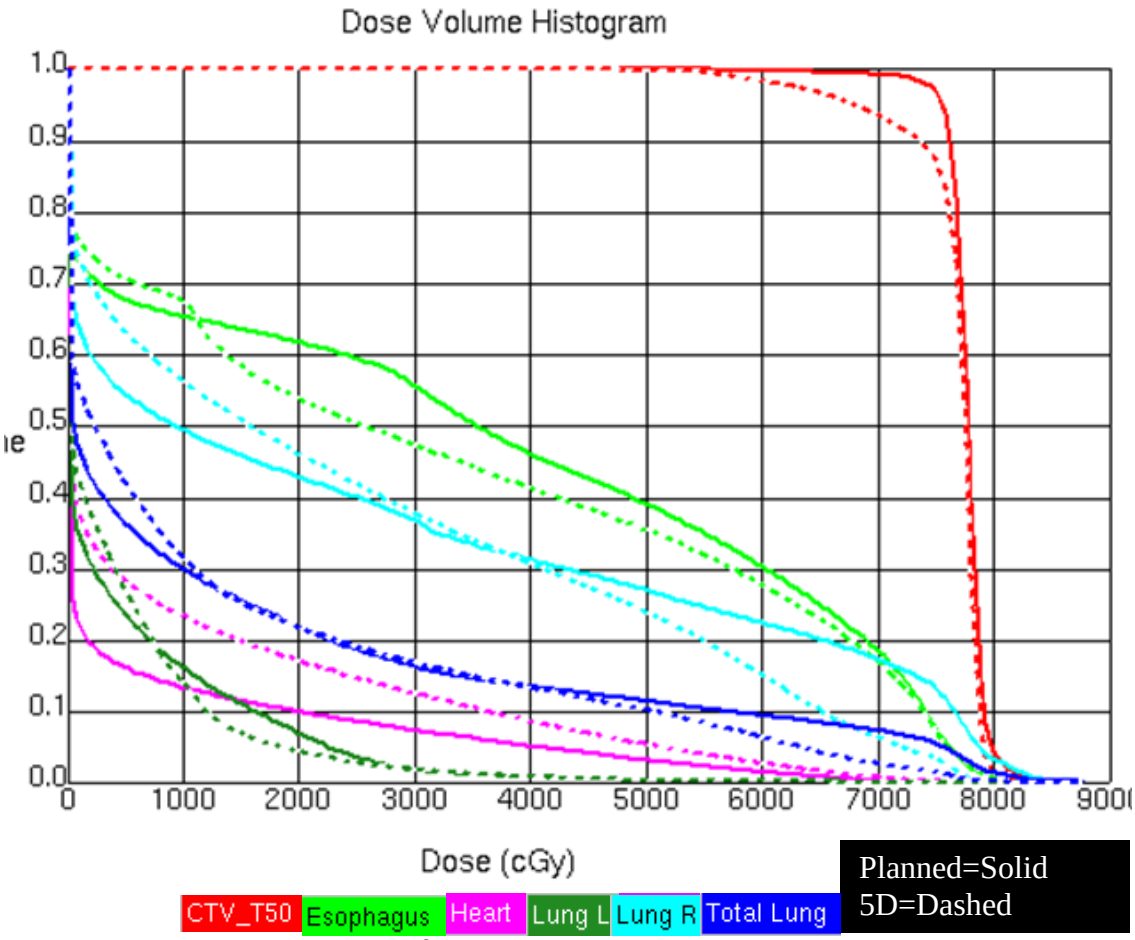

Figure B.28 Patient No. 7 DVH for PSPT plan

Table B.1 CTV V74 for each patient's IMRT plan

Patient No.	V74 (Planned)	V74 (Delivered)	%V diff (Delivered - Planned)
1	100	100	0
2	100	98	-2
3	98	98	0
4	100	100	0
5	100	100	0
6	98	98	0
7	99	93	-7

Table B.2 CTV V74 for each patient's PSPT plan

Patient No.	V74 (Planned)	V74 (Delivered)	%V diff (Delivered - Planned)
1	99	99	0
2	100	100	0
3	97	97	0
4	98	98	0
5	97	99	2
6	100	100	0
7	98	89	-9

Table B.3 Total Lung V5 for each patient's IMRT plan

Patient No.	V5 (Planned)	V5 (Delivered)	%V diff (Delivered - Planned)
1	61	62	1
2	35	38	3
3	43	46	3
4	50	51	1
5	58	59	1
6	58	62	3
7	51	56	5

Table B.4 Total Lung V10 for each patient's IMRT plan

Patient No.	V10 (Planned)	V10 (Delivered)	%V diff (Delivered - Planned)
1	45	45	1
2	23	25	2
3	31	33	3
4	39	40	1
5	43	44	1
6	43	46	3
7	36	40	4

Table B.5 Total Lung V20 for each patient's IMRT plan

Patient No.	V20 (Planned)	V20 (Delivered)	%V diff (Delivered - Planned)
1	26	26	0
2	17	18	1
3	23	25	2
4	31	32	1
5	31	32	1
6	32	35	2
7	22	24	2

Table B.6 Total Lung Mean Lung Dose for each patient's IMRT plan

Patient No.	Mean Lung Dose (Planned)	Mean Lung Dose (Delivered)	MLD diff (Delivered - Planned) [cGy]
1	1675	1694	19
2	1161	1213	52
3	1462	1583	121
4	2036	2096	61
5	2097	2170	74
6	2056	2230	173
7	1528	1585	57

Table B.7 Total Lung V5 for each patient's PSPT plan

Patient No.	V5 (Planned)	V5 (Delivered)	%V diff (Delivered - Planned)
1	43	49	6
2	21	22	1
3	43	47	4
4	45	46	1
5	37	40	4
6	53	56	3
7	36	42	6

Table B.8 Total Lung V10 for each patient's PSPT plan

Patient No.	V10 (Planned)	V10 (Delivered)	%V diff (Delivered - Planned)
1	38	42	4
2	19	20	1
3	39	42	3
4	42	43	1
5	34	36	2
6	49	53	3
7	30	31	2

Table B.9 Total Lung V20 for each patient's PSPT plan

Patient No.	V20 (Planned)	V20 (Delivered)	%V diff (Delivered - Planned)
1	31	33	2
2	18	18	0
3	30	33	3
4	39	39	0
5	29	31	1
6	43	48	4
7	22	22	0

Table B.10 Total Lung Mean Lung Dose for each patient's PSPT plan

Patient No.	Mean Lung Dose (Planned)	Mean Lung Dose (Delivered)	MLD diff (Delivered - Planned) [cGy]
1	1604	1682	78
2	1083	1092	9
3	1664	1804	140
4	2002	2034	32
5	1721	1827	106
6	2408	2693	285
7	1329	1282	-47

Table B.11 Esophagus V55 for each patient's IMRT plan

Patient No.	V55 (Planned)	V55 (Delivered)	%V diff (Delivered - Planned)
1	26	26	0
2	0	0	0
3	33	37	3
4	35	36	1
5	13	13	0
6	36	37	0
7	43	43	0

Table B.12 Esophagus V55 for each patient's PSPT plan

Patient No.	V65 (Planned)	V65 (Delivered)	%V diff (Delivered - Planned)
1	25	24	-1
2	0	0	0
3	18	22	3
4	27	28	1
5	5	5	0
6	28	29	1
7	32	29	-3

Table B.13 Heart V45 for each patient's IMRT plan

Patient No.	V45 (planned)	V45 (Delivered)	%V diff (Delivered - Planned)
1	1	2	1
2	0	0	0
3	0	0	0
4	22	21	-1
5	7	8	1
6	19	19	-1
7	2	6	4

Table B.14 Heart V45 for each patient's PSPT plan

Patient No.	V45 (planned)	V45 (Delivered)	%V diff (Delivered - Planned)
1	1	1	0
2	0	0	0
3	0	1	0
4	4	4	1
5	8	9	1
6	20	20	0
7	4	7	3

Table B.15 Mean Heart Dose for each patient's IMRT plan

Patient No.	Mean Heart Dose (planned)	Mean Heart Dose (Delivered)	MHD diff (Delivered-Planned) [cGy]
1	779	854	75
2	1468	1442	-25
3	98	103	6
4	2151	2125	-26
5	1155	1277	122
6	1810	1802	-8
7	807	1290	483

Table B.16 Mean Heart Dose for each patient's PSPT plan

Patient No.	Mean Heart Dose (planned)	Mean Heart Dose (Delivered)	MHD diff (Delivered-Planned) [cGy]
1	187	358	171
2	88	68	-20
3	188	279	91
4	595	767	172
5	746	873	127
6	1787	1743	-44
7	500	869	370

Table B.17 Max Spinal Cord Dose for each patient's IMRT plan

Patient No.	Max Cord Dose (Planned)	Max Cord Dose (Delivered)	MCD diff (Delivered-Planned) [cGy]
1	4406	4516	110
2	3010	2832	-178
3	4202	4595	393
4	4852	5026	174
5	4648	4665	17
6	4344	4464	120
7	4536	4677	141

Table B.18 Max Spinal Cord Dose for each patient's PSPT plan

Patient No.	Max Cord Dose (Planned)	Max Cord Dose (Delivered)	MCD diff (Delivered-Planned) [cGy]
1	4239	4069	-169
2	1542	2733	1191
3	4476	4483	7
4	3870	3868	-2
5	2657	3306	649
6	4929	4841	-88
7	5269	4486	-783

References

1. Bucci, M. K., A. Bevan, and M. Roach. 2005. Advances in radiation therapy: Conventional to 3D, to IMRT, to 4D, and beyond. Int J Radiat Oncol Biol Phys 55:117-134.
2. Galvin, J. M., G. Ezzell, A. Eisbrauch, C. Yu, B. Butler, Y. Xiao, I. Rosen, J. Rosenman, M. Sharpe, L. Xing, P. Xia, T. Lomax, D. A. Low, and J. Palta. 2004. Implementing IMRT in clinical practice: A joint document of the American Society for Therapeutic Radiology and Oncology and the American Association of Physicists in Medicine. Int J Radiat Oncol Biol Phys 58:1616-1634.
3. Takahashi, S., and T. Matsuda. 1960. Axial transverse laminagraphy applied to rotational therapy. Radiol 74:61-64.
4. Brahme, A. 1988. Optimal Setting of Multileaf Collimators in Stationary Beam Radiation-Therapy. Strahlentherapie Und Onkologie 164:343-350.
5. Bortfeld, T., J. Burkelbach, R. Boesecke, and W. Schlegel. 1990. Methods of Image-Reconstruction from Projections Applied to Conformation Radiotherapy. Phys Med Biol 35:1423-1434.
6. Hall, E. J., and C. S. Wuu. 2003. Radiation-induced second cancers: The impact of 3D-CRT and IMRT. Int J Radiat Oncol Biol Phys 56:83-88.
7. Luxton, G., S. L. Hancock, and A. L. Boyer. 2004. IMRT versus conformal 3-D planning for prostate cancer: Comparison of biological model calculations of NTCP and TCP. Medic Phy 31:1894-1894.
8. Vlachaki, M. T., T. N. Teslow, C. Amosson, N. W. Uy, and S. Ahmad. 2005. IMRT versus conventional 3DCRT on prostate and normal tissue dosimetry using an endorectal balloon for prostate immobilization. Med Dosim 30:69-75.
9. Yom, S. S., Z. X. Liao, H. H. Liu, S. L. Tucker, C. S. Hu, X. Wei, X. M. Wang, S. L. Wang, R. Mohan, J. D. Cox, and R. Komaki. 2007. Initial evaluation of treatment-related pneumonitis in advanced-stage non-small-cell lung cancer patients treated with concurrent chemotherapy and intensity-modulated radiotherapy. Int J Radiat Oncol Biol Phys 68:94-102.

10. Tobias, C. A., J. H. Lawrence, J. L. Born, R. K. Mccombs, J. E. Roberts, H. O. Anger, B. V. A. Lowbeer, and C. B. Huggins. 1958. Pituitary Irradiation with High-Energy Proton Beams - Preliminary Report. Cancer Resea 18:121-123.
11. Slater, J. M., D. W. Miller, and J. W. Slater. 1991. Developing a Clinical Proton Accelerator Facility - Consortium-Assisted Technology-Transfer. Conference Record of the 1991 Ieee Particle Accelerator Conference, Vols 1-5:532-536.
12. Konski, A., W. Speier, A. Hanlon, J. R. Beck, and A. Pollack. 2007. Is proton beam therapy cost effective in the treatment of adenocarcinoma of the prostate? J Clinical Oncol 25:3603-3608.
13. Brada, M., M. Pijls-Johannesma, and D. De Ruysscher. 2007. Proton therapy in clinical practice: Current clinical evidence. J Clinical Oncol 25:965-970.
14. Olsen, D. R., O. S. Bruland, G. Frykholm, and I. N. Norderhaug. 2007. Proton therapy - A systematic review of clinical effectiveness. Radiother Oncol 83:123-132.
15. Goitein, M., and J. D. Cox. 2008. A patient's perspective on randomized clinical trials for proton radiotherapy - Reply. J Clinical Oncol 26:2593-2596.
16. Chang, J. Y., X. Zhang, X. Wang, Y. Kang, B. Riley, S. Bilton, R. Mohan, R. Komaki, and J. D. Cox. 2006. Significant reduction of normal tissue dose by proton radiotherapy compared with three-dimensional conformal or intensity-modulated radiation therapy in Stage I or Stage III non-small-cell lung cancer. Int J Radiat Oncol Biol Phys 65:1087-1096.
17. Dosoretz, D. E., M. J. Katin, P. H. Blitzer, J. H. Rubenstein, S. Salenius, M. Rashid, R. A. Dosani, G. Mestas, A. D. Siegel, T. T. Chadha. 1992. Radiation therapy in the management of medically inoperable carcinoma of the lung: results and implications for future treatment strategies. Int J Radiat Oncol Biol Phys 24:3-9.
18. Zhang, X., Y. Li, X. Pan, L. Xiaoqiang, R. Mohan, R. Komaki, J. D. Cox, and J. Y. Chang. 2005. Intensity-modulated proton therapy reduces the dose to normal tissue compared with intensity-modulated radiation therapy or passive scattering proton therapy and enables individualized radical radiotherapy for extensive

stage IIIB non-small-cell lung cancer: a virtual clinical study. Int J Radiat Oncol Biol Phys 77:357-366.

19. Macbeth, F. 2008. Measuring the outcomes of lung cancer treatment. J Thorac Oncol 3:455-456.
20. Halperin, E. C. 2000. Overpriced technology in radiation oncology. Int J Radiat Oncol Biol Phys 48:917-918.
21. Lodge, M., M. Pijls-Johannesma, L. Stirk, A. J. Munro, D. De Ruysscher, and T. Jefferson. 2007. A systematic literature review of the clinical and cost-effectiveness of hadron therapy in cancer. Radiother Oncol 83:110-122.
22. Glimelius, B., and A. Montelius. 2007. Proton beam therapy - do we need the randomised trials and can we do them? Radiother Oncol 83:105-109.
23. Glasziou, P., I. Chalmers, M. Rawlins, and P. McCulloch. 2007. When are randomised trials unnecessary? Picking signal from noise. BMJ 334:349-351.
24. Vedam, S. S., P. J. Keall, V. R. Kini, and R. Mohan. 2001. Determining parameters for respiration-gated radiotherapy. Med Phys 28:2139-2146.
25. Ford, E. C., G. S. Mageras, E. Yorke, K. E. Rosenzweig, R. Wagman, and C. C. Ling. 2002. Evaluation of respiratory movement during gated radiotherapy using film and electronic portal imaging. Int J Radiat Oncol Biol Phys 52:522-531.
26. Balter, J. M., K. L. Lam, C. J. McGinn, T. S. Lawrence, and R. K. Ten Haken. 1998. Improvement of CT-based treatment-planning models of abdominal targets using static exhale imaging. Int J Radiat Oncol Biol Phys 41:939-943.
27. Keall, P. J., G. S. Mageras, J. M. Balter, R. S. Emery, K. M. Forster, S. B. Jiang, J. M. Kapatoes, D. A. Low, M. J. Murphy, B. R. Murray, C. R. Ramsey, M. B. Van Herk, S. S. Vedam, J. W. Wong, and E. Yorke. 2006. The management of respiratory motion in radiation oncology report of AAPM Task Group 76. Med Phys 33:3874-3900.
28. Pan, T., T. Y. Lee, E. Rietzel, and G. T. Chen. 2004. 4D-CT imaging of a volume influenced by respiratory motion on multi-slice CT. Med Phys 31:333-340.

29. Pan, T., T. Y. Lee, E. Rietzel, and G. T. Y. Chen. 2004. 4D-CT imaging of a volume influenced by respiratory motion on multi-slice CT. Med Phy 31:333-340.
30. Admiraal, M. A., D. Schuring, and C. W. Hurkmans. 2008. Dose calculations accounting for breathing motion in stereotactic lung radiotherapy based on 4D-CT and the internal target volume. Radiother Oncol 86:55-60.
31. Cachier, P., and X. Pennec. 2000. 3D non-rigid registration by gradient descent on a Gaussian-windowed similarity measure using convolutions. In Proceedings of the Workshop on Mathematical Methods in Biomedical Image Analysis. 182-189.
32. Brock, K. K., D. L. McShan, R. K. Ten Haken, S. J. Hollister, L. A. Dawson, and J. M. Balter. 2003. Inclusion of organ deformation in dose calculations. Med Phys 30:290-295.
33. Liang, J., and D. Yan. 2003. Reducing uncertainties in volumetric image based deformable organ registration. Med Phys 30:2116-2122.
34. Thirion, J. P. 1998. Image matching as a diffusion process: an analogy with Maxwell's demons. Med Image Anal 2:243-260.
35. Wang, H., L. Dong, M. F. Lii, A. L. Lee, R. De Crevoisier, R. Mohan, J. D. Cox, D. A. Kuban, and R. Cheung. 2005. Implementation and validation of a three-dimensional deformable registration algorithm for targeted prostate cancer radiotherapy. Int J Radiat Oncol Biol Phys 61:725-735.
36. Wang, H., L. Dong, M. F. Lii, A. L. Lee, R. de Crevoisier, R. Mohan, J. D. Cox, D. A. Kuban, and R. Cheung. 2005. Implementation and validation of a three-dimensional deformable registration algorithm for targeted prostate cancer radiotherapy. Int J Radiat Oncol Biol Phys 61:725-735.
37. Schaly, B., J. A. Kempe, G. S. Bauman, J. J. Battista, and J. Van Dyk. 2004. Tracking the dose distribution in radiation therapy by accounting for variable anatomy. Phys Med Biol 49:791-805.
38. Bender, E. T., N. Hardcastle, and W. A. Tome. On the dosimetric effect and reduction of inverse consistency and transitivity errors in deformable image registration for dose accumulation. Med Phys 39:272-280.

39. Yeo, U. J., M. L. Taylor, J. R. Supple, R. L. Smith, L. Dunn, T. Kron, and R. D. Franich. Is it sensible to "deform" dose 3D experimental validation of dose-warping. Med Phys 39:5065-5072.
40. Paganetti, H. Range uncertainties in proton therapy and the role of Monte Carlo simulations. Phys Med Biol 57:R99-117.
41. Engelsman, M., T. F. DeLaney, and T. S. Hong. Proton radiotherapy: the biological effect of treating alternating subsets of fields for different treatment fractions. Int J Radiat Oncol Biol Phys 79:616-622.
42. Lomax, A. J. 2008. Intensity modulated proton therapy and its sensitivity to treatment uncertainties 1: the potential effects of calculational uncertainties. Phys Med Biol 53:1027-1042.
43. Lomax, A. J. 2008. Intensity modulated proton therapy and its sensitivity to treatment uncertainties 2: the potential effects of inter-fraction and inter-field motions. Phys Med Biol 53:1043-1056.
44. Unkelbach, J., T. C. Chan, and T. Bortfeld. 2007. Accounting for range uncertainties in the optimization of intensity modulated proton therapy. Phys Med Biol 52:2755-2773.
45. Moyers, M. F., M. Sardesai, S. Sun, and D. W. Miller. Ion stopping powers and CT numbers. Med Dosim 35:179-194.
46. Yang, M., X. R. Zhu, P. C. Park, U. Titt, R. Mohan, G. Virshup, J. E. Clayton, and L. Dong. Comprehensive analysis of proton range uncertainties related to patient stopping-power-ratio estimation using the stoichiometric calibration. Phys Med Biol 57:4095-4115.
47. Paganetti, H., A. Niemierko, M. Ancukiewicz, L. E. Gerweck, M. Goitein, J. S. Loeffler, and H. D. Suit. 2002. Relative biological effectiveness (RBE) values for proton beam therapy. Int J Radiat Oncol Biol Phys 53:407-421.
48. Zhang, X., L. Dong, A. K. Lee, J. D. Cox, D. A. Kuban, R. X. Zhu, X. Wang, Y. Li, W. D. Newhauser, M. Gillin, and R. Mohan. 2007. Effect of anatomic motion on proton therapy dose distributions in prostate cancer treatment. Int J Radiat Oncol Biol Phys 67:620-629.

49. Hui, Z. G., X. D. Zhang, G. Starkschall, Y. P. Li, R. Mohan, R. Komaki, J. D. Cox, and J. Y. Chang. 2008. Effects of Interfractional, Motion and Anatomic Changes on Proton Therapy Dose Distribution in Lung Cancer. Int J Radiat Oncol Biol Phys 72:1385-1395.
50. Albertini, F., A. Bolsi, A. J. Lomax, H. P. Rutz, B. Timmerman, and G. Goitein. 2008. Sensitivity of intensity modulated proton therapy plans to changes in patient weight. Radiother Oncol 86:187-194.

51. Barker, J. L., A. S. Garden, K. K. Ang, J. C. O'Daniel, H. Wang, L. E. Court, W. H. Morrison, D. I. Rosenthal, K. S. C. Chao, S. L. Tucker, R. Mohan, and L. Dong. 2004. Quantification of volumetric and geometric changes occurring during fractionated radiotherapy for head-and-neck cancer using an integrated CT/linear accelerator system. Int J Radiat Oncol Biol Phys 59:960-970.
52. Hansen, E. K., M. K. Bucci, J. M. Quivey, V. Weinberg, and P. Xia. 2006. Repeat CT imaging and replanning during the course of IMRT for head-and-neck cancer. Int J Radiat Oncol Biol Phys 64:355-362.
53. O'Daniel, J. C., A. S. Garden, D. L. Schwartz, H. Wang, K. K. Ang, A. Ahamad, D. I. Rosenthal, W. H. Morrison, J. A. Asper, L. Zhang, S. M. Tung, R. Mohan, and L. Dong. 2007. Parotid gland dose in intensity-modulated radiotherapy for head and neck cancer: Is what you plan what you get? Int J Radiat Oncol Biol Phys 69:1290-1296.
54. Lomax, A. J. 2008. Intensity modulated proton therapy and its sensitivity to treatment uncertainties 1: the potential effects of calculational uncertainties. Phys Med Biol 53:1027-1042.
55. Lomax, A. J. 2008. Intensity modulated proton therapy and its sensitivity to treatment uncertainties 2: the potential effects of inter-fraction and inter-field motions. Phys Med Biol 53:1043-1056.
56. Gerweck, L. E., and S. V. Kozin. 1999. Relative biological effectiveness of proton beams in clinical therapy. Radiother Oncol 50:135-142.

57. Paganetti, H., A. Niemierko, M. Ancukiewicz, L. E. Gerweck, M. Goitein, J. S. Loeffler, and H. D. Suit. 2002. Relative biological effectiveness (RBE) values for proton beam therapy. Int J Radiat Oncol Biol Phys 53:407-421.
58. Wilkens, J. J., and U. Oelfke. 2004. A phenomenological model for the relative biological effectiveness in therapeutic proton beams. Phys Med Biol 49:2811-2825.
59. Chen, Y., and S. Ahmad. 2012. Empirical model estimation of relative biological effectiveness for proton beam therapy(dagger). Radia Protect Dosi 149:116-123.
60. Strongin, A., S. Yovino, R. Taylor, J. Wolf, K. Cullen, A. Zimrin, S. Strome, W. Regine, and M. Suntharalingam. Primary tumor volume is an important predictor of clinical outcomes among patients with locally advanced squamous cell cancer of the head and neck treated with definitive chemoradiotherapy. Int J Radiat Oncol Biol Phys 82:1823-1830.
61. Wang, H., L. Dong, J. O'Daniel, R. Mohan, A. S. Garden, K. K. Ang, D. A. Kuban, M. Bonnen, J. Y. Chang, and R. Cheung. 2005. Validation of an accelerated 'demons' algorithm for deformable image registration in radiation therapy. Phys Med Biol 50:2887-2905.

62. Cho, K. H., D. Shin, S. J. Cho, J. Jang, S. H. Lee, Y. H. Kim, D. H. Choi, E. S. Kim, and S. Il Kwon. 2007. The Effect of the CT Number for Each CT on Photon Dose Calculation. World Congress on Med Phys Bio 2006, Vol 14, Pts 1-6 14:1984-1986.
63. Lomax, A. J. 2008. Intensity modulated proton therapy and its sensitivity to treatment uncertainties 1: the potential effects of calculational uncertainties. Phys Med Biol 53:1027-1042.
64. Lomax, A. J. 2008. Intensity modulated proton therapy and its sensitivity to treatment uncertainties 2: the potential effects of inter-fraction and inter-field motions. Phys Med Biol 53:1043-1056.
65. Zhu, S. Y., T. Mizowaki, Y. Norihisa, K. Takayama, Y. Nagata, and M. Hiraoka. 2008. Comparisons of the impact of systematic uncertainties in patient

setup and prostate motion on doses to the target among different plans for definitive external-beam radiotherapy for prostate cancer. Int J Radiat Oncol Biol Phys 13:54-61.

66. Zhang, Y., D. Boye, C. Tanner, A. J. Lomax, and A. Knopf. 2012. Respiratory liver motion estimation and its effect on scanned proton beam therapy. Phys Med Biol 57:1779-1795.

67. Yang, M., X. R. Zhu, P. C. Park, U. Titt, R. Mohan, G. Virshup, J. E. Clayton, and L. Dong. 2012. Comprehensive analysis of proton range uncertainties related to patient stopping-power-ratio estimation using the stoichiometric calibration. Phys Med Biol 57:4095-4115.

68. Moyers, M. F., D. W. Miller, D. A. Bush, and J. D. Slater. 2001. Methodologies and tools for proton beam design for lung tumors. Int J Radiat Oncol Biol Phys 49:1429-1438.

69. Engelsman, M., and H. M. Kooy. 2005. Target volume dose considerations in proton beam treatment planning for lung tumors. Med Phys 32:3549-3557.

70. Albertini, F., A. Bolsi, A. J. Lomax, H. P. Rutz, B. Timmerman, and G. Goitein. 2008. Sensitivity of intensity modulated proton therapy plans to changes in patient weight. Radiother Oncol 86:187-194.

71. Wang, Y., J. A. Efstathiou, G. C. Sharp, H. M. Lu, I. F. Ciernik, and A. V. Trofimov. 2011. Evaluation of the dosimetric impact of interfractional anatomical variations on prostate proton therapy using daily in-room CT images. Med Phys 38:4623-4633.

72. Hui, Z. G., X. D. Zhang, G. Starkschall, Y. P. Li, R. Mohan, R. Komaki, J. D. Cox, and J. Y. Chang. 2008. Effects of Interfractional, Motion and Anatomic Changes on Proton Therapy Dose Distribution in Lung Cancer. Int J Radiat Oncol Biol Phys 72:1385-1395.

73. Kang, Y. X., X. D. Zhang, J. Y. Chang, H. Wang, X. Wei, Z. X. Liao, R. Komaki, J. D. Cox, P. A. Balter, H. Liu, X. R. Zhu, R. Mohan, and L. Dong. 2007. 4D proton treatment planning strategy for mobile lung tumors. Int J Radiat Oncol Biol Phys 67:906-914.

74. Schwarz, M. 2011. Treatment planning in proton therapy. Euro Phys J Plus 126.

75. Zhang, M., D. C. Westerly, and T. R. Mackie. 2011. Introducing an on-line adaptive procedure for prostate image guided intensity modulate proton therapy. Phys Med Biol 56:4947-4965.
76. Schwartz, D. L. 2012. Current Progress in Adaptive Radiation Therapy for Head and Neck Cancer. Curr Oncol Rep 14:139-147.
77. Hurkmans, C. W., I. Dijckmans, M. Reijnen, J. van der Leer, C. van Vliet-Vroegindeweij, and M. van der Sangen. 2012. Adaptive radiation therapy for breast IMRT-simultaneously integrated boost: Three-year clinical experience. Radiother Oncol 103:183-187.
78. Jensen, A. D., S. Nill, P. E. Huber, R. Bendl, J. Debus, and M. W. Munter. 2012. A Clinical Concept for Interfractional Adaptive Radiation Therapy in the Treatment of Head-and-Neck Cancer. Int J Radiat Oncol Biol Phys 82:590-596.
79. Ahn, P. H., C. C. Chen, A. I. Ahn, L. Hong, P. G. Scripes, J. Shen, C. C. Lee, E. Miller, S. Kalnicki, and M. K. Garg. 2011. Adaptive Planning in Intensity-Modulated Radiation Therapy for Head and Neck Cancers: Single-Institution Experience and Clinical Implications. Int J Radiat Oncol Biol Phys 80:677-685.
80. Nishimura, Y., T. Shibata, K. Nakamatsu, S. Kanamori, R. Koike, T. Nishikawa, I. Tachibana, and K. Ishikawa. 2011. Adaptive Radiation Therapy Scheme of a Two-step Intensity Modulated Radiation Therapy (IMRT) Method for Nasopharyngeal Cancer (NPC). Int J Radiat Oncol Biol Phys 81:S512-S513.
81. Lee, A. K., R. J. Kudchadker, R. A. Amos, J. L. Johnson, S. L. Choi, D. A. Kuban, J. D. Cox, R. Mohan, M. Gillin, and L. Dong. 2007. Proton therapy vs. IMRT for prostate cancer: A dosimetric comparison. Int J Radiat Oncol Biol Phys 69:S342-S342.
82. Chang, J. Y., X. D. Zhang, X. C. Wang, Y. X. Kang, B. Riley, S. Bilton, R. Mohan, R. Komaki, and J. D. Cox. 2006. Significant reduction of normal tissue dose by proton radiotherapy compared with three-dimensional conformal or intensity-modulated radiation therapy in Stage I or Stage III non-small-cell lung cancer. Int J Radiat Oncol Biol Phys 65:1087-1096.
83. Mohan, R., X. Zhang, J. Matney, J. Bluett, L. Dong, P. Balter, M. Engelsman, N. Choi, R. Komaki, and Z. Liao. 2010. IMRT vs. Passively Scattered Proton

Therapy (PSPT) for Locally Advanced Non-small Cell Lung CA (LA NSCLC) Randomized Trial - Is there Equipoise? Int J Radiat Oncol Biol Phys 78:S201-S202.

84. Engelsman, M., and H. Kooy. 2004. Target volume dose considerations in proton beam treatment planning for lung tumors. Med Phys 31:1918-1918.

85. Berman, A. T., M. Ingram, S. Both, and L. L. Lin. 2008. Dose-volume comparison of combined IMRT and proton therapy vs. IMRT for pelvis and para-aortic radiotherapy in gynecologic malignancies. Int J Radiat Oncol Biol Phys 72:S370-S371.

86. Krengli, M., F. Bourhaleb, L. Cozzi, G. Loi, A. Fogliata, D. Beldi, G. Nicolini, A. Clivio, M. C. Bassi, and R. Orecchia. 2006. Treatment planning comparison of photon IMRT, active and passive proton therapy, and carbon ion therapy for treatment of head and neck tumors. Int J Radiat Oncol Biol Phys 66:S669-S669.

87. Yeung, D., R. S. Malyapa, W. M. Mendenhall, Z. Li, D. Louis, C. Liu, R. J. Amdur, J. R. Palta, and N. P. Mendenhall. 2006. Dosimetric comparison of IMRT and proton therapy for head and neck tumors. Int J Radiat Oncol Biol Phys 66:S412-S412.

88. Ingram, M., A. Kassaee, and J. McDonough. 2007. Treatment planning advantages of proton scattered beam and intensity modulated proton therapy over IMRT for pancreas tumors. Med Phys 34:2499-2499.

89. Velec, M., J. Moseley, L. A. Dawson, and K. K. Brock. 2009. Importance of Deformation, Including Baseline Shifts and Breathing Variation, on Dose Accumulation in Liver SBRT. Int J Radiat Oncol Biol Phys 75:S25-S26.

90. Lu, W. G., G. H. Olivera, Q. Chen, K. J. Ruchala, J. Haimerl, S. L. Meeks, K. M. Langen, and P. A. Kupelian. 2006. Deformable registration of the planning image (kVCT) and the daily images (MVCT) for adaptive radiation therapy. Phys Med Biol 51:4357-4374.

91. Brock, K. K., M. Lee, C. L. Eccles, M. Velec, J. L. Moseley, and L. A. Dawson. 2008. Deformable registration and dose accumulation to investigate marginal liver cancer recurrences. Int J Radiat Oncol Biol Phys 72:S538-S538.

92. Janssens, G., J. O. de Xivry, S. Fekkes, A. Dekker, B. Macq, P. Lambin, and W. van Elmpt. 2009. Evaluation of nonrigid registration models for interfraction dose accumulation in radiotherapy. Med Phys 36:4268-4276.
93. Wang, H., L. Dong, J. O'Daniel, R. Mohan, A. S. Garden, K. K. Ang, D. A. Kuban, M. Bonnen, J. Y. Chang, and R. Cheung. 2005. Validation of an accelerated 'demons' algorithm for deformable image registration in radiation therapy. Phys Med Biol 50:2887-2905.
94. Gao, S., L. F. Zhang, H. Wang, R. de Crevoisier, D. D. Kuban, R. Mohan, and L. Dong. 2006. A deformable image registration method to handle distended rectums in prostate cancer radiotherapy. Med Phys 33:3304-3312.
95. Wang, H., S. Krishnan, X. Wang, A. Beddar, T. Briere, C. Crane, R. Mohan, and L. Dong. 2006. Improving soft tissue contrast in 4D CT images of liver cancer patients using deformable image registration method. Med Phys 33:2039-2039.

VITA

Yi Pei “Patty” Chen was born in Taipei, Taiwan. She attended University of California, San Diego in La Jolla, CA and received a Bachelor of Science in mechanical engineering degree in June 2008. After she moved to Houston, she started to work under the guidance of Dr. Lei Dong at the beginning of 2009. In September of 2011, she entered the medical physics program of The University of Texas Health Science Center at Houston Graduate School of Biomedical Sciences. She currently resides in Houston, Texas with her husband and her new born son.